

General Disclaimer

One or more of the Following Statements may affect this Document

- This document has been reproduced from the best copy furnished by the organizational source. It is being released in the interest of making available as much information as possible.
- This document may contain data, which exceeds the sheet parameters. It was furnished in this condition by the organizational source and is the best copy available.
- This document may contain tone-on-tone or color graphs, charts and/or pictures, which have been reproduced in black and white.
- This document is paginated as submitted by the original source.
- Portions of this document are not fully legible due to the historical nature of some of the material. However, it is the best reproduction available from the original submission.

NI
(NASA-CR-162334) HIGH TEMPERATURE - LOW
MASS SOLAR BLANKET Final Report (TRW
Defense and Space Systems Group) 121 p
HC A06/MF A01

N79-33559

CSCL 10A

Unclas

G3/44

35870

FINAL REPORT

ON

HIGH TEMPERATURE - LOW MASS SOLAR BLANKET

JPL Contract No. 955139

TRW No. 32809.000

Prepared For:

JET PROPULSION LABORATORY
CALIFORNIA INSTITUTE OF TECHNOLOGY
4800 Oak Grove Drive, Pasadena, California 91103

This work was performed for the Jet Propulsion Laboratory,
California Institute of Technology, under NASA Contract NAS7-100

AUGUST 1979

Prepared By: H. G. MESCH



TRW

DEFENSE AND SPACE SYSTEMS GROUP

ONE SPACE PARK • REDONDO BEACH • CALIFORNIA 90278

POWER/ELECTROMECHANICAL MFG. & TEST DEPARTMENT

FINAL REPORT

ON

**HIGH TEMPERATURE - LOW MASS
SOLAR BLANKET**

JPL Contract No. 955139

TRW No. 32809.000

Prepared For:

**JET PROPULSION LABORATORY
CALIFORNIA INSTITUTE OF TECHNOLOGY
4800 Oak Grove Drive, Pasadena, California 91103**

**This work was performed for the Jet Propulsion Laboratory,
California Institute of Technology, under NASA Contract NAS7-100**

AUGUST 1979

Prepared By: H. G. MESCH

TRW

DEFENSE AND SPACE SYSTEMS GROUP

ONE SPACE PARK • REDONDO BEACH • CALIFORNIA 90278

POWER/ELECTROMECHANICAL MFG. & TEST DEPARTMENT

TECHNICAL CONTENT

This report contains information prepared by TRW Systems under JPL sub-contract. Its content is not necessarily endorsed by the Jet Propulsion Laboratory, California Institute of Technology, or the National Aeronautics and Space Administration.

CONTENTS

	Page
1. ABSTRACT	1-1
2. INTRODUCTION	2-1
3. TECHNICAL DISCUSSION	3-1.1
3.1 Requirements	3.1-1
3.2 Interconnector Development	3.2-1
3.2.1 Configuration Analysis and Selection	3.2-1
3.2.2 Stress and Fatigue Analysis	3.2-2
3.3 Exploratory P/G - Welding	3.3-1
3.3.1 Equipment Description	3.3-1
3.3.2 Preliminary Welding Study	3.3-2
3.3.3 Optimizing Weld Parameters	3.3-2
3.3.4 Cell Contact Surface Roughness	3.3-43
3.3.5 Data Correlation, NDT Versus Pull-Strength	3.3-46
3.4 Process Development	3.4-1
3.4.1 Front Contact Attachment	3.4-1
3.4.2 Cover-to-Cell Bonding	3.4-3
3.4.3 Rear Contact Attachment	3.4-4
3.4.4 Cell-to-Substrate Bonding	3.4-5
3.4.5 Discussion of Critical Areas	3.4-5
3.5 Hardware Fabrication	3.5-1
3.5.1 Component Description	3.5-1
3.5.2 Test Coupons	3.5-1
3.5.3 Module Solar Blanket	3.5-6
3.6 Development Testing	3.6-1
3.7 Repair Study	3.7-1
3.7.1 Detailed Solar Cell Replacement	3.7-3
3.8 Usable Device Yield	3.8-1

CONTENTS (Continued)

	Page
3.9 Quality Assurance Procedures	3.9-1
3.9.1 Solar Cell	3.9-1
3.9.2 Cover Glass	3.9-2
3.9.3 Component and Assembly	3.9-3
4. CONCLUSIONS	4-1
5. RECOMMENDATIONS	5-1
6. NEW TECHNOLOGY	6-1
7. REFERENCES	7-1

1. ABSTRACT

Recent developments in ultrathin ($\sim 50 \mu\text{m}$) silicon solar cell technology have demonstrated that this type of cell possesses the highest power-to-mass ratio as well as the best performance under space radiation of any silicon solar cell yet produced. This report describes TRW's efforts oriented towards incorporating this unique device into photovoltaic blankets for space applications envisioned by NASA/JPL.

Interconnect materials and designs for use with ultrathin cells are discussed, as well as the results of TRW's investigation of the applicability of parallel-gap resistance welding for interconnecting these cells. Data relating contact pull strength and cell electrical degradation to variations in welding parameters such as time, voltage and pressure are presented.

Methods for bonding ultrathin cells to flexible substrates and for bonding thin ($75 \mu\text{m}$) covers to these cells are described. Also, factors influencing fabrication yield and approaches for increasing yield are discussed. The successful results of vacuum thermal cycling and thermal soak tests on prototype ultrathin cell test coupons and one solar module blanket are presented herein.

2. INTRODUCTION

The basic technology used to assemble solar cells into panels and to accommodate the many changes necessary to develop arrays which have higher power and lower mass per unit area are the primary objectives of this study. These improvements have been brought about mainly by the employment of flexible lightweight substrates, interconnecting by welding rather than solder, thinner cover-glasses, and the use of thinner more efficient solar cells. The development of 50 μm thick silicon solar cells with AMO conversion efficiencies in excess of twelve percent presents a unique assembly challenge to basic panel fabrication technology (Reference 1). The purpose of this work is to examine the prospects for fabricating solar panels employing ultrathin solar cells and covers via conventional assembly processes.

3. TECHNICAL DISCUSSION

This section contains the results of the analysis, experiments and manufacturing processes developed which are required for the manufacturing of a lightweight solar array blanket utilizing thin solar cells and covers, bonded to a thin flexible Kapton substrate.

3.1 REQUIREMENTS

The contract requirements call for a development and technology program for a welded solar array using 50-micron-thick, 2- by 2-centimeter solar cell assemblies covered with 75-micron-thick microsheet glass. The interconnectors are to be welded to front cell contact prior to cover-glassing. During these operations the thin cell's electrical performance variations are to be determined due to welding and cover glass application. Once series-parallel interconnected, the cell assemblies are to be bonded to 50-micron-thick Kapton substrates using a minimum mass of adhesive. The resulting technology shall be demonstrated by fabricating fifteen space quality solar cell coupons consisting of nine 2- by 2-centimeter, 50-micron-thick solar cells (electrically interconnected three cells in series and three cells in parallel, all bonded to 50-micron-thick Kapton substrates). The first five coupons are to be delivered to JPL and the remaining ten coupons shall be subjected to the following tests prior to shipment:

- a) Twenty-four hours of thermal soak at a high temperature of 120°C and an additional soak at 170°C for 24 hours.
- b) Twenty-four hours of thermal soak at a low temperature of -120°C and an additional soak at -180°C for 24 hours.
- c) Thereafter the ten test coupons are to be incrementally tested to 100 thermal vacuum cycles between -180° to $+120^{\circ}\text{C}$ with 30-minute soaks at the temperature extremes.

Upon successful completion of the test and written JPL approval, three High Temperature-Low Mass Solar Blankets are to be fabricated, each consisting of four cells in parallel and twenty cells connected in series for further JPL extended evaluation for the components as well as for the completed module solar blanket. One of the 3 modules solar blankets shall be subjected to 24 thermal vacuum cycles between $+70^{\circ}$ and -110°C with 30 minute soaks at the temperature extremes.

3.2 INTERCONNECTOR DEVELOPMENT

While the techniques for assembling thin cell test coupons were being developed, a parallel effort was initiated aimed at producing a suitable interconnect design for the thin cell coupons. In order to make the coupons compatible with the concept of either foldout or rollout array deployment schemes, inplane stress relief interconnect designs were examined.

3.2.1 Configuration Analysis and Selection

Five inplane stress relief interconnects were analyzed for electrical resistance and stress relief capability (Figure 3.2-1). All calculations were based on silver-plated 25 μm (0.001 inch) Invar interconnects. Of the five designs, the box interconnect offers the greatest stress relief at the lowest resistance. The rounded interconnect is equivalent in the region of interest ($H/L \approx 3$). Three variations of the rounded interconnect (Figure 3.2-2) were selected for test evaluation. For this phase of the investigations, ten coupons of thin cells were fabricated, using the same parallel and series circuit configuration. The single loop series interconnector (Figure 3.2-2) was used in assembling seven of the coupons. The remaining three coupons were assembled using the double loop series interconnect (Figure 3.2-2). All coupons utilized the same parallel interconnectors (Figure 3.2-2).

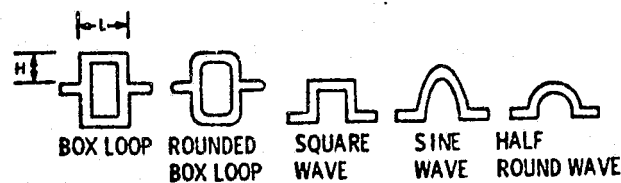


Figure 3.2-1. Five In-Plane Stress Relief Interconnector Design Configurations

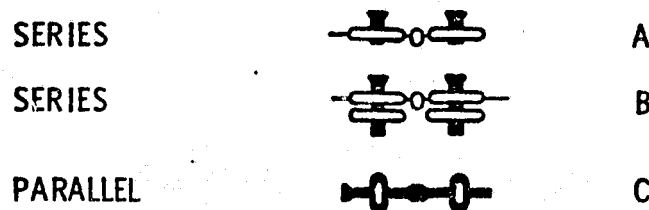


Figure 3.2-2. Coupon Series and Parallel Interconnect Designs

3.2.2 Stress and Fatigue Analysis

This section presents the results of a stress analysis of the proposed solar cell assemblies. Due to the large difference in the thermal coefficients of expansion of the silicon cell, the substrate, and the interconnector materials, the welded joint (between the interconnector and cell) is subjected to a large thermal stress amplitude as the solar array undergoes thermal cycles. The stresses come from two sources: (1) The actual differential expansion or contraction of the weld materials themselves, and (2) The forces applied to the weld by the interconnector. The former stresses are dependent on the selection of the weld materials and the thicknesses of the materials, while the latter stresses are dependent on the interconnector stiffnesses and thermal displacement between the cells. The thermal displacement can be minimized by the choice of different dimensions and materials of solar cell assemblies and is discussed in Section 3.2.2.1. Three different solar cell assemblies were studied. The interconnector stiffness can be minimized by the selection of the interconnector materials and the interconnector configuration. Three different interconnector configurations were investigated. The fatigue lives of these interconnector solar cell welds for the solar cell design which has the lowest thermal displacement were computed for two temperature ranges from -180° to 100°C and from -180° to 180°C .

3.2.2.1 Gap Displacements and Stresses of Solar Cell, Adhesive Material (RTV) and Substrate

The solar cell is bonded to the substrate by use of an adhesive as shown in Figure 3.2-3. The adhesive material is more flexible than either the cell or the substrate layers. Thus, as the temperature is cycled, a relative motion occurs between two layers at their interface. The analysis, neglecting the axial stiffness of the adhesive, has been discussed in Reference 2 for the case of thermal loading. The results are:

$$\sigma_1(X) = - \frac{E_1 \Delta \alpha \Delta T}{1 + mn} \left(1 - \frac{\cosh 2\beta X}{\cosh \beta L} \right) \quad (3-1)$$

$$\sigma_2(X) = - m \sigma_1(X) \quad (3-2)$$

$$\tau(X) = \frac{2E_1 t_1 \Delta \alpha \Delta T}{L(1+mn)} \frac{\beta L \sinh 2\beta X}{\cosh \beta L} \quad (3-3)$$

$$\Delta U = \Delta \alpha \Delta T L \frac{\tanh \beta L}{\beta L} + S \alpha_2 \quad (3-4)$$

where

$$\Delta \alpha = \alpha_2 - \alpha_1 \quad (3-5)$$

$$m = \frac{t_1}{t_2} \quad (3-6)$$

$$n = \frac{E_1}{E_2} \quad (3-7)$$

$$\beta^2 = \frac{1}{4} \frac{G_3}{t_3} \left(\frac{1}{E_1 t_1} + \frac{1}{E_2 t_2} \right) \quad (3-8)$$

in which

- t_1 thickness of cell
- t_2 thickness of adhesive
- t_3 thickness of substrate
- σ_1 the axial stress in the cell layer
- σ_2 the axial stress in the substrate layer
- τ the shear stress in the adhesive layer
- E_1 Young's modulus of the cell layer
- E_2 Young's modulus of the substrate layer
- G_3 the shear modulus of the adhesive layer
- S the intercell gap width
- α_1 the linear thermal expansion coefficient of the cell layer
- α_2 the linear thermal expansion coefficient of the substrate layer
- ΔU total gap displacement between adjacent cells
- L cell length
- X the distance from the midpoint of the cell

Three proposed cell and substrate designs, as well as the Fleet Satellite Communications (FLTSATCOM) and the Tracking Data Relay Satellite

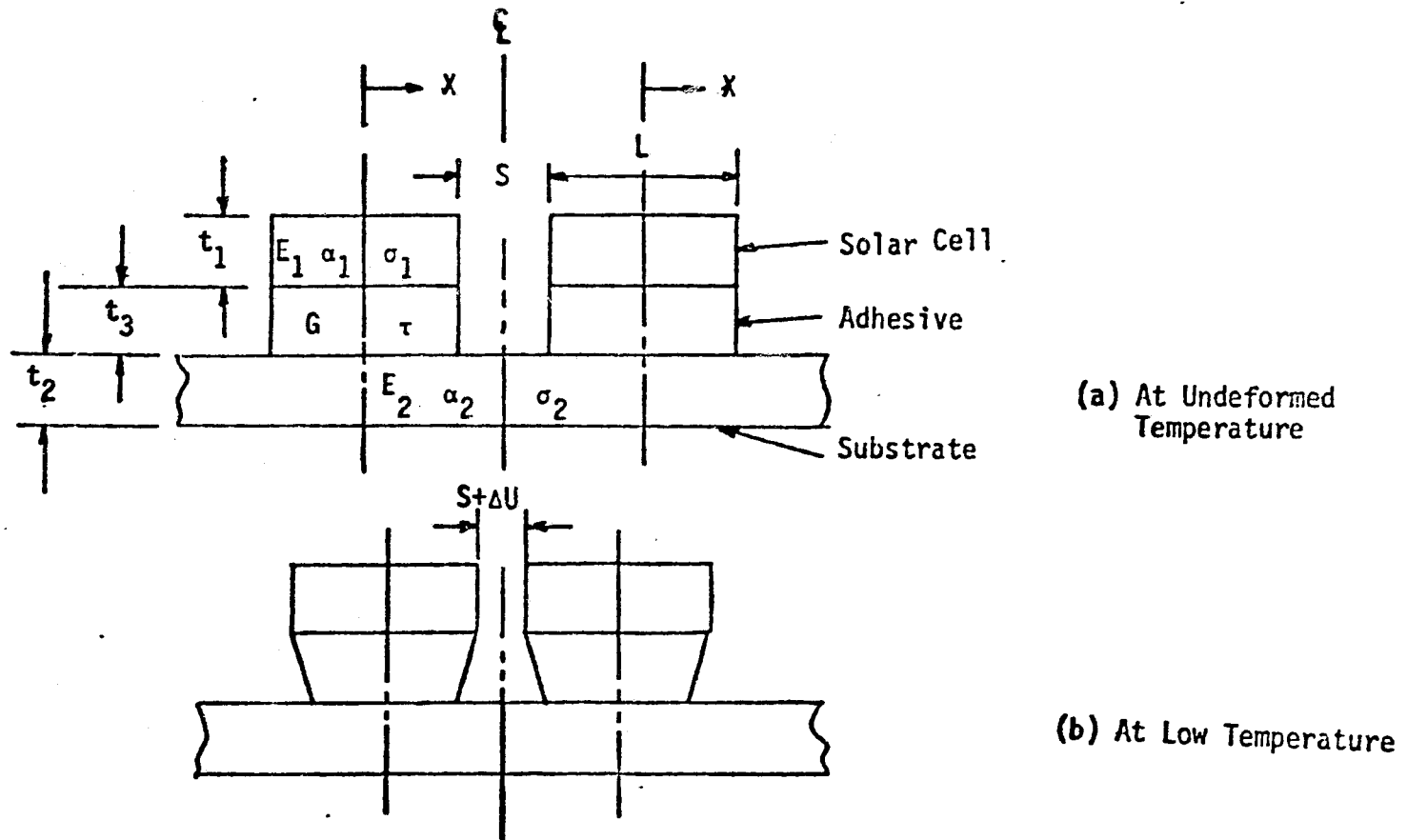


Figure 3.2-3. Cross Section of the Solar Cell Assembly at Equilibrium Undeformed Temperature and at Low Temperature

Table 3.2-1: Stresses and Gap Opening of Different Solar Cell Designs

Parameter	FLTSATCOM	TDRSS	Proposed I	Proposed II	Proposed III
t_1	0.008 in.	0.008 in.	0.002 in.	0.002 in.	0.002 in.
t_2	0.005 in. (Al)	0.002 in. (Kapton)	0.002 in. (Kapton)	0.002 in. (Kapton)	0.005 in. (Al)
t_3	0.004 in.	0.002 in.	0.001 in.	0.002 in.	0.001 in.
E_1 (psi)	1.7×10^7	1.7×10^7	1.7×10^7	1.7×10^7	1.7×10^7
E_2 (psi)	1.0×10^7	0.4×10^6	0.4×10^6	0.4×10^6	1.0×10^7
G(psi)	500	500	500	500	500
α_1 (in/in ⁰ F)	1.0×10^{-6}	1×10^{-6}	1×10^{-6}	1×10^{-6}	1×10^{-6}
α_2 (in/in ⁰ F)	13.0×10^{-6}	11×10^{-6}	11×10^{-6}	11×10^{-6}	13×10^{-6}
L	0.8 in	0.8	0.8	0.8	0.8
S	0.035 in	0.035	0.02	0.02	0.02
σ_1 max/ ΔT	-12.20	-0.993	-3.9	-3.9	-88.78
σ_2 max/ ΔT	19.53	3.97	3.9	3.9	35.51
τ max/ ΔT	0.51	0.141	0.198	0.140	1.163
$\Delta U/\Delta T$	8.618×10^{-6}	1.513×10^{-6}	1.011×10^{-6}	1.338×10^{-6}	4.911×10^{-6}

Systems (TDRSS) designs were analyzed. All calculations assumed a silicon cell and RTV adhesive material. The substrate material was either aluminum or Kapton as indicated in Table 3.2-1. The table also shows the remaining design parameters and the computed results.

The interconnector force is proportional to the gap displacement. Proposed Design I has the lowest gap displacement $\Delta U/\Delta T$. The displacement of FLTSATCOM design is about 8.5 times the displacement of Proposed Design I, while the displacement of TDRSS is about 1.4 times. The Proposed Design II is 1.3 times as large, while Proposed Design III is about 4.8 times. It is seen that the axial stresses σ_1 in the silicon cell and σ_2 in the substrate in the I and II designs are unaffected by the adhesive (RTV)

thickness. However, the shear stress τ in the adhesive in the II design is about 70 percent of the shear stress in the I design. It is concluded that Proposed Design I is the best candidate for the improved solar cell design since it causes the smallest interconnector force and therefore should result in the highest weld fatigue life. The slight increase in the adhesive shear stress τ -max compared to Proposed Design II is not critical. It is already considerably lower than the value for the FLTSATCOM design.

For service temperature deltas of 360°C and 280°C , the maximum stresses in the silicon cell, the substrate and the adhesive are:

	ΔT	
	280°C	360°C
σ_1 (mn/m^2)	6.8	8.7
σ_2 (mn/m^2)	6.8	8.7
τ (mn/m^2)	0.35	0.44

3.2.2.2 Stiffness of Interconnector

3.2.2.2.1 Simple Beam Theory. The solar cell interconnector must bridge the gap between two adjacent cells. The gap is deformed ΔU during a thermal cycle. In order to maintain the attachment, the interconnector is subjected to a separating force F which is proportional to the magnitude of ΔU times the stiffness of the interconnector. Thus, minimizing the interconnector stiffness will reduce the stresses in the welding joint between the interconnector and the solar cell and in the interconnector itself. Analytical solutions for the beam stiffness obtained by the simple beam theory are desirable for the dimensional or parametric studies. Various interconnector configurations were analyzed by the simple beam theory and the results are expressed in the following:

- a) Single Rectangular Loop Interconnector. The geometry of a single rectangular loop interconnector is shown in Figure 3.2-4. Due to symmetry, a quarter of the interconnector as shown in Figure 3.2-4 was analyzed and the flexibility (1/K) is:

$$\frac{1}{K} = \frac{\Delta U}{F} = \frac{2}{Et} \left(\frac{H}{W}\right)^3 \left[\frac{1 + \frac{1}{3}\alpha}{2 + \frac{1}{3}\alpha} \frac{2L}{H} \right]$$

$$\text{where } \alpha = \frac{W_2}{W}$$

E = elastic modulus of interconnector material

t = thickness of interconnector

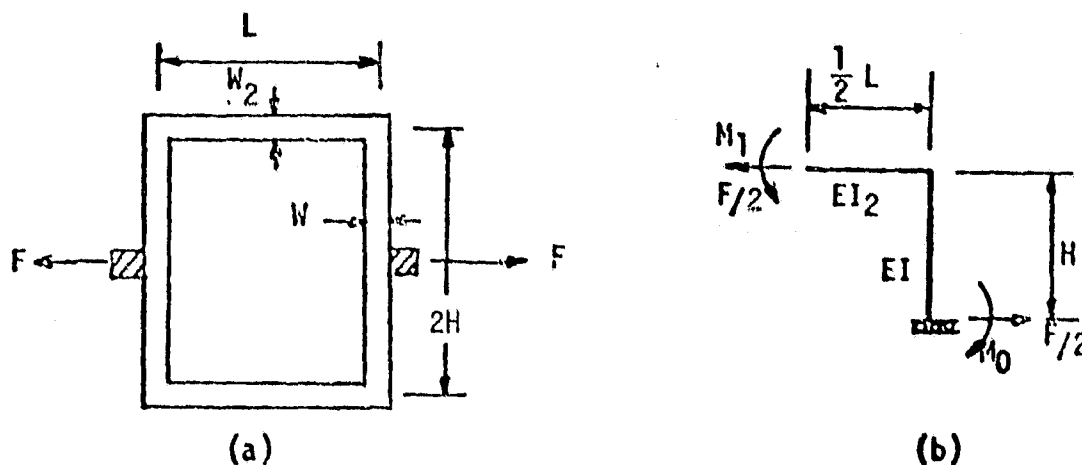


Figure 3.2-4. Single Loop Rectangular Interconnector

- b) Rectangular Wave Interconnector. A half wave length of a rectangular wave interconnector shown in Figure 3.2-5 was analyzed. The result is:

$$\frac{\Delta U}{FL} = \frac{1}{EtW} \left[12 \left(\frac{H}{W}\right)^2 \left(1 + \frac{2}{3} \left(\frac{H}{L}\right) \right) + 1 \right]$$

For a square wave interconnector, $L = 2H$

$$\frac{\Delta U}{F(2H)} = \frac{1}{EtW} \left[16 \left(\frac{H}{W}\right)^2 + 1 \right]$$

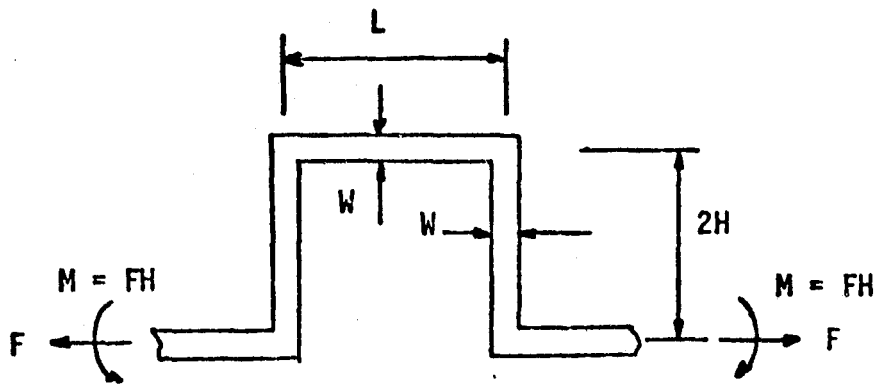


Figure 3.2-5. Rectangular Wave Interconnector

- c) Single Loop with Full Radius Interconnector. The geometry is shown in Figure 3.2-6, and the result is

$$\frac{\Delta U}{F} = \frac{J_2}{Et} \left(\frac{H}{W} \right)^3 f(\alpha)$$

where

$$f(\alpha) = \frac{\left(\frac{\pi}{16} - \frac{1}{28} \right) \alpha^4 + \frac{\pi}{8} \alpha^3 (1-\alpha) + \frac{1}{2} \alpha^2 (1-\alpha)^2 + \frac{\pi}{12} \alpha (1-\alpha)^3 + \frac{1}{24} (1-\alpha)^4}{1 + \left(\frac{\pi}{2} - 1 \right) \alpha}$$

$$\alpha = \frac{R}{H}$$

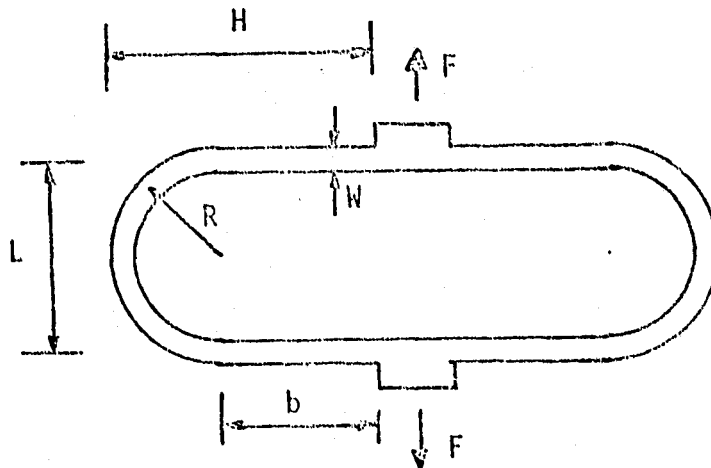


Figure 3.2-6. Single Loop with Full Radius Interconnector

The above analytical solutions were used for the choice interconnector dimensions such as W and H based on the optimized electric resistance versus stress relief ratio, Reference 2.

3.2.2.2.2 Finite Element Analyses. Three proposed design configurations: (1) single loop (A_{NS}), (2) double loop (B_{NS}), and (3) parallel type (C_{NP}) interconnectors were analyzed by use of the SAP4 finite element computer program. The powerful isoparametric membrane element was employed to calculate the stiffness. The interconnector was assumed fabricated from 1-mil Invar with two 0.4-mil layers of silver.

SAP4 finite element mathematical models of the three design configurations were constructed. The thick line mesh lines of Figures 3.2-7 through 3.2-9 show the geometries of the three models.

In order to compute the stiffness and deformation shapes of the design configurations subjected to thermal loading, two separate deformation loading cases were imposed on the model. The analysis of each design is described in the following:

- a) Single Loop Design (A_{NS}). Due to symmetry, only one half of the interconnector was modelled and is shown in Figures 3.2-7a and 3.2-7b (thick lines). Sections A-A and B-B are weld attachments to the cells, while Section C-C is the plane of symmetry.

The first loading case applied a 1-mil displacement at section A-A in Z direction with section B-B fixed. The deformation mesh is shown in Figure 3.2-7a (thin line). The computed force required to cause the 1-mil displacement at section A-A in Z direction is 0.275 pound. Hence, the stiffness of the system in Z direction is 275 lb/in. From the simple beam theory analysis, the stiffness is 291 lb/in.

The second loading case applied a 1-mil displacement at the symmetrical section C-C in the Y direction with both A-A and B-B sections fixed. The deformation mesh (thin line) is shown in Figure 3.2-7b. The SAP4 results showed that 51 percent of the displacement occurred in the right half vertical loop. The required force to cause the 1-mil displacement is 2.726 pounds and the system stiffness in Y direction is 2726 lb/in.

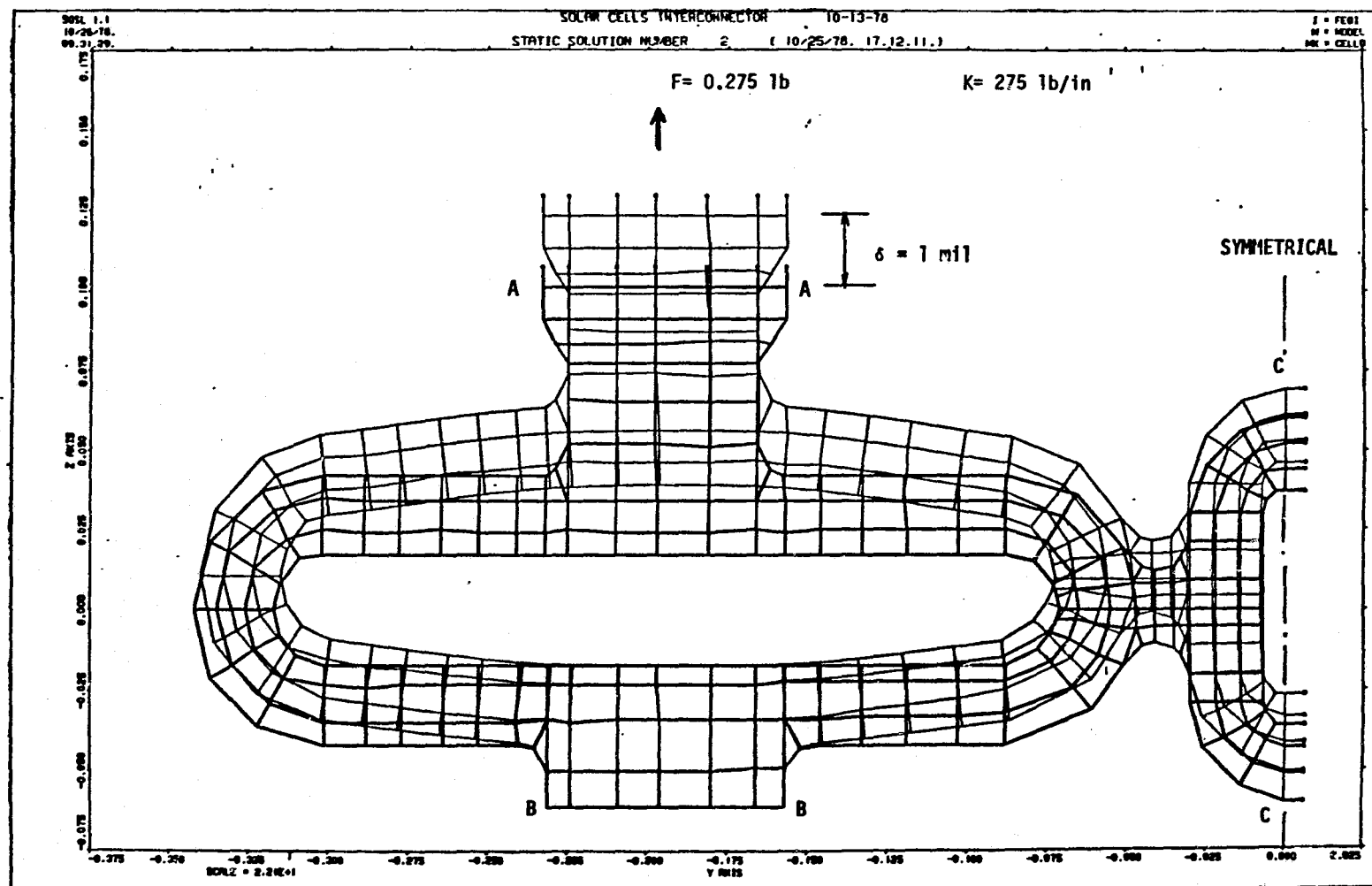


Figure 3.2-7a. Finite Element Undeformed and Deformed Mesh of a Single Loop Interconnector for 1-mil Z Displacement Applied at Section A-A

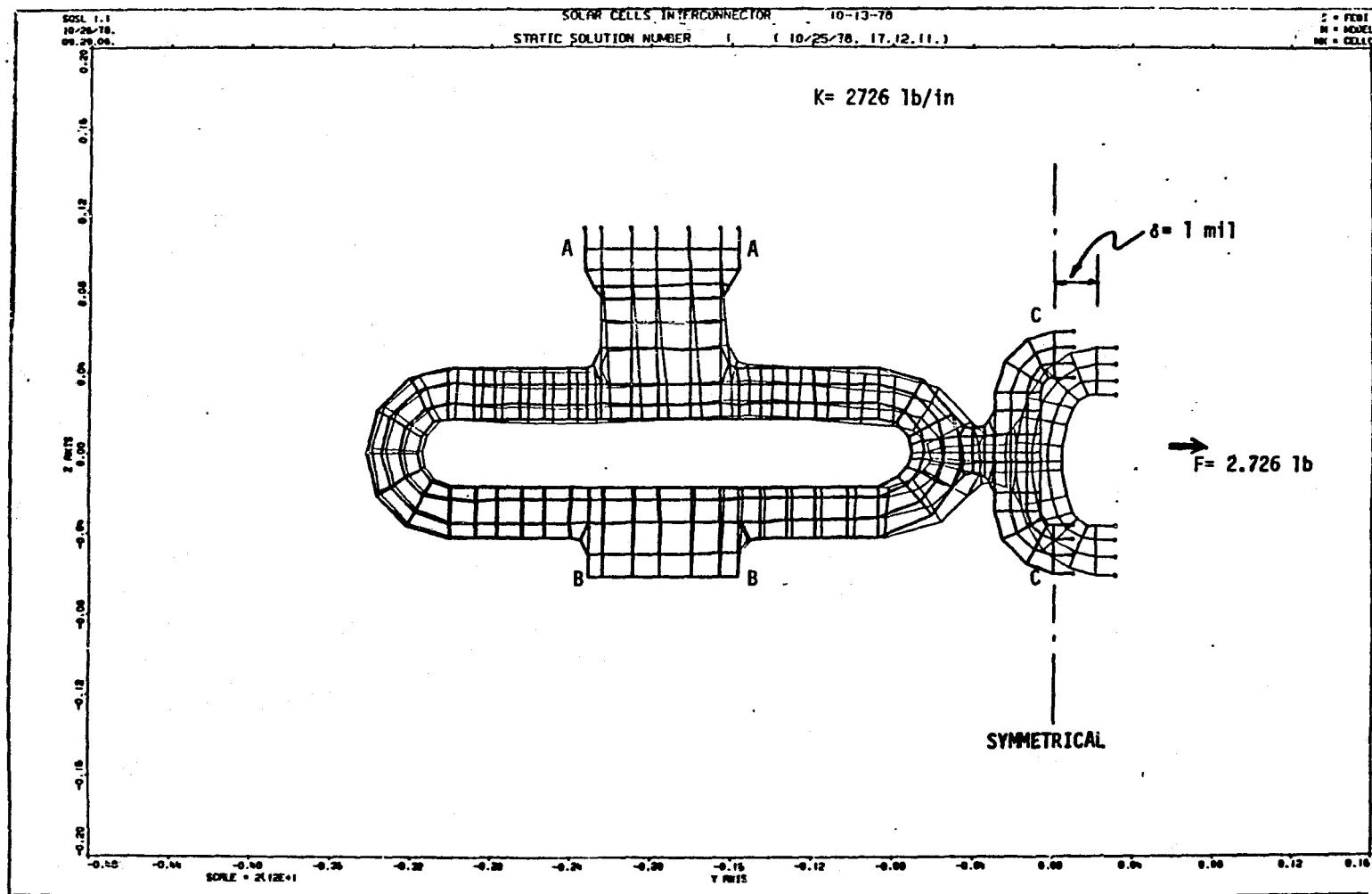


Figure 3.2-7b. Finite Element Undeformed and Deformed Mesh of a Single Loop Interconnector for 1-mil Y Displacement Applied at Section C-C

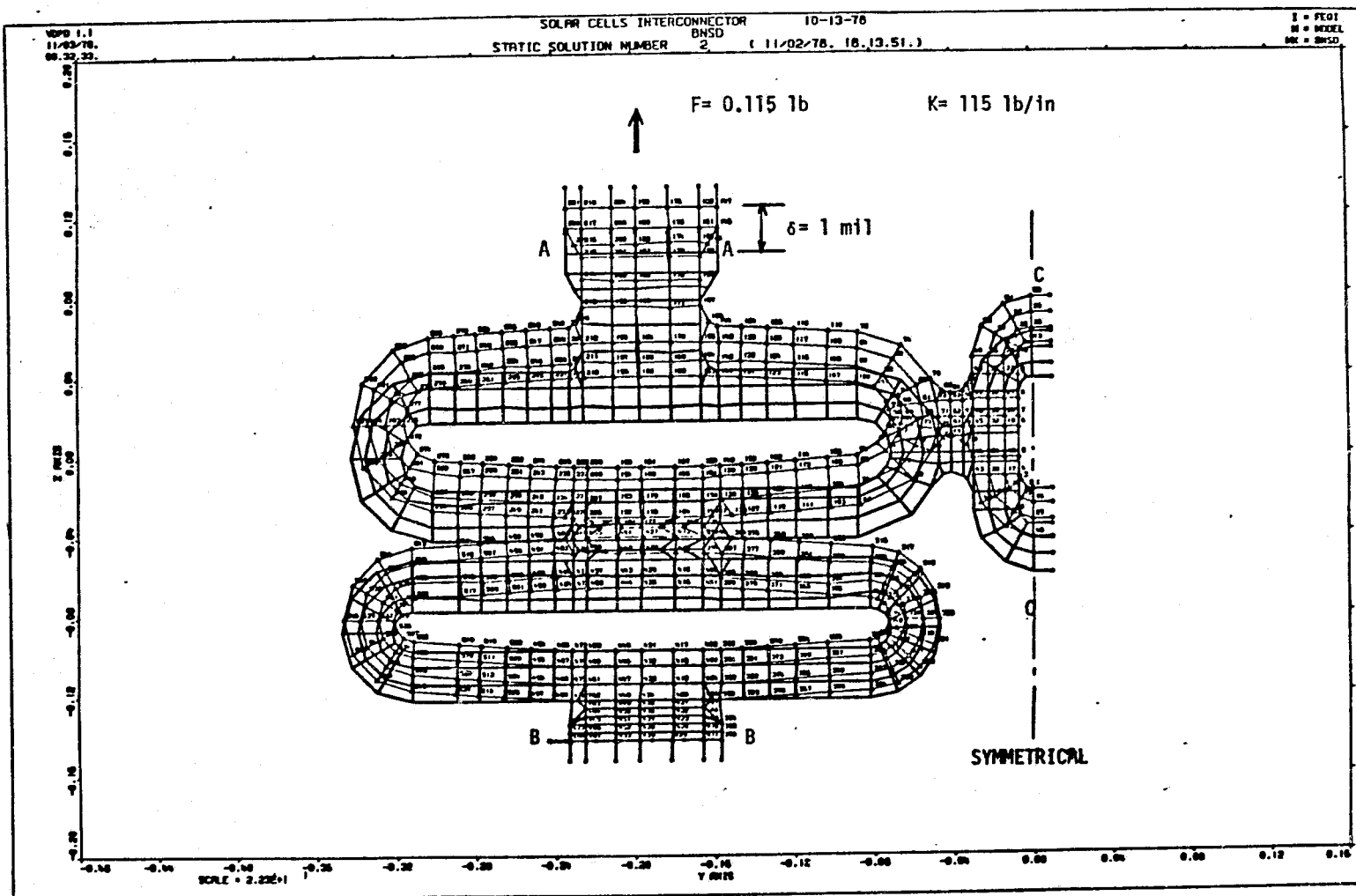


Figure 3.2-8a. Finite Element Undeformed and Deformed Mesh of a Double Loop Interconnector for 1-mil Z Displacement Applied at Section A-A

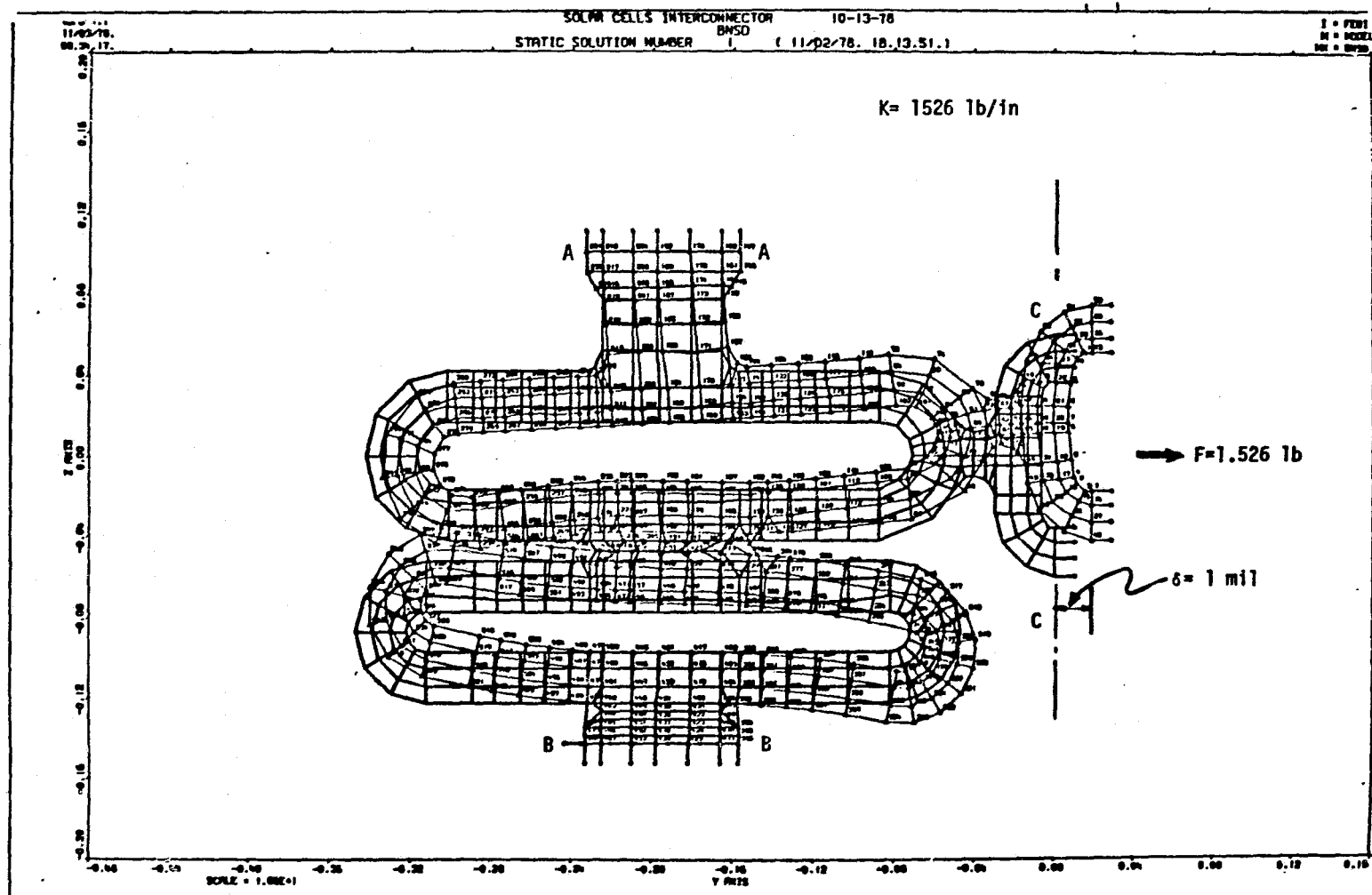


Figure 3.2-8b. Finite Element Undeformed and Deformed Mesh of a Double Loop Interconnector for 1-mil Y Displacement Applied at Section C-C

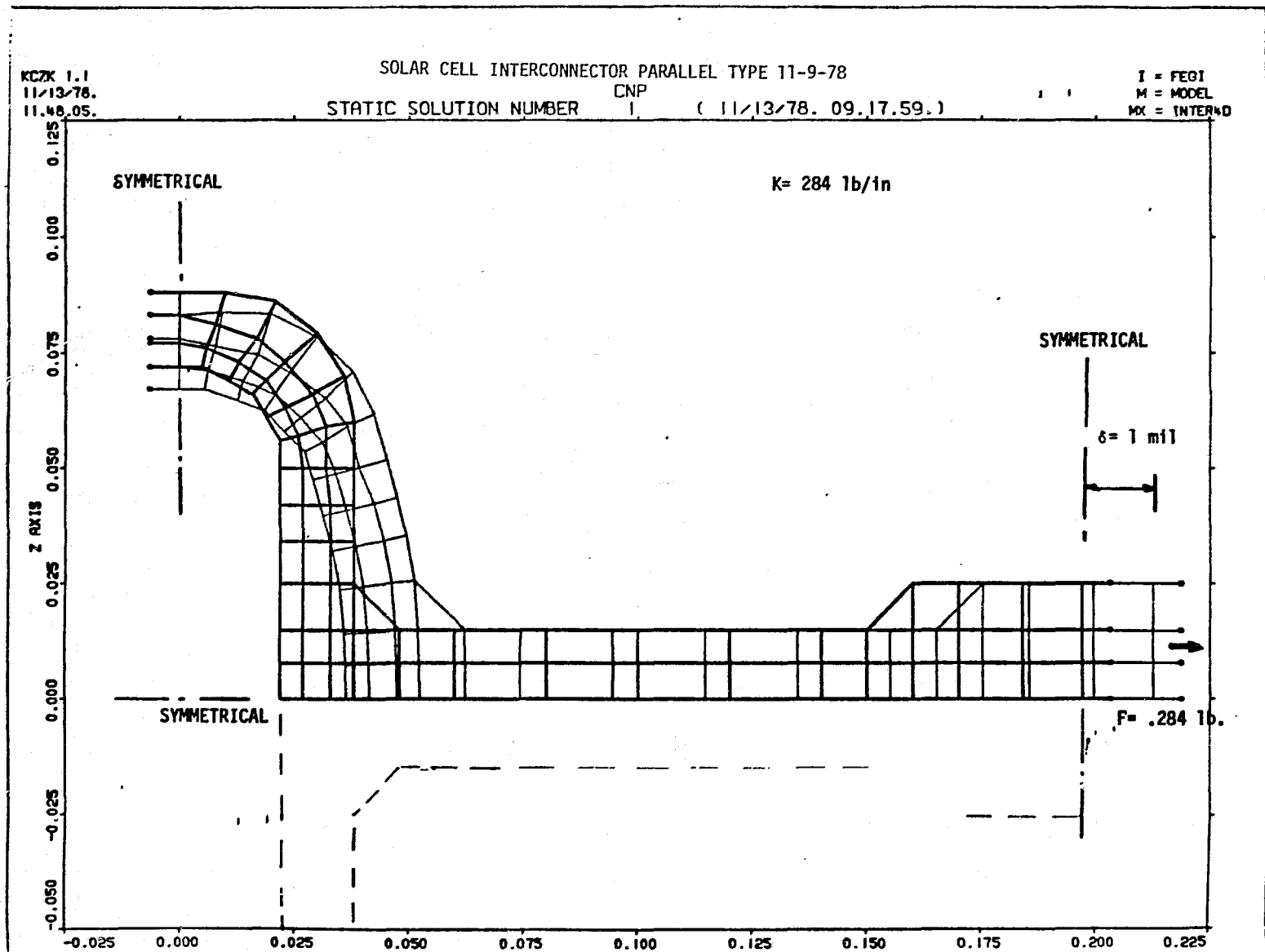


Figure 3.2-9. Finite Element Deformed and Undeformed Mesh of a Parallel Type Interconnector for 1-mil Y Displacement Applied at Section C-C

- b) Double Loop Design (B_{NC}). Similar to the analysis of the single loop design, only one half of the double loop interconnector was considered. The mesh geometry (thick line) is shown in Figures 3.2-8a and 3.2-8b. Sections A-A, B-B, and C-C have the same definition as for the above case. The same two types of loading were applied. The deformed shape (thin line) for the displacements in the Z and Y directions are shown in Figures 3.2-8a and 3.2-8b, respectively. The stiffness of the system in Z and Y directions are 115 lb/in and 1526 lb/in, respectively. For this configuration, the right hand vertical loop provided only 27 percent of the total Y displacement. Thus, elimination of the loop would increase the Y stiffness to 2090 lb/in. The stiffness of the system in Z direction obtained by the simple beam theory is 149 lb/in.
- c) Parallel Type Design (C_{NP}). Due to symmetry, a quarter of a unit of a parallel type interconnector was modelled and shown in Figure 3.2-9 (thick line). One loading case was considered. A 1-mil displacement was applied to the symmetrical section C-C in the Y direction. The deformation mesh is shown in Figure 3.2-9 (thin line). The required force to cause the 1-mil Y displacement is 0.284 pound. Hence, the stiffness of the system in Y direction is 284 lb/in. From the beam analysis the value of the stiffness is bounded by 234 lb/in and 369 lb/in.

The results obtained by the execution of SAP4 finite element computer program are in good agreement with equations based on the simple beam theory. However, in applying the beam theory equations, the thickened sections adjacent to the weld must be treated as being infinitely stiff.

3.2.2.3 Fatigue Life Analysis

The fatigue life of the welded joint between the interconnector and cell is affected by the forces applied to the weld by the interconnector. To decrease the force it is necessary either to reduce the gap displacement ΔU or the stiffness of the interconnector. The lowest ΔU of the Proposed Design I of the solar cell assembly was of interest. From Table 3.2-1, ΔU is 1.01×10^{-6} in/ $^{\circ}\text{F}$. Hence, for a service temperature range $\Delta T = 360^{\circ}\text{C}$ (180 to -180°C) (648 $^{\circ}\text{F}$), the total displacement amplitude between the cell is

$$1.01 \times 10^{-6} \times 648 = 6.54 \times 10^{-4} \text{ (in.)}$$

Over the same temperature range the thermal change in length of the Invar interconnector is

$$\Delta T \alpha L$$

Thus, the changes in interconnector length for three designs are:

$$\begin{array}{lll}
 A_{NS} & 0.163 & 0.90 \times 10^{-4} \text{ (in.)} \\
 B_{NS} & 648 \times 0.85 \times 10^{-6} \times 0.234 = & 1.29 \times 10^{-4} \text{ (in.)} \\
 C_{NP} & 0.320 & 1.76 \times 10^{-4} \text{ (in.)}
 \end{array}$$

Neglecting the flexibilities of the cell and substrate combination, the interconnectors have to accommodate displacement of (for each design)

$$\begin{array}{lll}
 A_{NS} & 0.90 \times 10^{-4} & 5.64 \times 10^{-4} \text{ (in.)} \\
 B_{NS} & 6.54 \times 10^{-4} - 1.29 \times 10^{-4} = & 5.25 \times 10^{-4} \text{ (in.)} \\
 C_{NP} & 1.76 \times 10^{-4} & 4.78 \times 10^{-4} \text{ (in.)}
 \end{array}$$

$$\Delta T = 180^{\circ}\text{C} - (-180^{\circ}\text{C}) = 360^{\circ}\text{C} \text{ (648}^{\circ}\text{F)}$$

The values of axial loads of interconnectors are obtained from the products of the stiffnesses of each interconnector design and the relative thermal displacement between welded joints of adjacent cells. Thus:

$$F = K\Delta U$$

$$\begin{array}{lll}
 A_{NS} & 275 \times 5.64 \times 10^{-4} = 0.155 \text{ (lb)} & 0.690 \text{ (N)} \\
 B_{NS} & 115 \times 5.25 \times 10^{-4} = 0.060 \text{ (lb)} & 0.269 \text{ (N)} \\
 C_{NP} & 284 \times 4.78 \times 10^{-4} = 0.36 \text{ (lb)} & 0.604 \text{ (N)}
 \end{array}$$

It was assumed that there were two weld spots at each end of the interconnector; hence, each welding spot was subjected to one half of axial force in the interconnector

$$\begin{array}{ll}
 A_{NS} & 0.345 \text{ (N)} \\
 B_{NS} & 0.134 \text{ (N)} \\
 C_{NP} & 0.302 \text{ (N)}
 \end{array}$$

Similar calculations were performed for a service temperature range

$$\Delta T = 280^{\circ}\text{C} \text{ (-180 to } 100^{\circ}\text{C) (504}^{\circ}\text{F)}$$

The total gap displacements between the cells are

$$1.01 \times 10^{-6} \times 504 = 5.09 \times 10^{-4} \text{ (in.)}$$

The interconnector thermal elongations are

$$\begin{array}{llll}
 A_{NS} & & 0.163 & 0.698 \times 10^{-4} \text{ (in.)} \\
 B_{NS} & 504 \times 0.85 \times 10^{-6} \times & 0.234 & = 1.002 \times 10^{-4} \text{ (in.)} \\
 C_{NP} & & 0.320 & 1.371 \times 10^{-4} \text{ (in.)}
 \end{array}$$

Thus, the net displacements are

$$\begin{array}{llll}
 A_{NS} & & 0.698 \times 10^{-4} & 4.39 \times 10^{-4} \text{ (in.)} \\
 B_{NS} & 5.09 \times 10^{-4} & - 1.002 \times 10^{-4} & = 4.09 \times 10^{-4} \text{ (in.)} \\
 C_{NP} & & 1.371 \times 10^{-4} & 3.72 \times 10^{-4} \text{ (in.)}
 \end{array}$$

and the axial forces are

$$\begin{array}{ll}
 A_{NS} & 275 \times 4.39 \times 10^{-4} = 0.121 \text{ (lb)} \\
 B_{NS} & 115 \times 4.09 \times 10^{-4} = 0.047 \text{ (lb)} \\
 C_{NP} & 284 \times 3.72 \times 10^{-4} = 0.106 \text{ (lb)}
 \end{array}$$

For each welding spot

$$\begin{array}{lll}
 A_{NS} & 0.0605 & 0.269 \text{ (N)} \\
 B_{NS} & 0.0235 \text{ (lb)} = & 0.105 \text{ (N)} \\
 C_{NP} & 0.0503 & 0.224 \text{ (N)}
 \end{array}$$

The fatigue life of welded joints subjected to different interconnector forces and over different temperature ranges had been studied in Reference 4. In Reference 4, the interconnector is constructed of 15- μ m-thick Invar with two 5- μ m layers of silver plating while the silicon cell thickness is assumed to be 254 μ m with 3- μ m silver-plating. The analyses used the SAAS III computer program. The total effective strains $\Delta\epsilon^{-t}$ in the silver were obtained as a function of the temperature ranges for various axial loads. These data were shown in Figure 3.2-10 and extrapolated to the temperature range of 400°C. The total effective strain of silver at the weld joint over temperature ranges of $\Delta T = 280^\circ\text{C}$ and $\Delta T = 369^\circ\text{C}$ was computed for each interconnector design configuration from Figure 3.2-7. These values of the effective strain ranges were then plotted on Manson's empirical curve for the fatigue life of silver.

$$\Delta\epsilon^{-t} = 0.00903 N_f^{-0.12} + 0.770 N_f^{-0.6}$$

to obtain the fatigue life N_f (cycles to failure) in Figure 3.2-11. Figure 3.2-11 also shows the fatigue lives of the weld joint without the interconnector (zero axial force). The results are tabulated in the following:

Fatigue Life N_f (Cycles to Failure)		
	$\Delta T = 280^{\circ}\text{C}$	$\Delta T = 360^{\circ}\text{C}$
Weld Alone	3000	1600
A_{NS}	1700	900
B_{NS}	2400	1300
C_{NP}	2000	1250

For both temperature ranges the life of the single loop configuration is 56 percent of the life of the weld joint without the interconnector, while the life of the double loop configuration is 80 percent and the life of the parallel loop is about 63 percent.

3.2.2.4 Discussion of the Results

The fatigue lives of the weld joint obtained in the previous section were based on the curves shown in Reference 4. It should be noted that the present solar cell assemblies design have dimensions which are somewhat different from those of Reference 4. In Reference 4, the Invar interconnector silver plating thickness was $5\text{ }\mu\text{m}$, and the solar cell silver-plating thickness was $3\text{ }\mu\text{m}$; while in the present investigation, the Invar interconnector silver plating thickness is $10\text{ }\mu\text{m}$ (0.4 mil), and the solar cell silver-plating thickness is $7.6\text{ }\mu\text{m}$ (0.3 mil).

Reference 5 studied the effects of silver-plating thickness on the fatigue life of the weld joints alone without the interconnector. It concluded that reducing the silver-plating thickness on a Kovar interconnector from $5\text{ }\mu\text{m}$ to $3\text{ }\mu\text{m}$ reduced the maximum strain in the weld area and therefore increased the fatigue life by 31 percent (for an Invar interconnector this value would be larger); while increasing the solar cell silver-plating thickness from $3\text{ }\mu\text{m}$ to $10\text{ }\mu\text{m}$ increased the fatigue life by 80 percent. Thus, it is advantageous with respect to the weld joint fatigue life to decrease the interconnector silver-plating thickness and to increase the solar cell plating thickness.

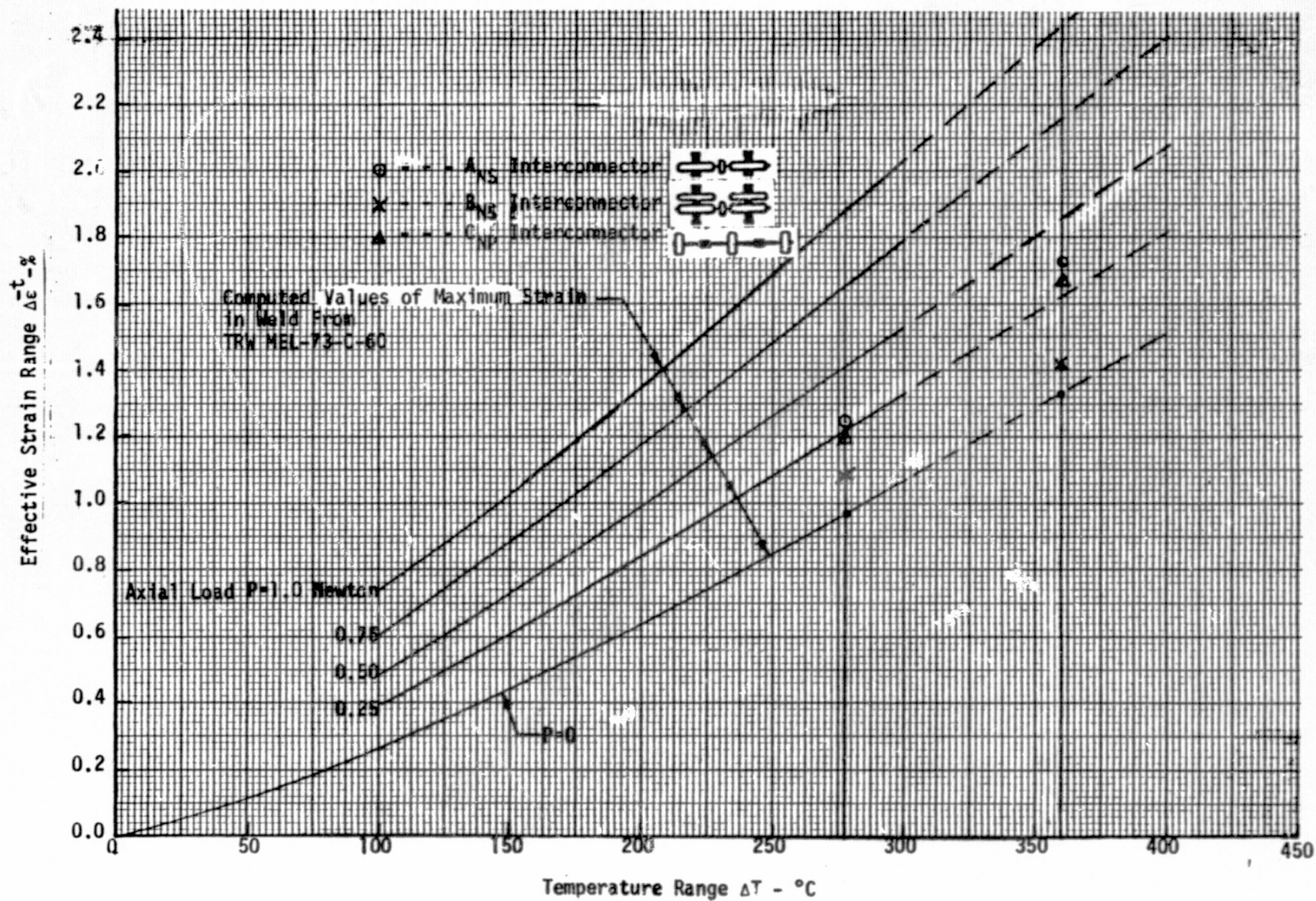


Figure 3.2-10. Maximum Effective Strain as Function of Temperature Range ΔT for Welds Loaded by Various Axial Loads P

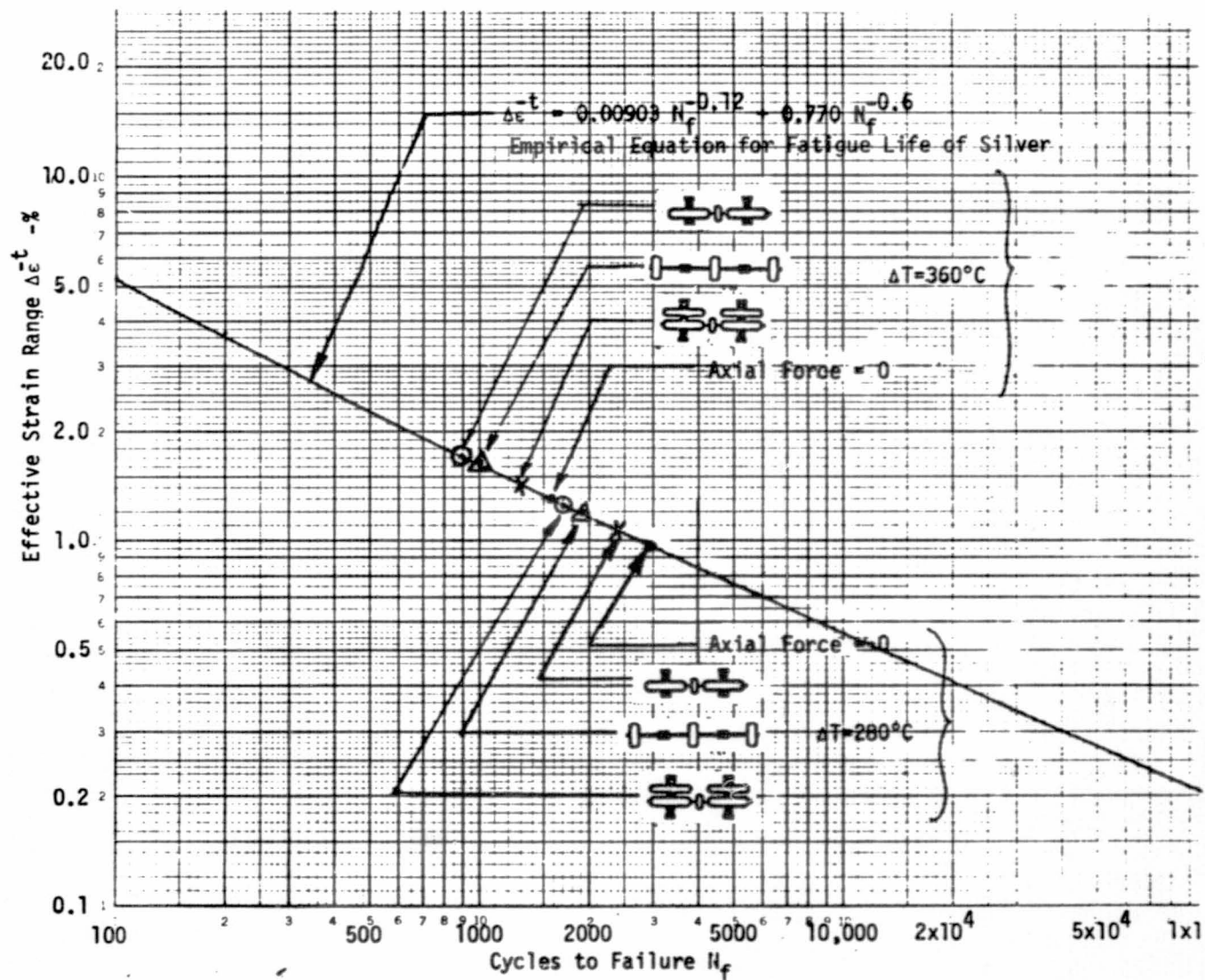


Figure 3.2-11. Computed Fatigue Lives for A_{NS} , B_{NS} and C_{NP} Interconnector Design Configurations

Using the results of Reference 5 (which were made for Kovar not Invar) the fatigue life for weld joint alone obtained in the previous section would be reduced 78 percent due to the increase in the interconnector silver plating thickness from 5 μm to 10 μm and increased 53 percent due to the increase in the solar cell silver-plating thickness from 3 μm to 7.6 μm . Thus, the effects tend to cancel out.

No detailed analysis has been made of the influence of the plating thickness on the reduction of the fatigue life due to the interconnector force. However, it is expected that increasing the thickness would tend to increase the fatigue life since it would increase the thermal coefficient of expansion to more closely approach that of the substrate and therefore reduce the interconnector force.

The computed fatigue lives are unrealistically low compared to results obtained from experimental measurement (Reference 4). As discussed in Reference 4, there are several probable reasons for this variation, the most important of which involves the definition of failure. For the mechanically loaded specimens upon which Manson's empirical curve is based, failure occurred soon after a crack developed. This resulted from the rapid increase in the local stress level once the crack developed. However, for the weld considered here, there is initially a built-in "crack" at the edge of the weld. Thus, failure in this case is measure of the time required for the weld crack to start growing and not the time at which the crack grows completely through the weld. Therefore, the useable life of the weld is underestimated. This factor, as well as the silver-plating thickness effects, apply to all three interconnector design configurations. However, it is expected that although the predicted lives are too conservative, the quantitative variation among these proposed designs will be accurate.

3.3 EXPLORATORY PARALLEL/GAP - WELDING

Although in the actual assembly of these test coupons other factors had greater impact on yield, a great deal of preliminary work had to be done in order to develop a technique for employing parallel-gap resistance welding as the interconnecting method.

3.3.1 Equipment Description

The welding equipment used in this effort consisted of a Model MCW-550 constant voltage power supply and a Model VTA-66 variable tip weld head, both manufactured by Hughes Aircraft Company. A constant voltage is maintained at the weld electrodes by varying the current during the weld cycle to compensate for variations in resistance occurring in or across the weld. Voltage is regulated to within 25 mV for any dial adjustment over the typical weld voltage range from 0.5 volt to 1.0 volt. The power supply compensates for load changes in less than 100 microseconds during the weld duration. Equipment repeatability was excellent.

Although the weld voltage is held constant, weld current varies from one weld to the next. This variation results from differences in cell and interconnect silver-plating thickness and is also a function of weld electrode tip cleanliness. TRW has previously developed nondestructive test (NDT) equipment which monitors the time integrated weld current. Time integrated weld current values are displayed on a digital voltmeter. Readings below a previously specified limit trigger a red light directing the operator to clean the electrodes using an aluminum oxide chip.

The weld electrodes are made of molybdenum. Two electrode sizes are used; 0.38 by 0.64 mm (0.015 by 0.025 inch) for the cell front contact and 0.64 and 1.14 mm (0.025 by 0.045 inch) for the cell rear contact.

A specially modified Unitek Model 6-092-03 pull tester was used to measure the shear strength of weld joints rather than performing a conventional pull test at a 45° angle, because the fragile thin cell would have failed prior to the weld joint failure at that angle. The modification decreased the pull rate from 6 sec/cm (15 sec/inch) to 12 sec/cm (30 sec/inch) and allowed weld joint shear strengths to be measured without having to bond each cell to a rigid substrate.

The objective was to demonstrate that acceptable welds could be made to thin solar cells. It was arbitrarily decided to classify a weld as acceptable if the weld strength measured in shear was equal to or greater than 300 grams.

3.3.2 Preliminary Welding Study

During the preliminary experimental work with the thin cell it soon became clear that the weld parameters previously used for thicker solar cells were not appropriate for thin cells.

For this reason the maximum weld parameters were defined experimentally and some ground rules were established early in the program. For example, cell electrical degradation due to front contact welding was not to exceed 1 percent. (Electrical degradation generally occurs when the top or junction contact is welded. Because of the proximity of the junction, partial electrical shorting results.) Cell fracturing was encountered when the weld electrode pressure exceeded 2 kg; thus, 2 kg of pressure was identified as the upper limit during the systematic weld parameter evaluation that followed the preliminary study.

Excessive cell cracking was experienced with standard size 0.38 by 0.64 mm (0.015 x 0.025 inch) weld electrodes when welding to rear cell contacts of thin glassed solar cells. This cracking, or puncturing, resulted because the thin cell was supported only by a comparatively soft adhesive layer underneath the thin cell. This problem was overcome by increasing the electrode imprint size by a factor of three to 0.64 by 1.14 mm (0.025 by 0.045 inch).

3.3.3 Optimizing Weld Parameters

The preliminary study was followed by a systematic investigation of all weld parameters, such as the weld voltage; duration; pressure; and the related nondestructive test (NDT) data; consisting of the time integrated weld current, $\int i dt$.

3.3.3.1 Cell Front Contact

The results are shown in Figures 3.3-1 through 3.3-4 with each data point representing the average of three weld joints made and pull tested. Figure 3.3-1 shows the joint pull strength measured as a function of

WELD TIME: 100 ms

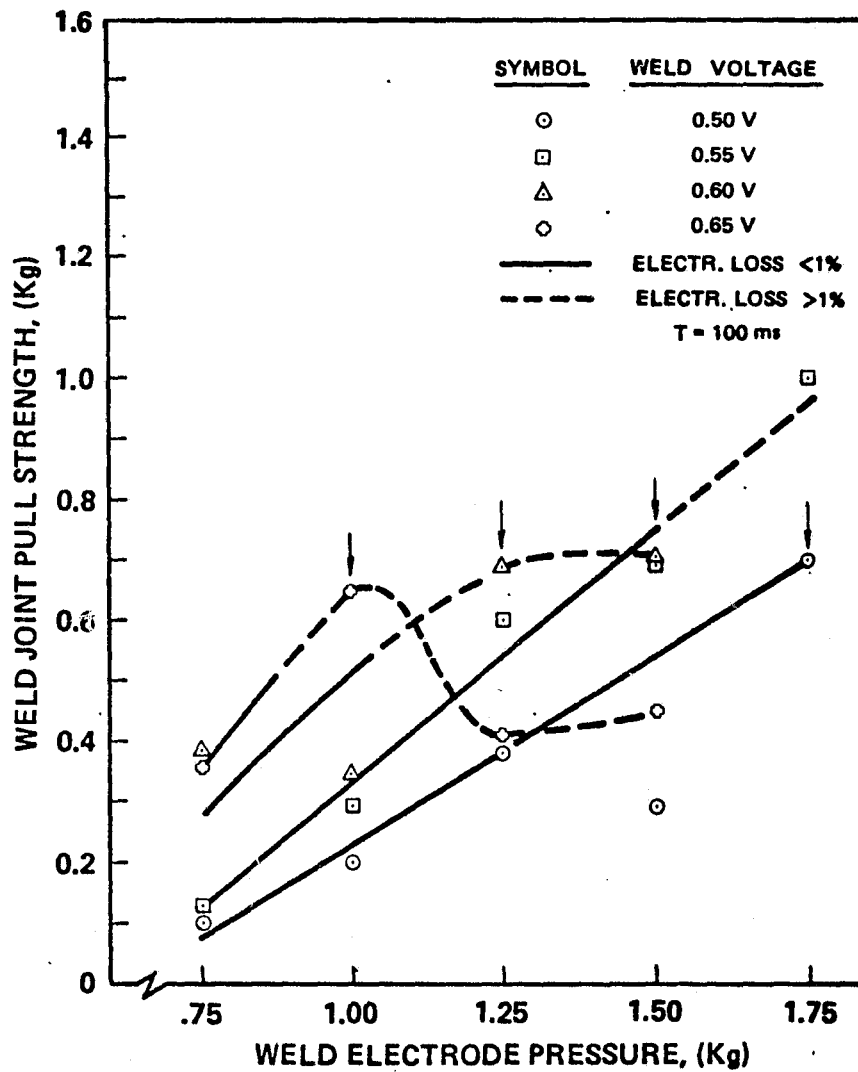


Figure 3.3-1. Front Cell Contact Weld Joint Pull Strength as a Function of Weld Electrode pressure for Various Weld Voltages

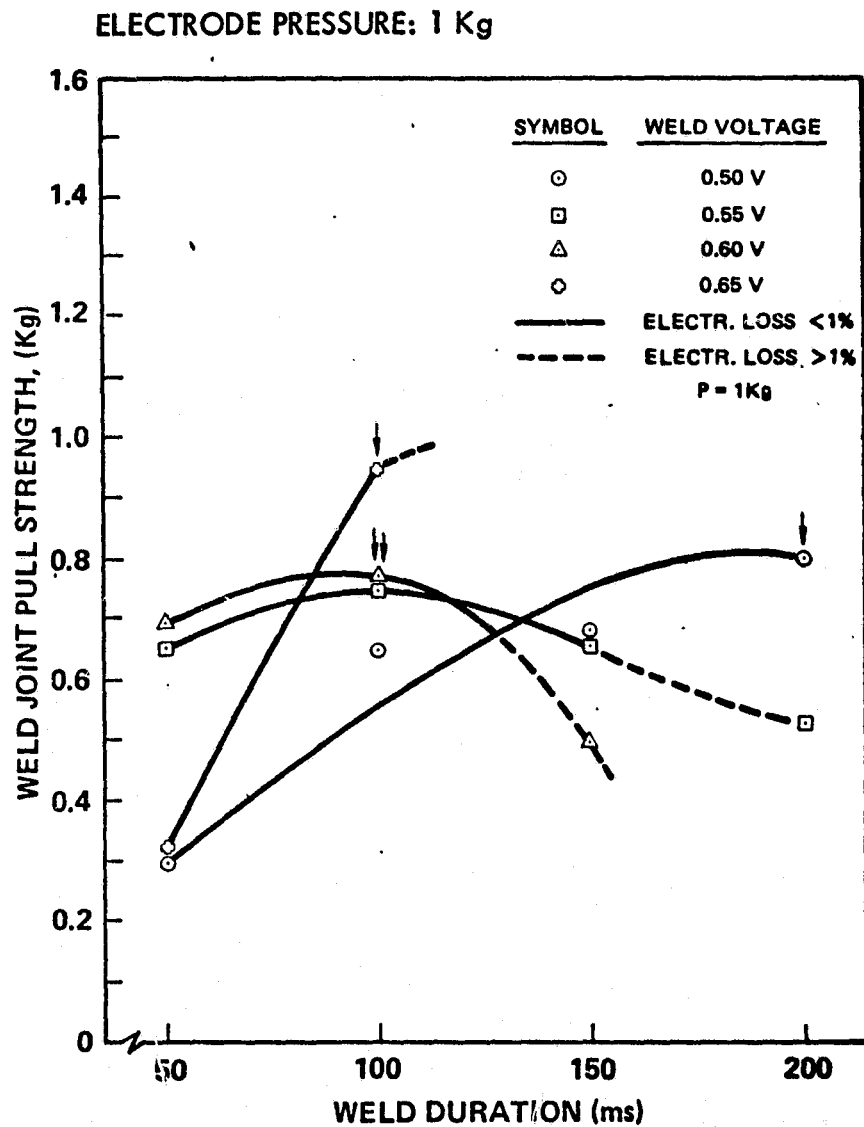


Figure 3.3-2. Front Cell Contact Weld Joint Pull Strength as a Function of Weld Duration for Various Weld Voltages

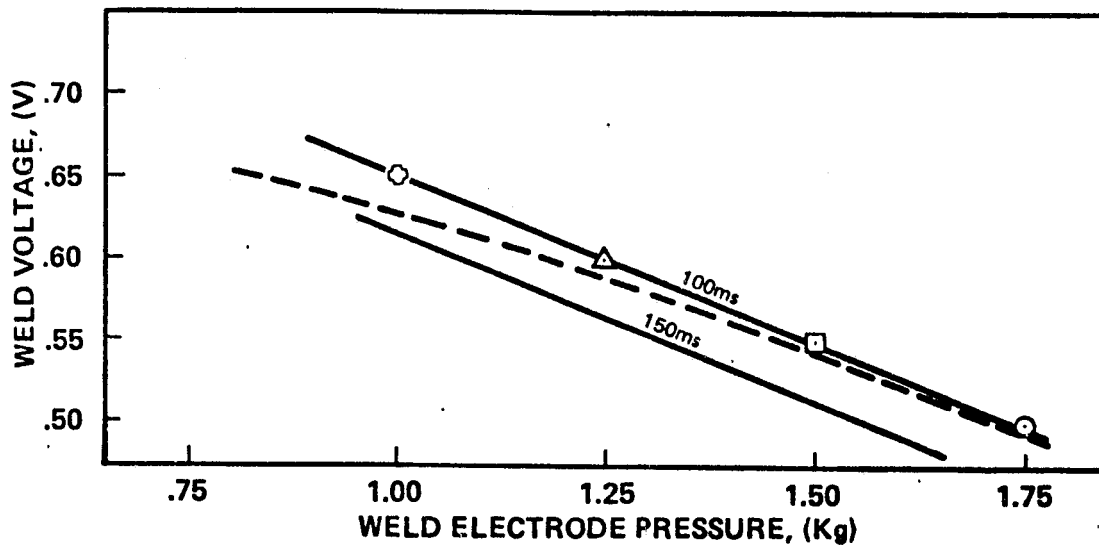


Figure 3.3-3. Optimum Weld Joint for Weld Voltage and Pressure Relationship, as Observed in Figure 3.3-1. Electrical Performance Loss $\geq 1\%$ Above Dotted Line

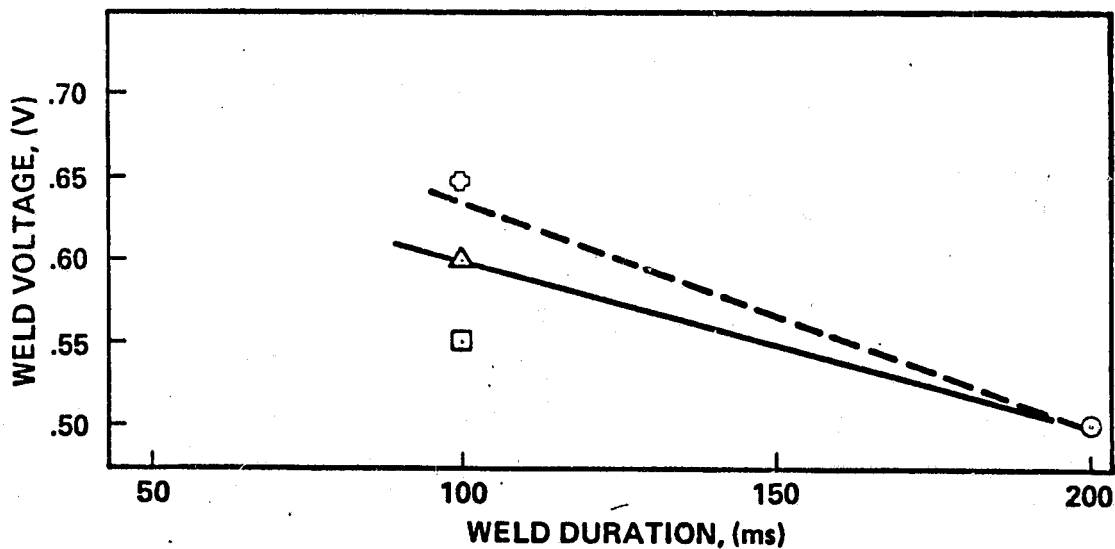


Figure 3.3-4. Optimum Weld Joint for Voltage and Weld Duration Relationship as Observed in Figure 3.3-2. Weld pressure: 1 kg. Electrical Performance Loss $\geq 1\%$ Above Dotted Line

electrode pressure for four weld voltages. Figure 3.3-2 shows the joint pull strength as a function of weld duration for the same weld voltages using a different group of solar cells.

It is suspected that the upper limit in joint pull strength for the various weld voltages may be caused by silicon fracturing due to a combination of excessive voltage (heat) and pressure impinging upon the silicon below the weld joint area.

Figures 3.3-3 and 3.3-4 were generated from the optimum joint pull strength data (as identified [↑] in Figures 3.3-1 and 3.3-2), in order to show the weld voltage as a function of weld electrode pressure and weld duration, respectively.

The region slightly below the solid line in these figures represents acceptable weld joints with pull strengths of ~750 g. The region above the dotted line represents the area where cell electrical degradation will be >1 percent. The weld strength of the front contact appears to be limited by the yield strength of the thin silicon since all welds ultimately failed due to cell breakage (with weld still intact) somewhere between 0.7 and 0.8 kg. This failure mode could also result from excessive heat and pressure developed in the silicon pad area.

Eight solar cell samples were submitted to the Materials and Processes Department for microsectioning. Fifty percent of the cells had interconnectors welded to the front side, and the remaining had interconnectors welded to the rear cell side. All weld joints were made with different weld schedules. Unfortunately, most of these samples were damaged during sample mounting, and could not serve for microsectioning. Improved mounting methods were developed and then employed on the second group of thin cells. The weld parameters were picked from the data summarized in Figures 3.3-1 through 3.3-4, selecting weld schedules above and below the threshold level where cell fracturing is expected to occur. All weld joint cross-sectioning is made approximately at the center of the weld joint depicting the imprint of the two weld electrodes and the 0.006-inch gap between them; thus, only a two-dimensional cross-section is presented. Additional lapping of the specimens weld joints No. 45 and No. 50 indicate some shifting of the bonded or welded area showing silver-to-silver bonds in the range of 0 to 80 percent, depending on the location of the cross-section. A good

weld joint, bonding a silver-plated Invar interconnector to a thin solar cell is shown in Figure 3.3-10 (joint No. 52). Some of the silver rear cell contact has separated from this and other cells as well, due to poor adhesion to the silicon. The evaluation of front contact weld joint micro-sectioning is summarized in Table 3.3-1. Cell fracturing was expected earlier and was partially confirmed in joints No. 44, 48, and 49; although joints No. 51 and 52 were an exception and remained intact. On the other hand joints No. 42 and 46 should not have fractured. Cell fracturing is predominantly seen below the weld joints, which has become the weakest link along the cell's edge after welding. It is difficult to assess the true cause of the fracture because the cells are subjected to handling after welding which includes cutting of the interconnector tab, (the part that overhangs the cell), cell potting, silicon carbide grinding (320, 400 and 600 grid) and polishing on nylon cloth using 1-micron alumina paste.



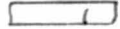
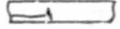
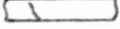



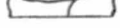





As one examines weld joints No. 41, and 52 in Figures 3.5-5, and 3.3-10, respectively, a certain waviness can be seen in the silicon, particularly when a clear straight edge is placed along the 200X magnification view. It is evident that the high spots, (up to 0.0002 inch) show better weld jointing than the low spots. In most of the low spot areas either some or no evidence of welding is found.

This waviness, or cratering, in the silicon is more clearly illustrated in Figure 3.3-11 where three views of the same cell contact and surrounding cell area are shown. View A shows the cell contact area after a welded interconnector is peeled off. The light circles show the peeled silver contact area. Only the upper-crater ridges were contacted and no welding is seen in the crater valleys. Views B and C show the same cell contact in more inclined angles to illustrate the cratering effect which is most likely caused by the chemical polishing of the silicon prior to cell diffusion.

3.3.3.2 Cell Rear Contact

A similar systematic investigation was made for the rear cell contact of glassed thin solar cells. The larger electrode used for the rear welds consistently yielded higher pull strength values from 0.8 to 1.2 kg as shown in Figures 3.3-12 and 3.3-13. The weld strength of the rear contact again appears to be limited by the yield strength of the thin silicon.

Table 3.3-1. Evaluation of Front Weld Joint Microsectioning

WELD JOINT NO.	MOUNT NO.	FIGURE NO.	WELD JOINT BOND AREA(%) [CROSS SECTION]		CELL FRACTURE	SEPARATED OR LIFTED SILVER PLATING		WELD SCHEDULE			ELECTRODE FOOT PRINT	SILVER MELTING BETWEEN ELECTRODES
			Left	Right		Front	Rear	P (Kg)	T (ms)	E (V)		
41	5	5	28	20		X		1.0	100	.57	Faint	
42	5	6	30	40		X		1.0	100	.60	Good	
43	6	7	10	45				1.0	100	.63	Good	
*44	6	8	80	90			X	1.0	100	.66	Heavy	X
45	7	9	0	0				1.0	150	.57	Heavy	
45a	7	10	80	70				1.0	150	.60	Heavy	
46	7	11	60	65				1.0	150	.60	Heavy	X
47	8	12	40	15				1.5	100	.53	Faint	
*48	8	13	0	30				1.5	100	.56	Faint	
*49	9	14	0	0		X	X	1.5	100	.59	Faint	
50	9	15	0	0			X	1.5	150	.50	Good	
50a	9	16	10	35			X	1.5	150	.50	Good	
*51	10	17	10	45			X	1.5	150	.53	Good	
*52	10	18	20	85			X	1.5	150	.56	Good	

* Cell cracking or fracturing is expected

ORIGINAL PAGE IS
OF POOR
QUALITY

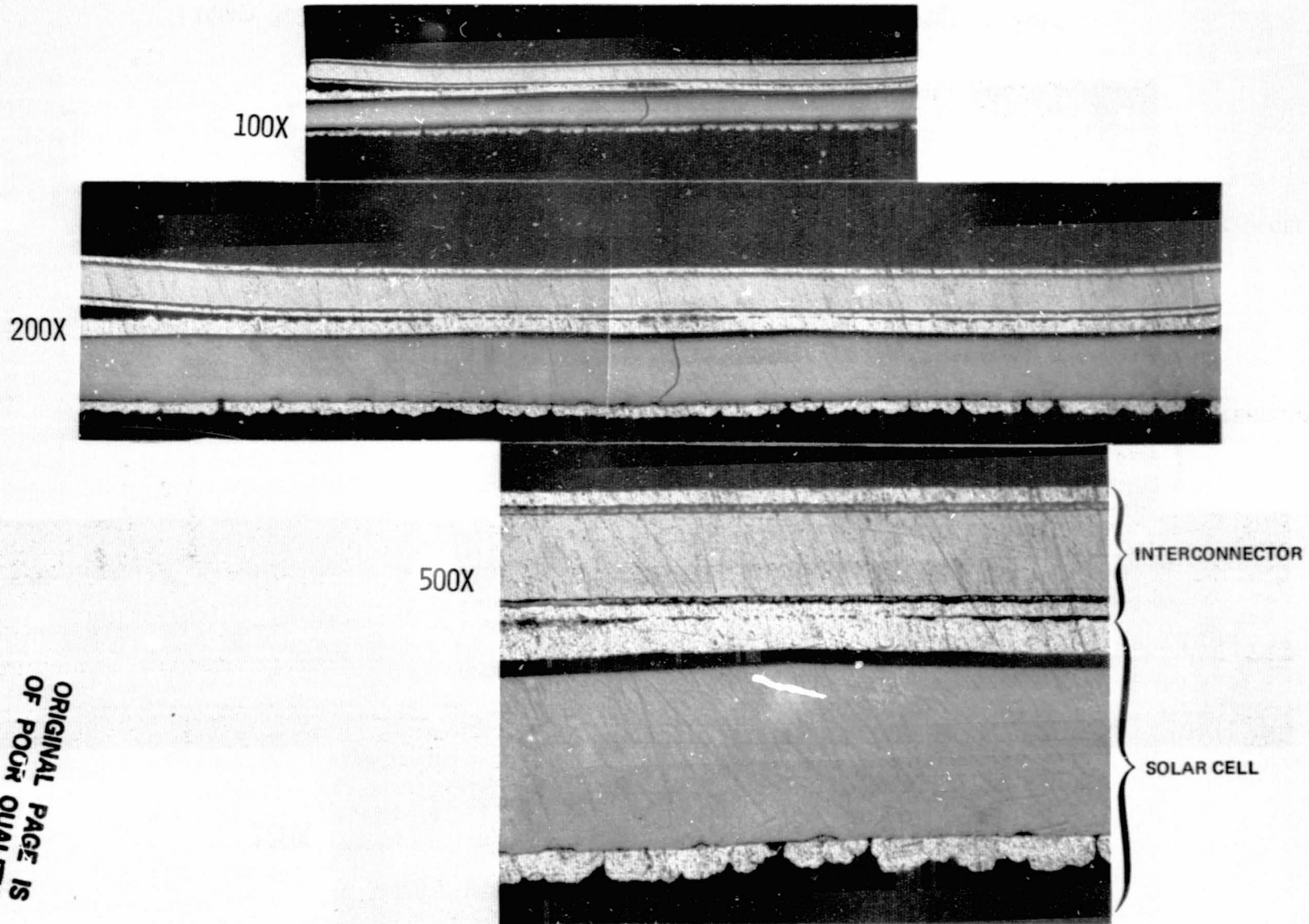


Figure 3.3-5. Joint No. 41, Cross Section of Cell Front Contact Weld

ORIGINAL PAGE IS
OF POOR QUALITY

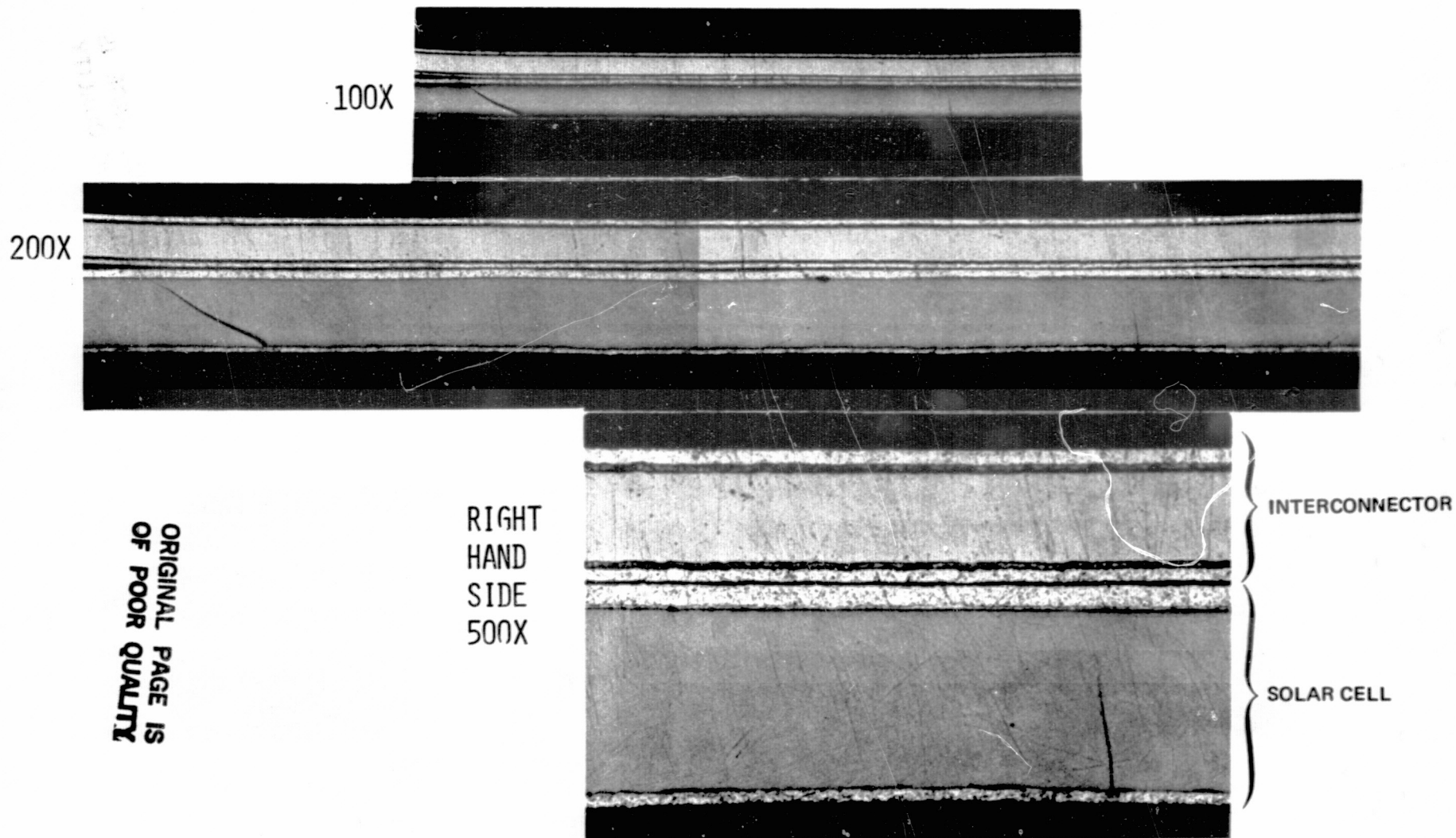


Figure 3.3-6. Joint No. 45, Cross Section of Cell Front Contact Weld

R5-002-79

3.3-11

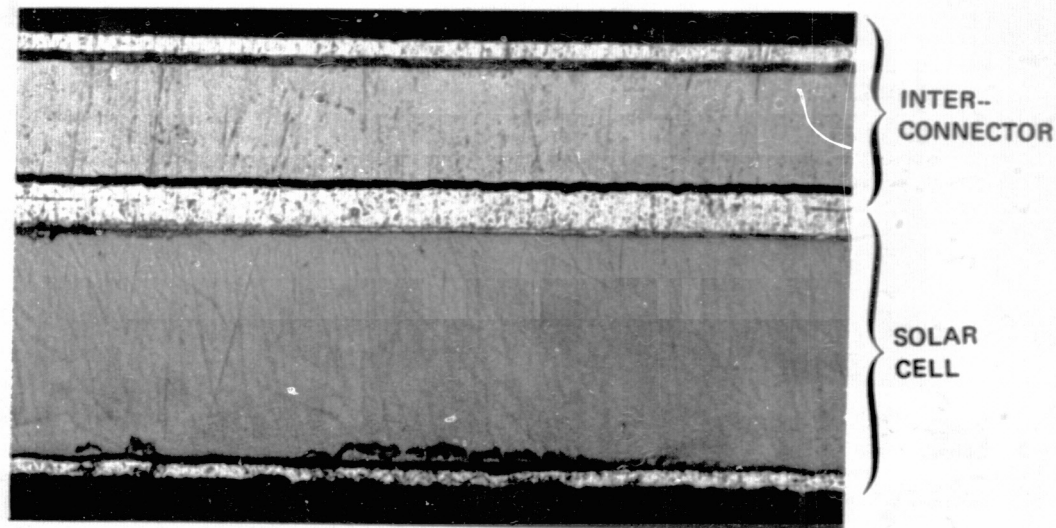
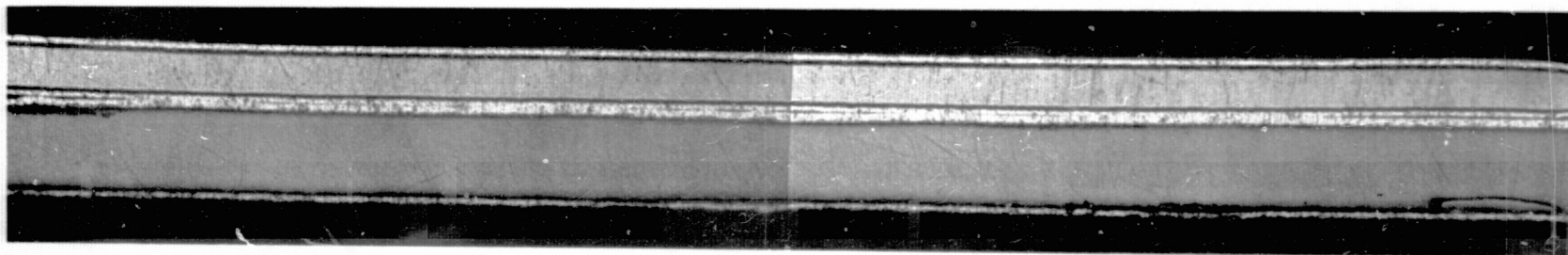


Figure 3.3-7. Joint No. 45A, Cross Section of Cell Front Contact Weld

R5-002-79

3.3-12

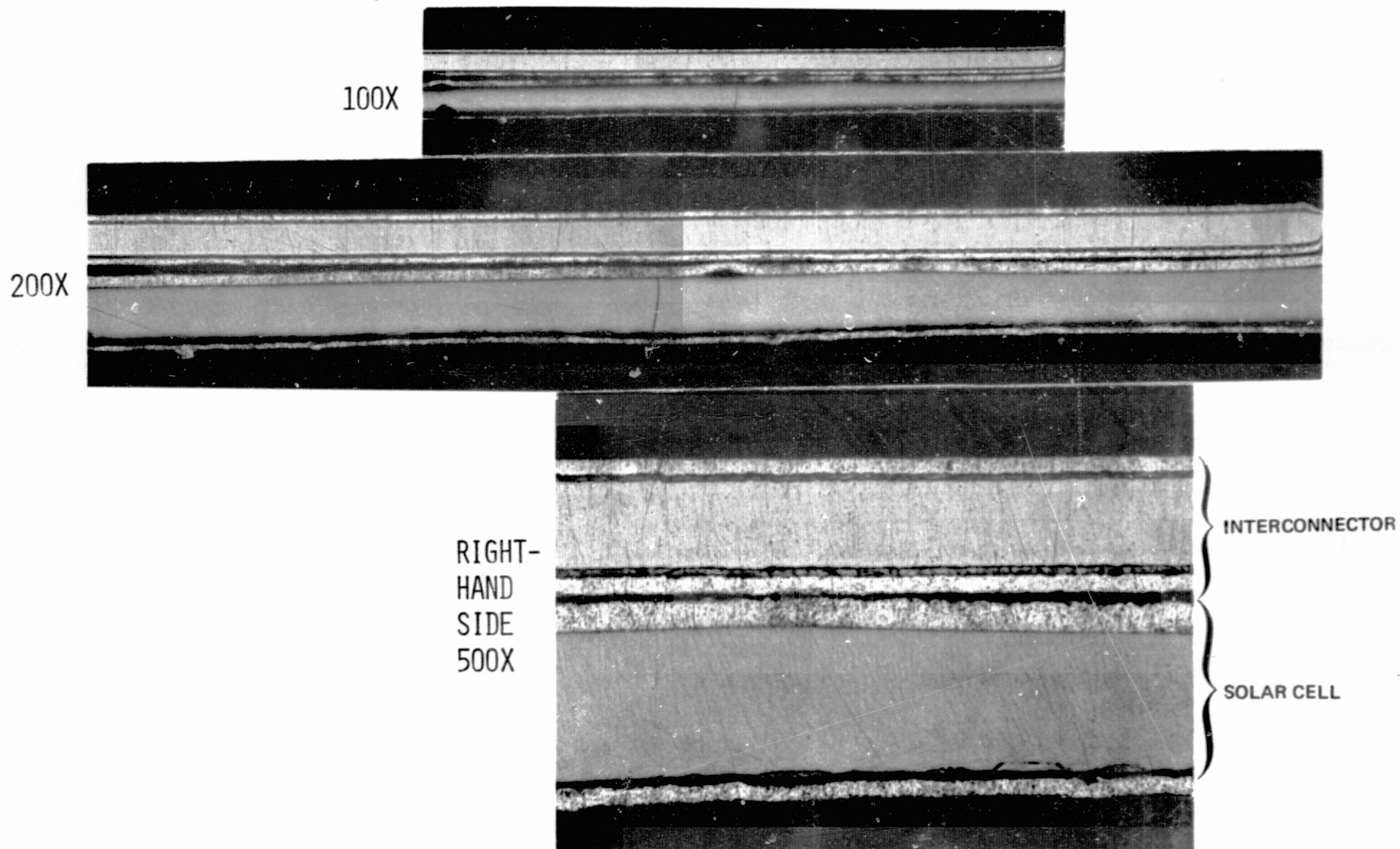


Figure 3.3-8. Joint No. 50, Cross Section of Cell Front Contact Weld

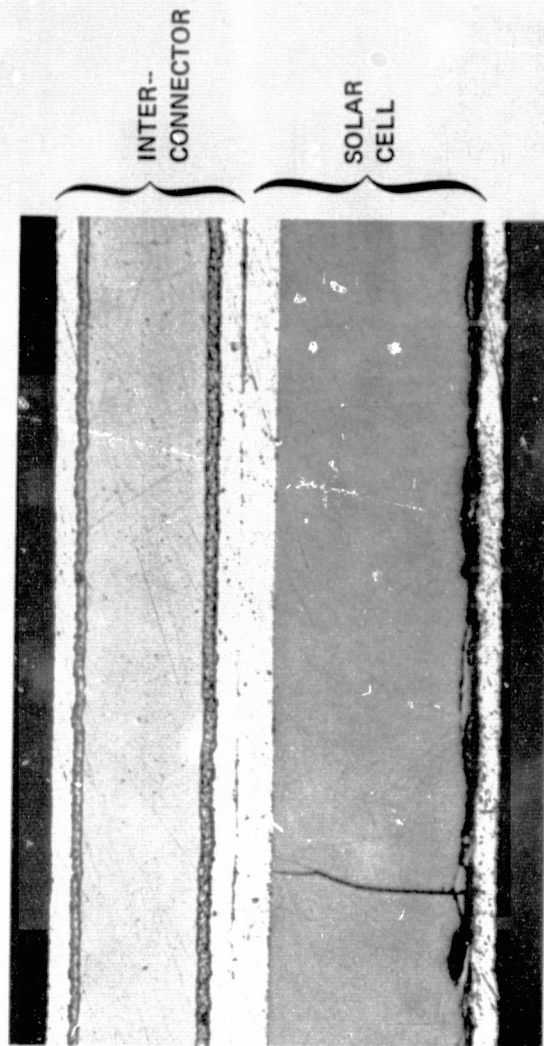
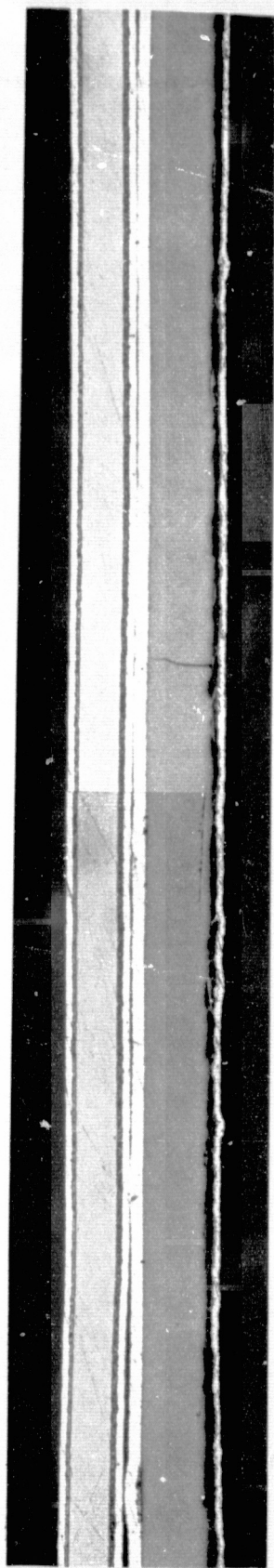


Figure 3.3-9. Joint No. 50A, Cross Section of Front Contact Weld

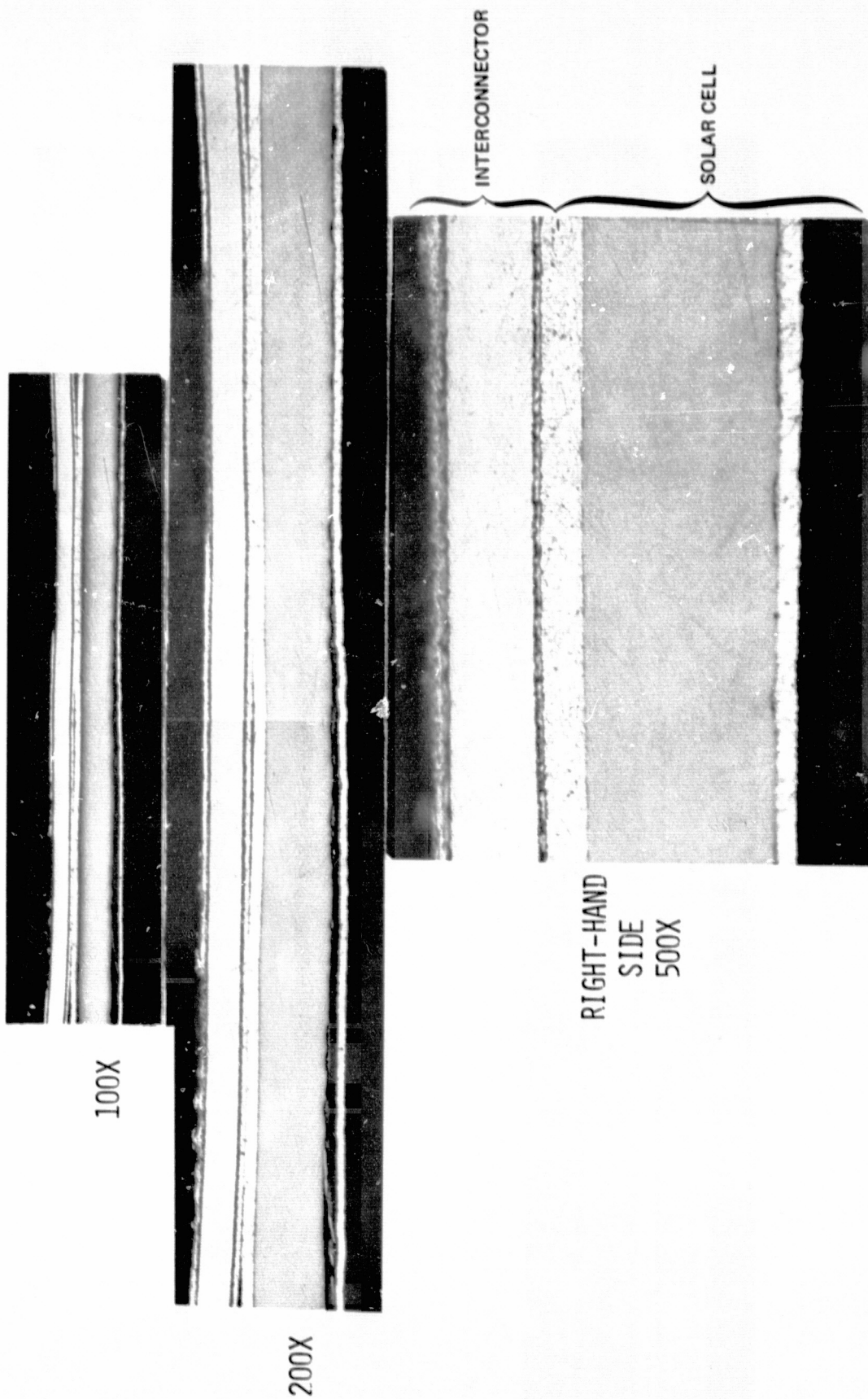
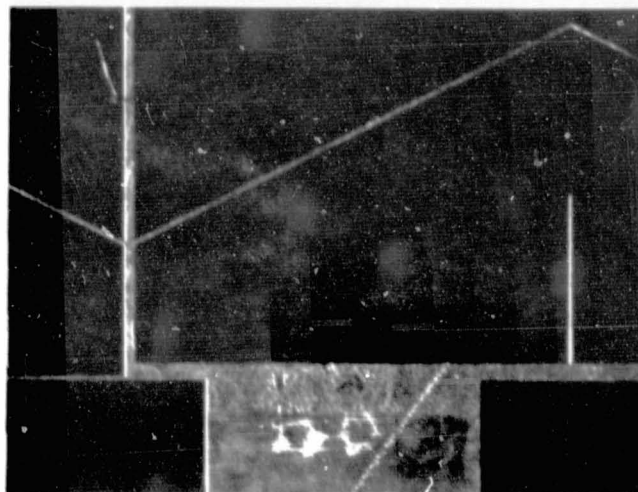
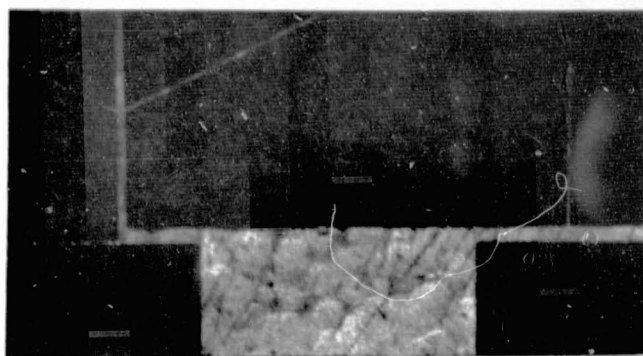


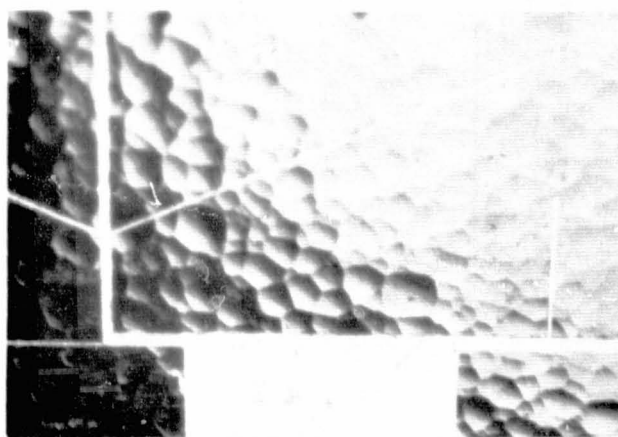
Figure 3.3-10. Joint No. 52, Cross Section of Cell Front Contact Weld



(A)



(B)



(C)

Figure 3.3-11. The Solarex Solar Cell Front Surface Cratering (Mosaic)
 A: Weld imprint after interconnector was peeled from cell contact.
 B&C: Same specimen shown at different angles.

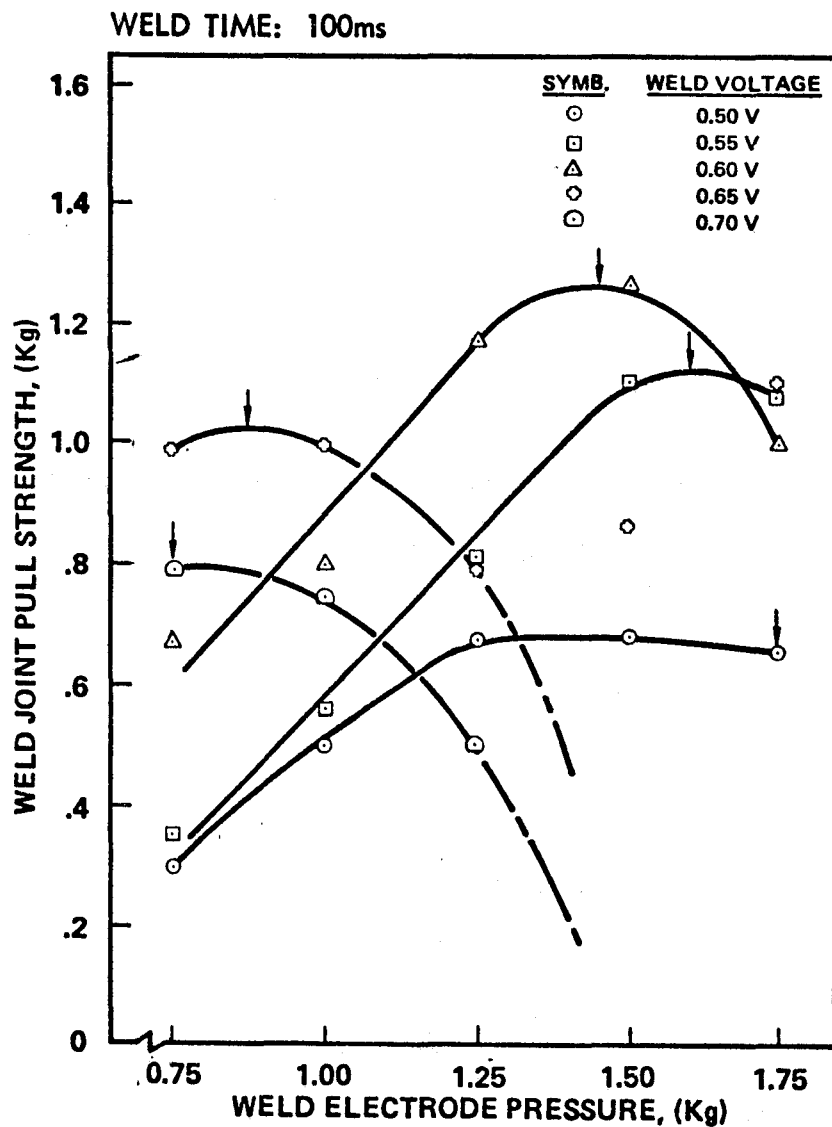


Figure 3.3-12. Results of Rear Cell Contact Weld Joint Pull Strength as a Function of Weld Electrode Pressure and Weld Voltage. Electrode size: 0.025 by 0.045 inch (2x); weld time: 100 ms

R5-002-79

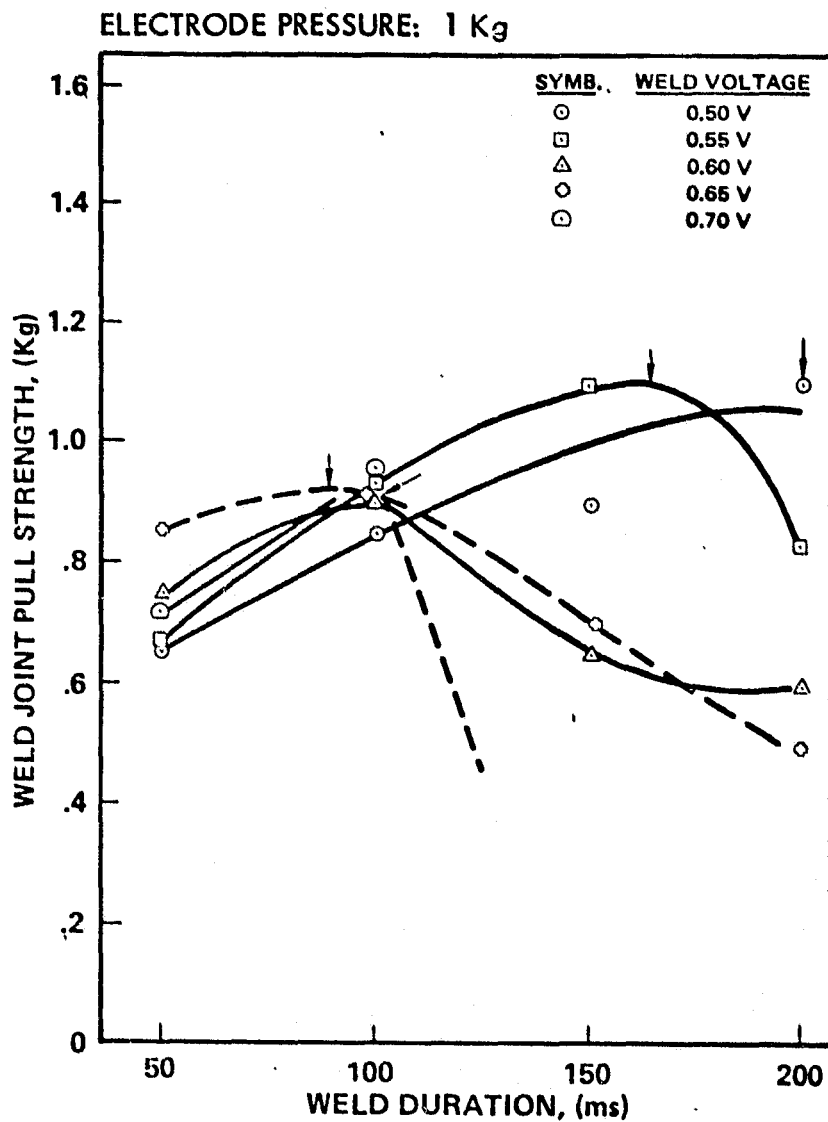


Figure 3.3-13. Results of Rear Cell Contact Weld Joint Pull Strength as a Function of Weld Duration for Various Weld Voltages. Electrode size: 0.025 by 0.045 inch (2x); electrode pressure: 1 kg

All welds ultimately failed due to silicon fracturing (with the weld still intact). The shaded areas of Figures 3.3-14 and 3.3-15 represent the regions where cell to cover adhesive delaminations occurred. Photographs of microsectioned rear cell weld joints show similar cell fracturing as seen on the front contact joints. The results are summarized in Table 3.3-2.

The microphotographs, presented in Figure 3.3-16 through 3.3-21, show this more clearly. The silver plated interconnector is shown on the top side of the cell. The grid lines can be seen below the cell in the form of small clusters of silver. Joints No. 21, and 27 are made to poor cell silver-plating surfaces having granular characteristics, which are further illustrated on a nonwelded cell in Figure 3.3-20a. Other plating problems, discussed in earlier reports, consist of silver-plating blistering (shown in Figure 3.3-20b).

It was expected for some time that the silicon fracturing was caused either during the welding or the microsectioning process. The cell microsectioning was refined to the point that it was ruled out as a source of silicon fracture. A surface roughness measurement of the weld fixture revealed that the fixture surface is sufficiently smooth and will not cause cell fracture. Finally, some bare cell edges of typical 2-mil-thick non-welded cells were viewed under an infrared microscope using 200X magnification. Some cells showed minor cracks, others more severe cracks, and still others none at all. Those cells that showed severe cracking, namely Nos. 400, 412 and 414, are shown in Figure 3.3-21. Interconnectors were welded to cells with and without cracks using different weld electrode pressure. No further cell damage was observed up to about 2 kg of weld pressure; thereafter it was noted that fractured cells did show fracture propagation at normal weld time and voltage settings. The fractured cell number No. 414, along with other fractured cells, was used in the assembly of test coupons.

The majority of what appeared to be edge microcracks may be merely the cosmetic residue of silicon saw chips clinging to the cell by the metallization.

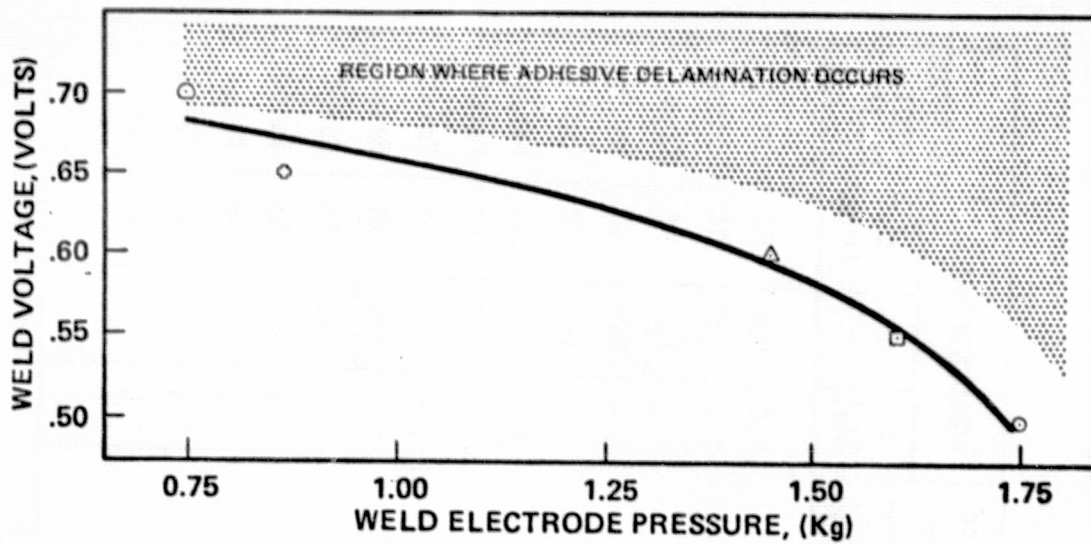


Figure 3.3-14. Weld-Voltage and Weld-Pressure Relationship for Optimum Weld Joint Strength (as observed in Figure 3.3-20)
Time = 100 ms

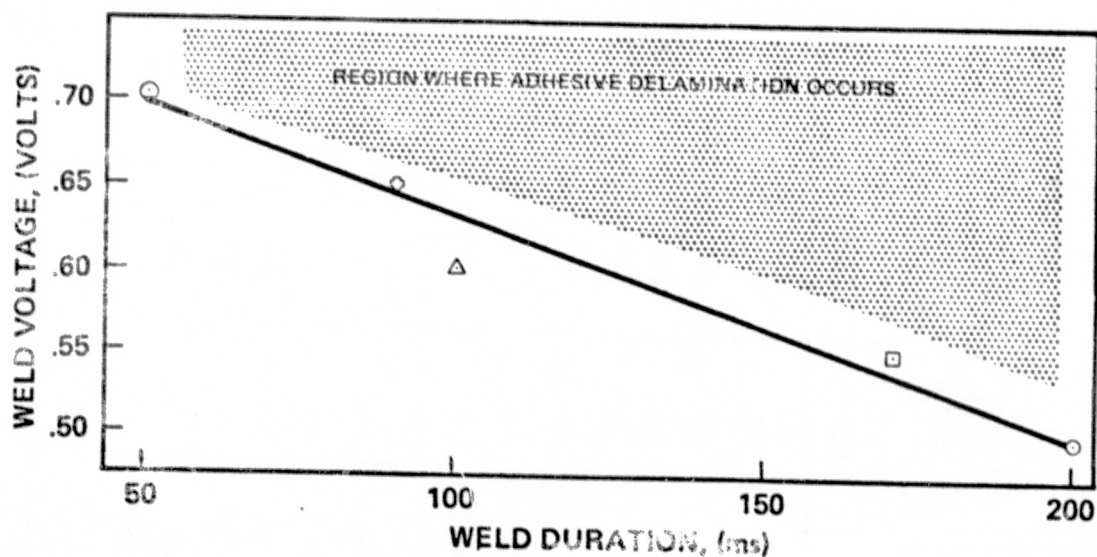


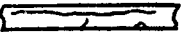



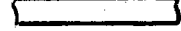


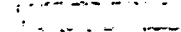

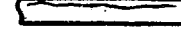




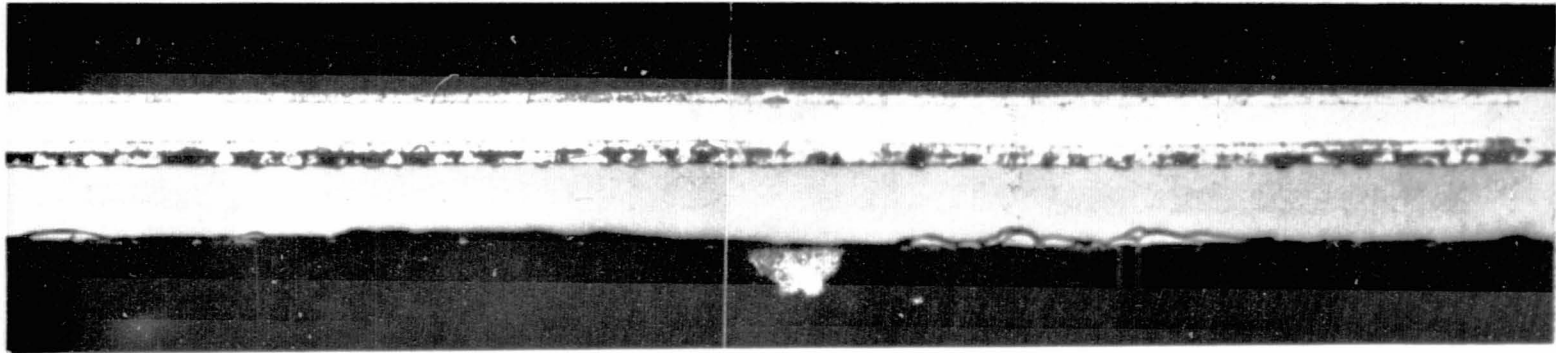
Figure 3.3-15. Weld-Voltage and Weld-Duration Relationship for Optimum Weld Joint Strength (as observed in Figure 3.3-21)
Pressure = 1 kg

Table 3.3-2. Evaluation of Rear Weld Joint Microsectioning

WELD JOINT NO.	MOUNT NO.	WELD JOINT BOND AREA(%) [CROSS SECTION]		CELL FRACTURE	REAR CELL CONTACT SILVER PLATING		WELD SCHEDULE			ELECTRODE FOOT PRINT
		LEFT	RIGHT		VOIDS	INSUFF. Ag THICK'	P (Kg)	T (ms)	E (V)	
21	15	40	50		X		1.0	100	.62	Faint
22	15	60	60		X		1.0	100	.64	Faint
23	16	60	70				1.0	100	.66	Good
24	16	0	40				1.0	150	.60	Faint
25	17	45	90				1.0	150	.62	Good
*26	17	90	25				1.0	150	.64	Heavy
27	18	0	0		X		1.5	100	.57	Faint
28	18	25	10		X		1.5	100	.59	Faint
29	--	--	--				1.5	100	.61	Faint
*30	--	--	--				1.5	150	.54	Faint
31	19	15	30			X	1.5	150	.56	Faint
*32	19	50	60			X	1.5	150	.58	Faint
*33	20	5	10				1.5	150	.60	Faint
*34	20	20	15				1.5	150	.62	Good

*Cell cracking or fracturing is expected

200X



500X

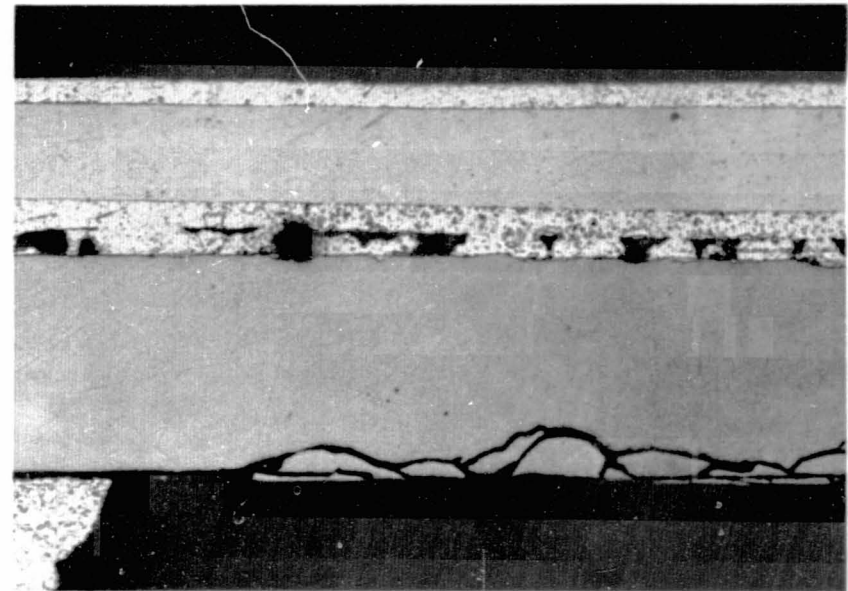
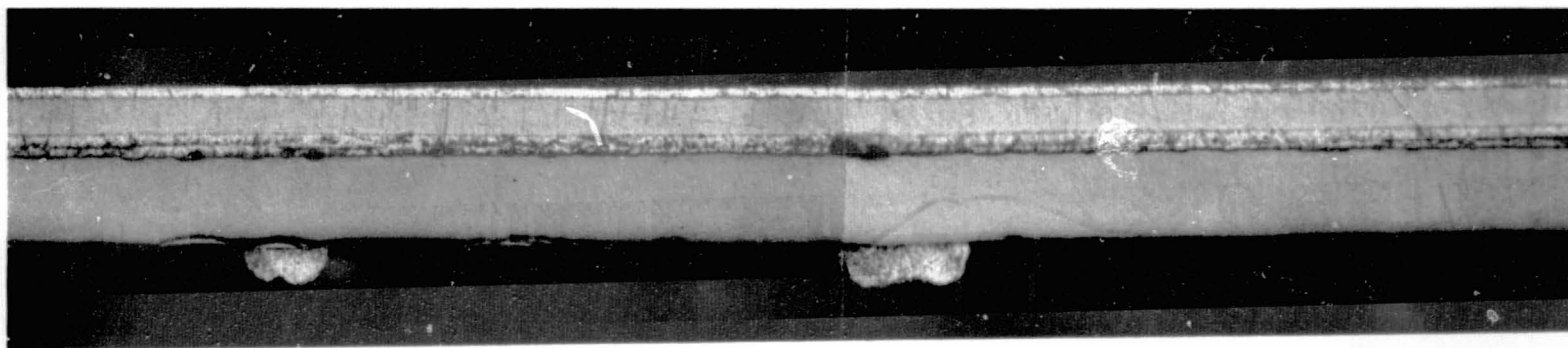
INTER-
CONNECTORSOLAR
CELL

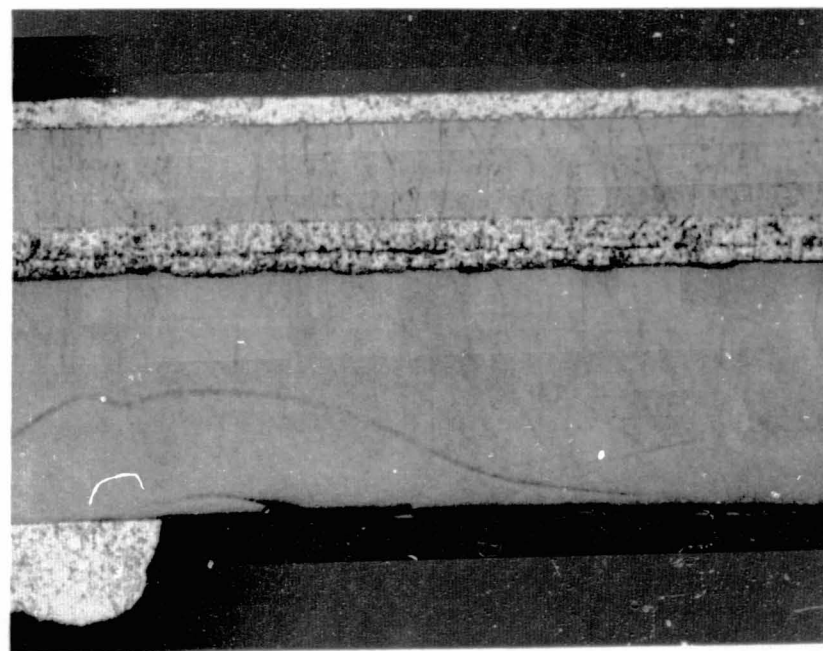
Figure 3.3-16. Joint No. 21, Cross Section of Cell Rear-Contact Weld

200X



3.3-22

500X



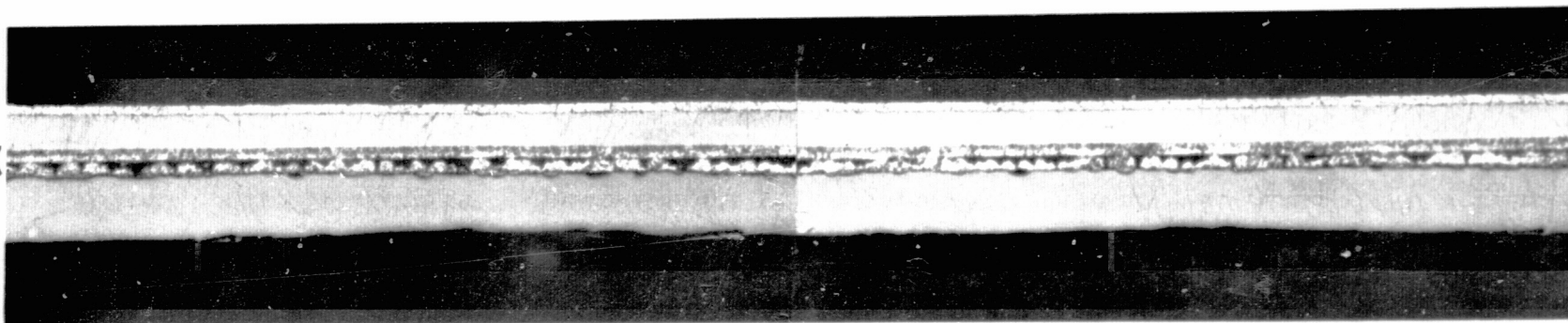
INTERCONNECTOR

SOLAR CELL

Figure 3.3-17. Joint No. 25, Cross Section of Cell Rear-Contact Weld

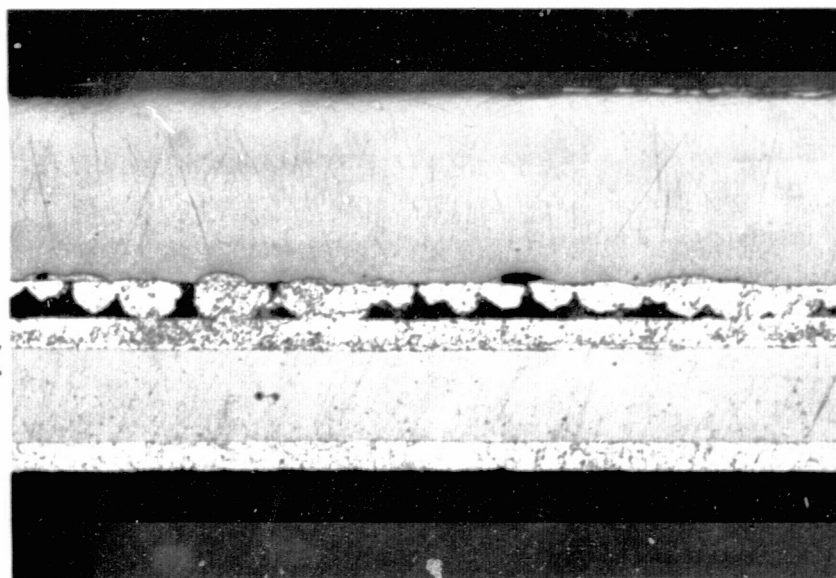
R5-002-79

200X



3.3-23

500X



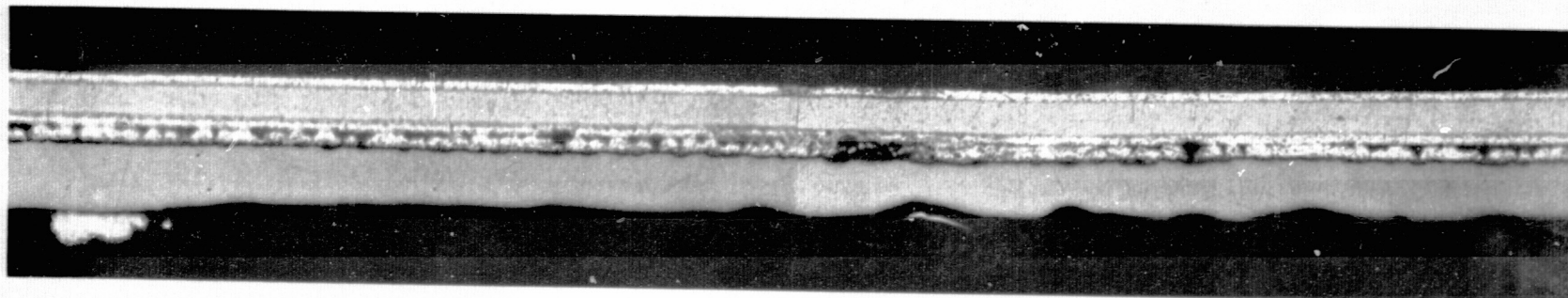
SOLAR CELL

INTERCONNECTOR

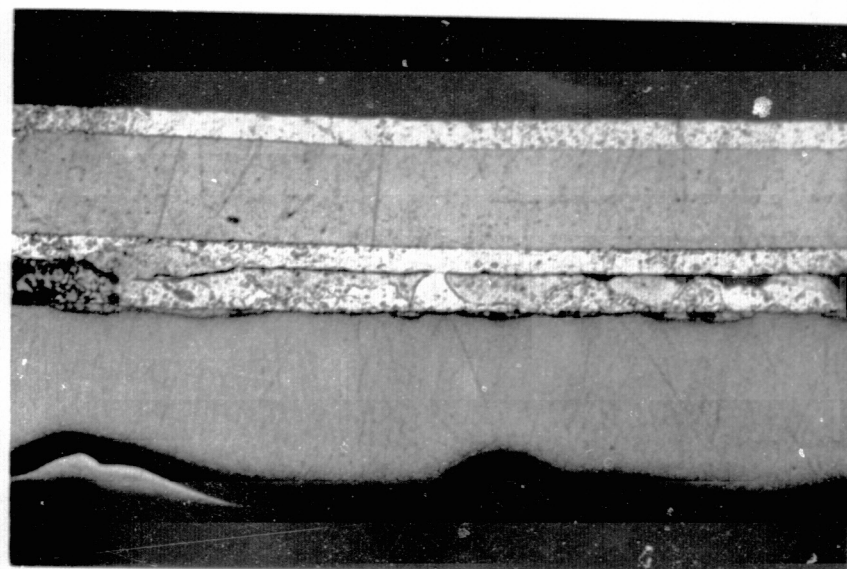
Figure 3.3-18. Joint No. 27, Cross Section of Cell Rear-Contact Weld

3.3-24

200X



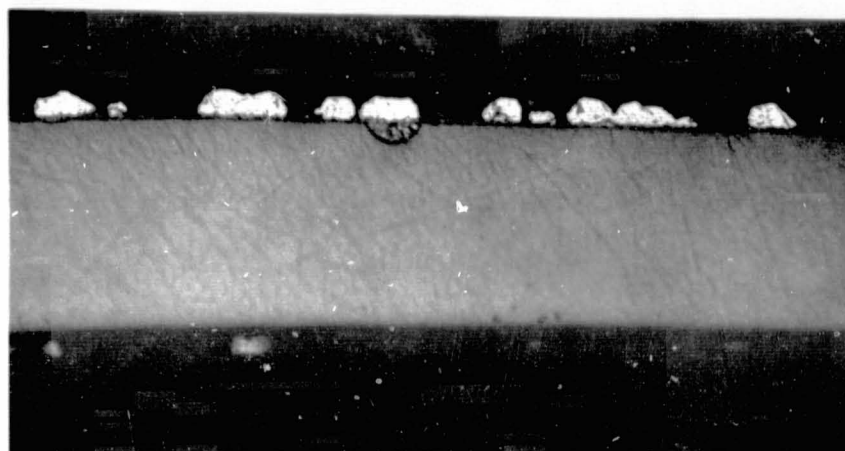
500X



INTERCONNECTOR

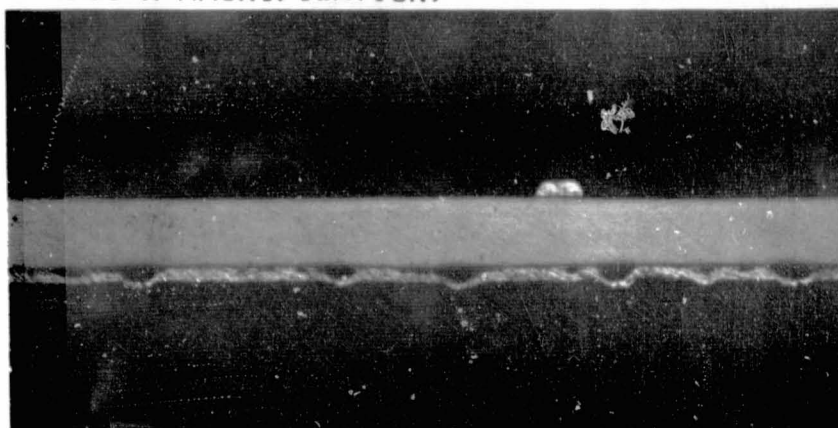
SOLAR CELL

Figure 3.3-19. Joint No. 28, Cross Section of Cell Rear-Contact Weld



A.

GRANULAR SILVER PLATED CELL CONTACT
(500 x MAGNIFICATION)



BLISTERED SILVER PLATED CELL CONTACT
(200 x MAGNIFICATION)

Figure 3.3-20. Silver Plating problems on Rear-Cell Surface of Non-Welded Thin Cells

CELL #412



CELL #414



CELL #400

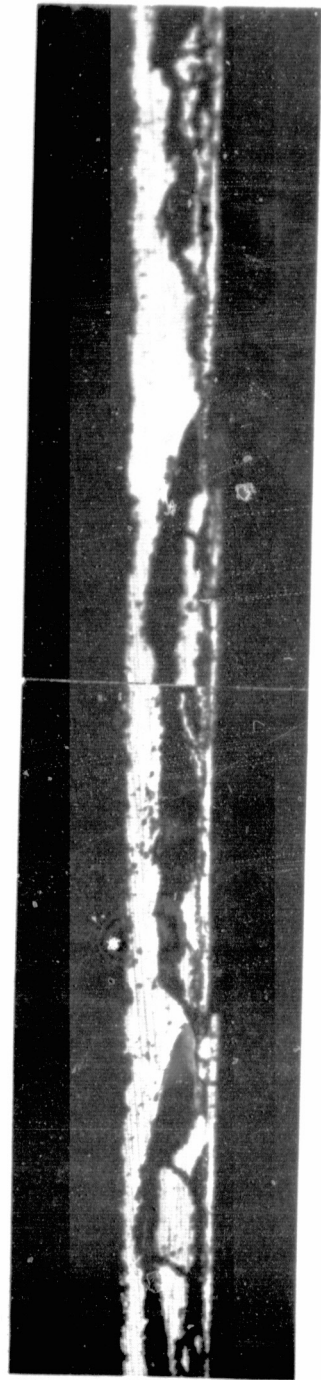


Figure 3.3-21. Microsectioning of Nonwelded, Virgin Thin Cells

Table 3.3-3. Weld Schedule

	FIRST GROUP OF TEST COUPONS (5)		MODULE SOLAR BLANKETS (3) AND SECOND GROUP OF TEST COUPONS (10)	
	Front Cell Contact	Rear Cell Contact	Front Cell Contact	Rear Cell Contact
<u>Weld Electrode</u>				
Size (inch)	.015 x .025	.030 x .050	.015 x .025	.025 x .045
Spacing (inch)	.006	.008	.006	.008
<u>Weld Schedule</u>				
Voltage (v)	0.58	0.65	0.58	0.68
Time (ms)	100	100	100	100
Pressure (kg)	1.0	1.0	1.0	1.0

The optimum weld schedule for front and rear cell contact welding is summarized in Table 3.3-3. This table also includes the preliminary weld schedule used for the assembly of the first five test coupons.

3.3.4 Cell Contact Surface Roughness

Previous data (Ref. 6) from welds made to conventional thick cells of varying contact smoothness show that better weld strengths are associated with smoother surfaces (Figure 3.3-22). Front and back contact surface roughness of five randomly selected thin cells are shown in Table 3.3-4. The measurements were made with a Bendix Corporation Profilometer, Type RLJ, Model 1 using a 0.0013-cm (0.0005-inch) radius stylus. The actual roughness plots are shown in Figures 3.3-23 and 3.3-24; vertical scale on these plots is in micro-inch, called "mk" on the graph paper. The arithmetic average is obtained by dividing the peak-to-valley actual distance by 3.3.

The TRW specification for weldable solar cells specifies a surface roughness of ≤ 500 nm. Referring to Figure 3.3-22, a pull strength of ≥ 1.5 kg can thus be obtained for conventional 200 μ m thick solar cells. As the weld electrode pressure is lowered to 1 kg (dotted line), the weld joint pull strength is reduced to about 1 kg for cells having a surface roughness of 500 nm. Since the weld electrode pressure of 1 kg was chosen for a safe limit for thin cells it can be seen from the data presented that an improvement in joint pull strength can be achieved only by providing smoother cell contact surfaces.

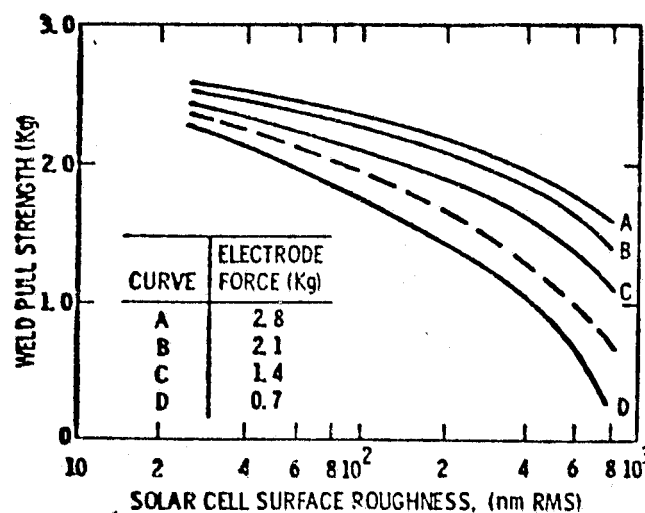


Figure 3.3-22. Conventional Thick Cell Pull Strength Versus Contact Surface Roughness (Ref. 6)

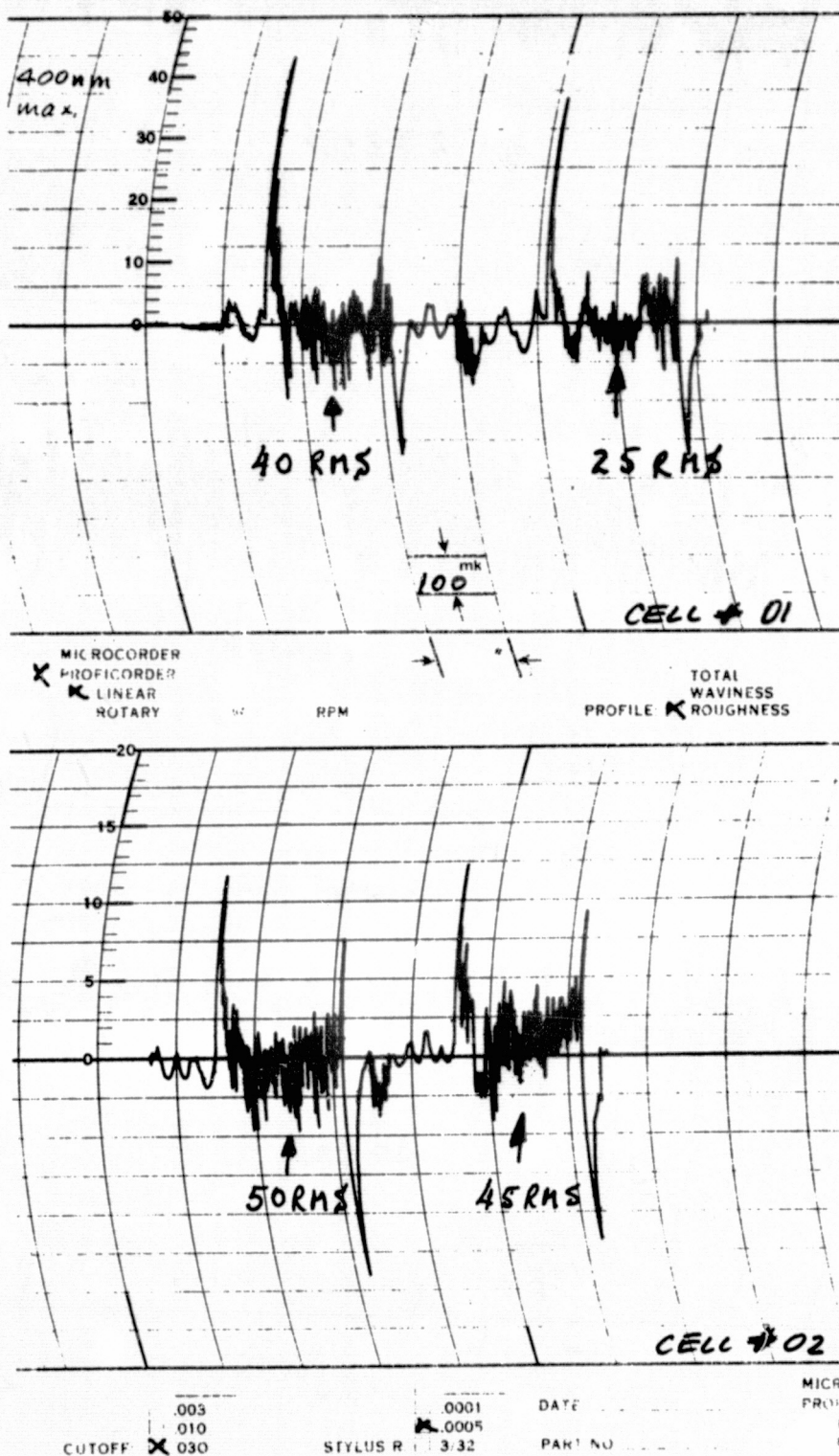


Figure 3.3-23. Surface Roughness Measurements of the Thin Solar Cell Front Silver Contacts

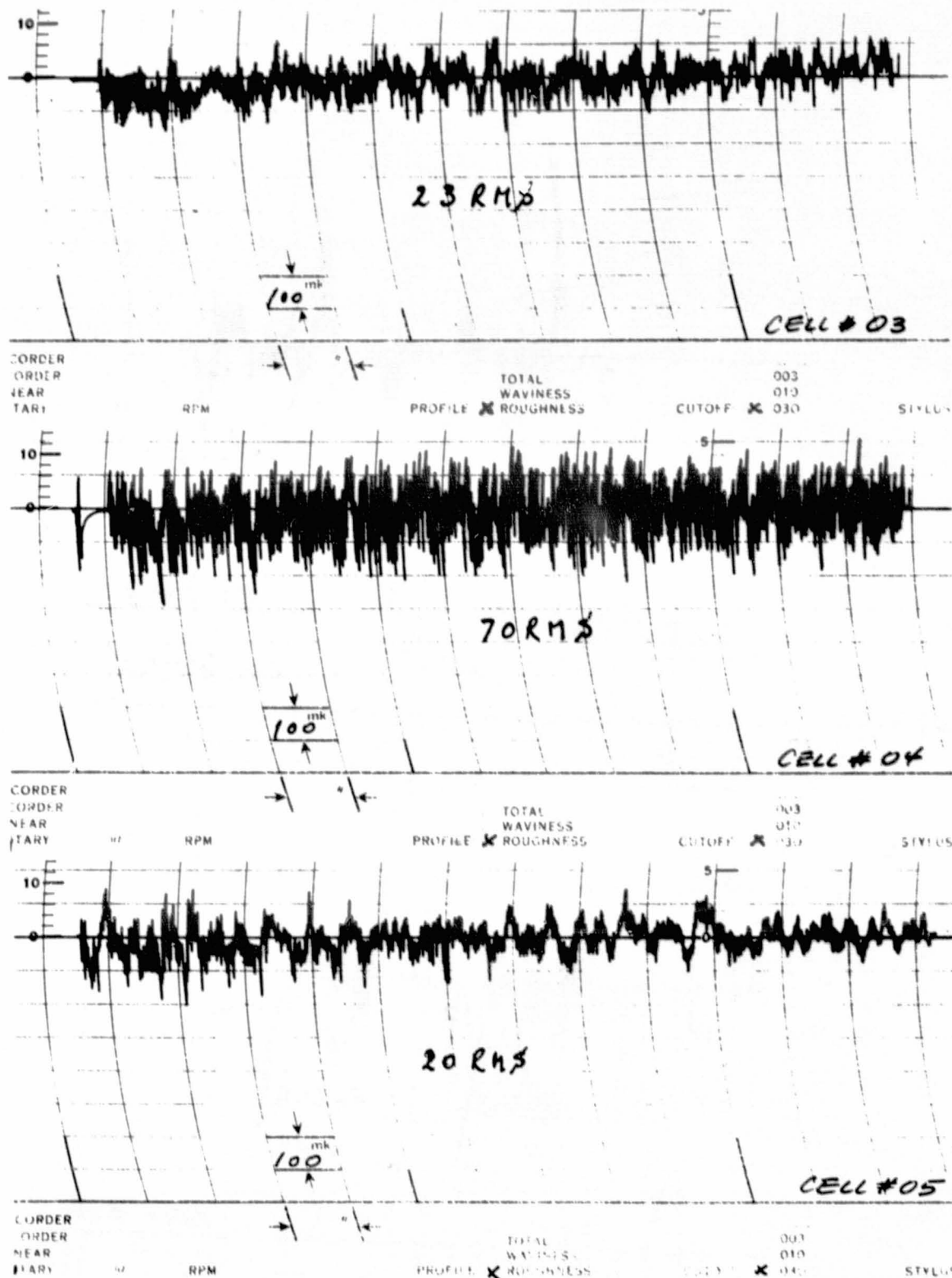


Figure 3.3-24. Surface Roughness Measurements of Solar Cell Rear Silver Contacts

Table 3.3-4. Surface Smoothness of 50 μ m Thick Solar Cells

Cell No.	SURFACE ROUGHNESS, RMS					
	FRONT SIDE				REAR SIDE	
	μ inch		nm		μ inch	nm
	A	B	A	B		
01	40	25	1030	640		
02	50	45	1240	1160		
03					23	590
04					70	1790
05					20	520

3.3.5 Data Correlation, NDT Versus Pull-Strength

The nondestructive test (NDT) equipment was employed throughout the exploratory parallel-gap welding and all welding during the test coupon and module solar blanket assembly in order to monitor the amount of current injected into each weld joint made. The magnitude of this reading is a function of the weld electrode cleanliness, the tip pressure and tip length and also takes into account the cell and interconnector contact cleanliness. The time-integrated weld current, $\int i dt$, is displayed on a digital voltmeter after each weld joint. The displayed readings are recorded by the weld operator.

Based on past experience the electrode cleaning operation is repeated after every twelfth weld joint or sooner, should the NDT monitor indicate a reading below 400 for front cell contact welding and below 450 for rear cell contact welding. It was found that the weld energy is reduced from weld-to-weld for the first twelve weld joints made without electrode cleaning by about 1 percent per weld for the front contact welds and about 3 percent per weld for the rear contact welds, as shown in Figures 3.3-25 and -26.

Figure 3.3-27 shows that a definite relationship exists between the NDT reading and the resulting weld joint pull strength. The data presented is based on more than 30 weld joints made without electrode cleaning between welds. Based on the data shown, the 15th weld joint made would produce a reject NDT reading of about 450, resulting in a joint pull strength of 0.3 kg.

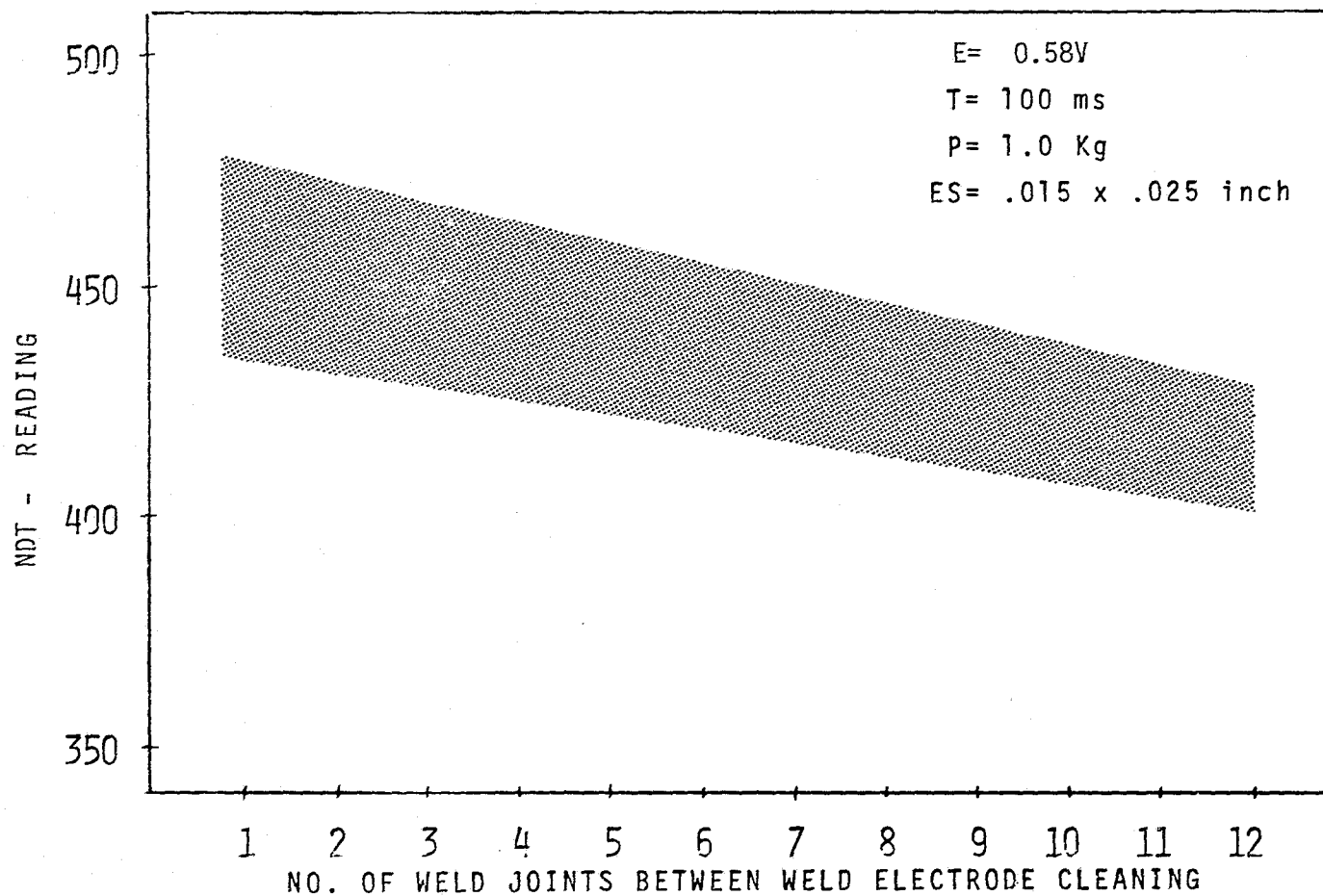


Figure 3.3-25. Nondestructive Test Data for Front Cell Contact Welds Made Without Electrode Cleaning

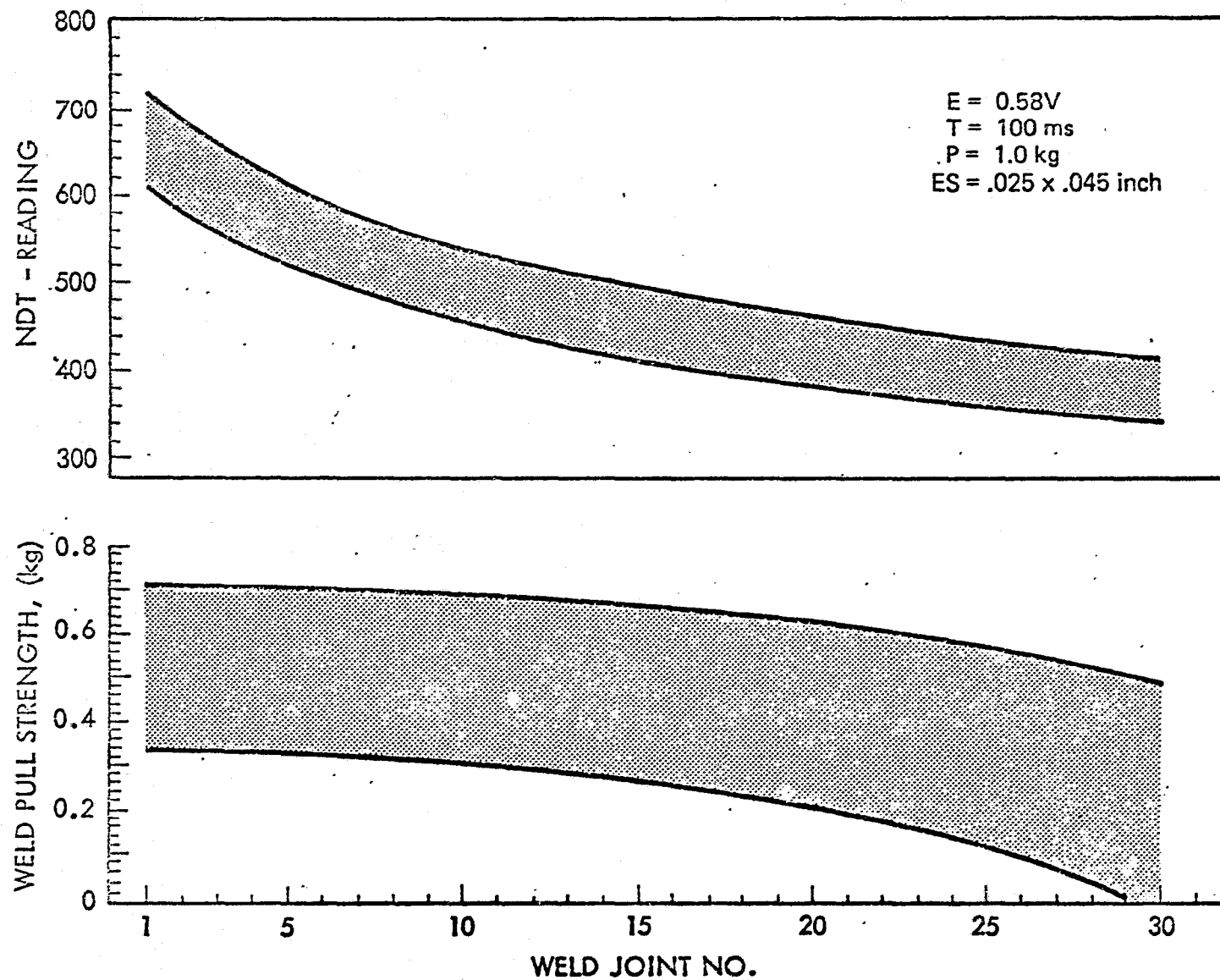


Figure 3.3-26. Range of Nondestructive Test - and Weld Pull Strength-Data Without Electrode Cleaning Between Welds for Rear Cell Contact Welding

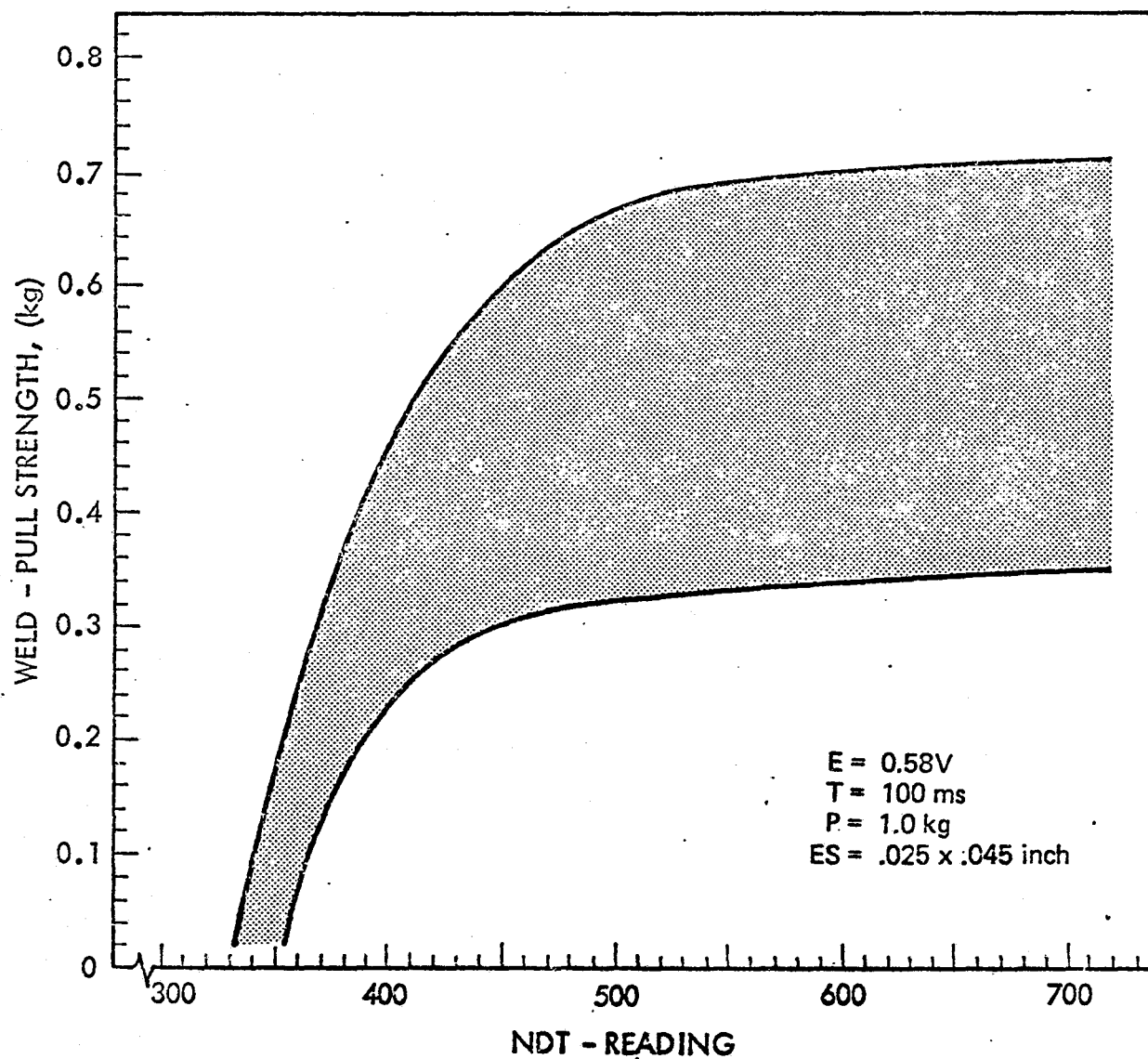


Figure 3.3-27. Pull Strength versus Relative Nondestructive Test Reading for Rear Cell Contact Welding

3.4 PROCESS DEVELOPMENT

During the process development work it was found that conventional manufacturing methods were not always suitable for the assembly of solar blankets utilizing thin as well as bowed cell assemblies. Different assembly methods were evaluated throughout the program. The various process problems encountered and the final process developed for the assembly of the test coupons and module solar blankets will be discussed in the following sections. A flow diagram is given in Figure 3.4-1. As shown in this diagram the front contact is attached prior to cell glassing, a deviation from the conventional assembly method which has several distinct advantages: (1) the cell contact is not contaminated with cover glass adhesive prior to welding, thus assuring a good metallic bond between interconnector and the cell ohmic contact; and (2) optimum cell protection from charged particle proton irradiation is guaranteed due to a four-sided cover glass overhang.

3.4.1 Front Contact Attachment

About halfway through the program a minor modification was made to the weld electrode pressure system assuring an automatic upper pressure limit, which was formerly controlled by the operator. Other than that, no additional modifications were made to the weld equipment described in Section 3.3.1.

All front contact welding was done on an aluminum fixture having six cavities, one for each thin 2- by 2-cm cell, which are separated by 250- m (0.010-inch) wide shims. Two locating pins near the outside cells (the first and the sixth cell) maintain interconnector strip positioning during cell front contact welding. When all 12 weld joints (2 per cell) have been completed, the two interconnector positioning loops, at the ends of the strip, are cut and removed from the pins. Cells with interconnectors are stored in styrofoam containers, awaiting cover glass bonding. Front cell contacts are attached with the conventional size electrodes, each 0.38 by 0.64 mm (0.015 by 0.025 inch) in size. Electrode tip cleaning is initiated by the operator prior to fixture reloading (after 12 weld joints), or sooner, should the nondestructive test (NDT) readout fall below a preset \int idt value. A ceramic material is employed for the electrode contact cleaning operation.

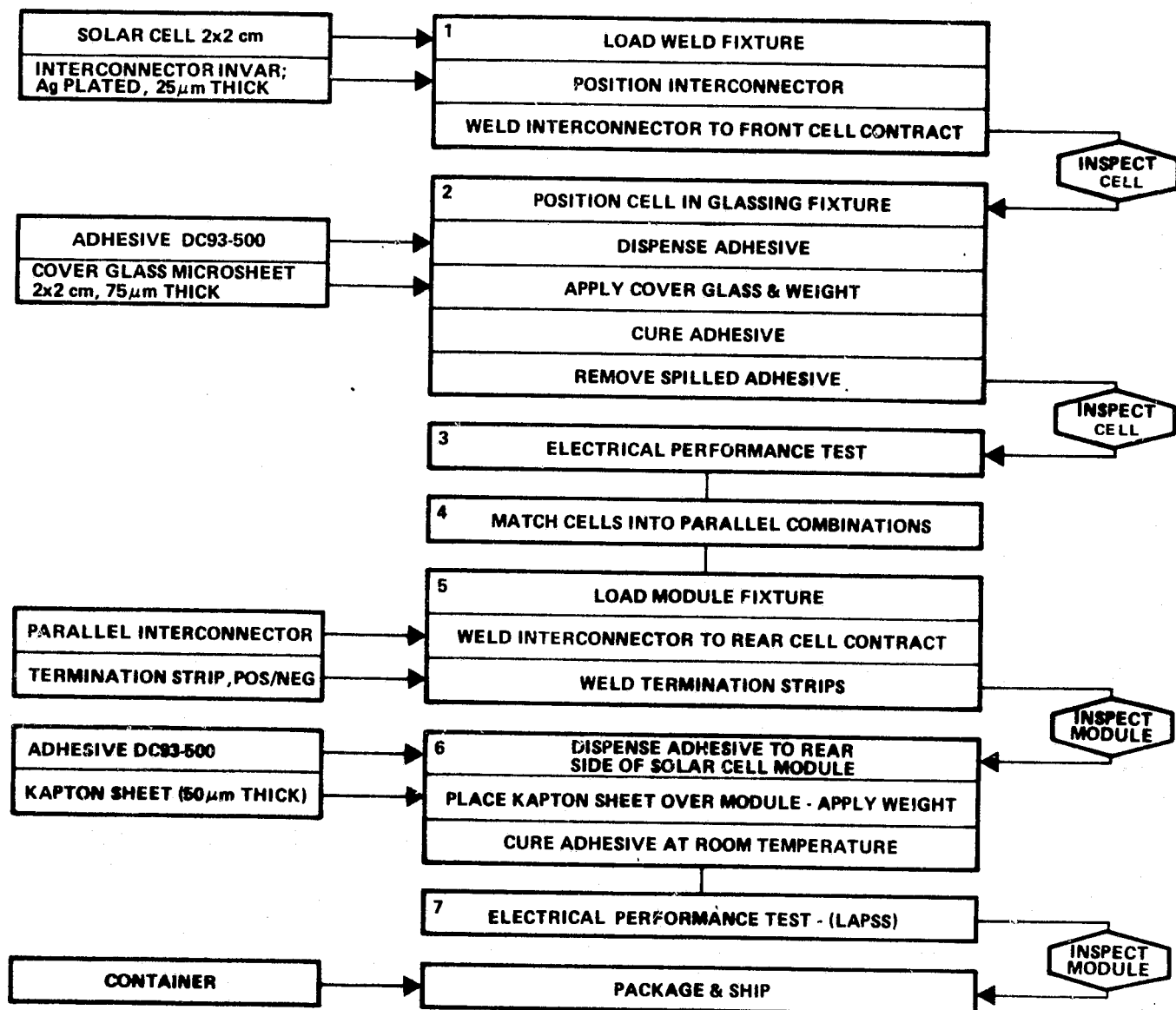


Figure 3.4-1. Flow Diagram for Solar Blanket Assembly

3.4.2 Cover-to-Cell Bonding

Most assembly difficulties were experienced in glassing the 50 μ m thin, bowed solar cells using 75 μ m thin microsheet covers. The initial cell bowing problem was overcome when a weight was applied on top of the assemblies. Cells having a bow radius up to $r = 40$ mm will straighten out with a weight of 12 grams. However, only a few cells had a radius smaller than $r = 40$ mm; more recent cell shipments were considerably larger than $r = 40$ mm. Bowing of thin cells is caused by one-sided silver-plating at high temperature, causing shrinkage of the silver at room temperature. Even though later cell shipments revealed less of a bowing problem the 12-gram weights were used throughout the program, thus reducing the DC93-500 adhesive bondline thickness to between 12 to 30 μ m. These thin bondlines did not inhibit adhesive curing, and bowed cells maintained their flatness after the cover glass application.

The second problem encountered in thin cell glassing was the partial bonding of cells to the glassing fixture, leading to cell and cover glass or cover glass breakage during the subsequent thin cell removal from the glassing fixture. A number of experiments were conducted with thin Tungsten wires, thin spatulas, and a mold release called FREKOTE, all without major improvements. In a separate experiment a total of five different mold release agents were evaluated by actually bonding cells to substrates about 30 minutes after treatment with the various mold releases. The test results are summarized in Table 3.4-1, identifying the CENCO WETTING AGENT as the best mold release for the DC93-500 adhesive. For the purpose of our investigation the mold release was applied to the fixtures with a small artist brush, although for actual production runs a spray technique is recommended.

The glassing fixture design is a flat plate concept with three slanted pins against which two sides of the cover glass and the cell rest as the fixture is tilted 30 degrees, thus having gravitational force aid in the cell to cover alignment and cover glass overhang.

Table 3.4-1. Results of Mold Release Evaluation Using Cover Glass Adhesive DC 93-500

Mold Release		
Name	Manufacturer	Evaluation
GARALEASE	Ram Chemicals Company	Fair
PLASTILEASE	Ram Chemicals Company	Fair
RAM	Ram Chemicals Company	Poor
CENCO Wetting Agent	Central Scientific Co.	Good
FREKOTE	Frekote Company	Very Poor

3.4.3 Rear Contact Attachment

Prior to the rear contact welding operation each glassed cell underwent a performance test at a 1 sun intensity (135.3 mW/cm^2) and a test temperature of 28°C . Matching of parallel cell combinations by electrical performance was accomplished by first determining the average cell current of all cells at hand at the predetermined optimum cell voltage (V_{op}), of 0.46 volt and then selecting those four parallel cells that will provide four times the average cell current at V_{op} for any particular parallel module combination.

As discussed in Section 3.3.2, the weld electrode size was increased by a factor of 3 to 0.64 by 1.14 mm (0.025 by 0.045 inch) for all rear cell contact welding.

An aluminum fixture with 80 cell cavities provided for series parallel cell spacing for the module solar blanket, consisting of 0.5 mm (0.020 inch) in the series direction and 0.25 mm (0.010 inch) for the parallel cell spacing. The module was assembled by adding four matched parallel cells at a time, welding their front contacts to the rear cell side of the next group already in position. A separate interconnector ribbon welded to the rear side of all cells completed the parallel connection. After welding completion the module's front and rear side were inspected. The module remained in the assembly fixture for the next operation.

3.4.4 Cell-to-Substrate Bonding

The initial adhesive choices were DC93-500 for cell-to-cover and RTV-566 for the cell-to-substrate bonding. However, it was difficult to obtain thin bondlines using the RTV-566 adhesive. This difficulty was overcome by employing DC93-500 for both, the cell-to-cover and cell-to-substrate adhesive.

Prior to cell-to-substrate bonding the back surfaces of all cells and the Kapton substrate are primed using 92-023 primer. One drop, or about 12 mg of DC93-500 adhesive is dispensed on the center rear side of each cell, as the interconnected cells rest in the welding fixture. The 50- μ m-thick pre-cut Kapton substrate is positioned and bonded to the cells, applying light pressure through a thin foam sheet for about 30 minutes. Thereafter the completed unit is removed from the fixture and placed on a flat surface where it remains for a minimum of 24 hours. Only minor adhesive cleanup is required thereafter.

The final electrical performance of each unit is determined with the Large Area Pulsed Solar Simulator (LAPSS) following the assembly and prior to and after environmental testing.

3.4.5 Discussion of Critical Areas

A great deal of practical information concerning the assembly and handling of these rather fragile cells and covers was obtained throughout the test coupon and module assembly. The major assembly difficulty was in the area of cell and module handling. The solution was personnel training. Everyone expressed fear in handling the thin device at the start. Some people adapted readily, others were somewhat slower.

The following are areas identified as critical handling steps:

- 1) Marking the cells for identification; only minimal pressure may be exerted; a flat hard surface below the cell is mandatory.
- 2) Electrical test probe pressure must be carefully controlled and the heat sink surface must be flat.
- 3) For front and rear welding absolutely flat clean surfaces with surface smoothness better than 500 nm (20 microinch) are necessary; careful adherence to the weld parameters is essential.

- 4) Good process control is essential for cell covering including critical monitoring of the amount of adhesive dispersed. (Most cell breakage occurs in the glassing operation.)
- 5) Increased module assembly time is necessary to allow for slower operation motion. Rushing the operator would increase cell breakage.

It has been noticed that some of the thin 50- μ m thick solar cells have been curled so that they require weight to flatten them when bonding the coverglass. The maximum rise at the center of the cell has been estimated as 0.06 inch, giving a curvature $1/R = 0.75 \text{ in}^{-1}$. Presumably this curvature is due to the application of the one-sided silver plating at a high temperature and the subsequent shrinkage of the silver to room temperature.

Thus the use of the ultrathin cells increases significantly both the curvature of the cell and the residual stresses in the silicon. Careful ideal flattening of the cell by applying distributed bending moments to the edges of the cell would actually reduce the silicon stresses.

Once the coverglass has been bonded on and the weight removed, the cell tends to return to its curled shape, but is restrained due to the bending resistance of the coverglass. This, in turn, causes tensile stresses to be developed in the top surface of the coverglass. For conventional cells, any further curling is essentially eliminated by bonding the silver surface of the cell to a relatively stiff aluminum substrate. However, the lightweight 50- μ m thick cells are bonded to a 50- μ m thick Kapton substrate which is very flexible, compared to both the silver and the silicon. Thus it provides negligible resistance to further curling. Therefore, when the temperature is lowered to the operational limits, the silver/silicon/coverglass sandwich continues to curl and to cause additional tensile stresses in the outer surface of the coverglass. Thus there will be a strong tendency for the coverglass to crack at low temperatures.

3.5 HARDWARE FABRICATION

3.5.1 Component Description

All test coupons and module blankets were assembled with 2 ohm-cm, N/P 2 by 2-cm solar cells ranging in thickness from 50 to 75 μm (0.002 to 0.003 inch). The cells had titanium-palladium-silver contacts and Ta_2O_5 AR coatings. The cells were manufactured by the Solarex Corporation, and were supplied to TRW by JPL. The cells were covered using 75 μm microsheet glass; in all cases the cover was oversized in order to overhang the cell on all four sides. The interconnect material was 25 μm silver-plated Invar, while the substrate was 50 μm Kapton^R. The cell to cover bonding adhesive was Dow Corning DC93-500 and the circuits were bonded to the substrate using DC93-500 primed with 93-023.

3.5.2 Test Coupons

A coupon consists of nine glassed thin solar cells, three cells in series and three cells connected in parallel, all bonded to the Kapton substrate, 4 by 6 inch in size. A typical test coupon is shown in Figure 3.5-1. Two groups of test coupons were made. The first group of five were assembled using a weld schedule which was based on previous experience since the coupons were to be delivered 2 months after contract go-ahead; the weld schedule had not been optimized at that time. The second group of ten coupons were assembled using the optimum weld parameters as well as primer for the attachment of cells-to-substrate. Two-thirds of the cells received single loop interconnectors and one-third of the cells were fabricated with the double loop interconnector. The assembly of these coupons was followed by thermal soak testing and thermal vacuum cycling testing and then the ten coupons were delivered to JPL for further evaluation.

Electrical single cell performance was measured under the X-25 solar simulator, after cell receipt, after welding and once more after glassing.

The essential data points of the first coupon group such as I_{sc} , V_{oc} and I_{op} at 0.46 volt have been recorded in Tables 3.5-1 through 3.5-3 for comparison. From these results it can be seen that the average cell performance dropped 1.7 percent after welding and showed a performance gain of 2.8 percent after glassing; due to the presence of a Ta_2O_5 coating on these Solarex cells.

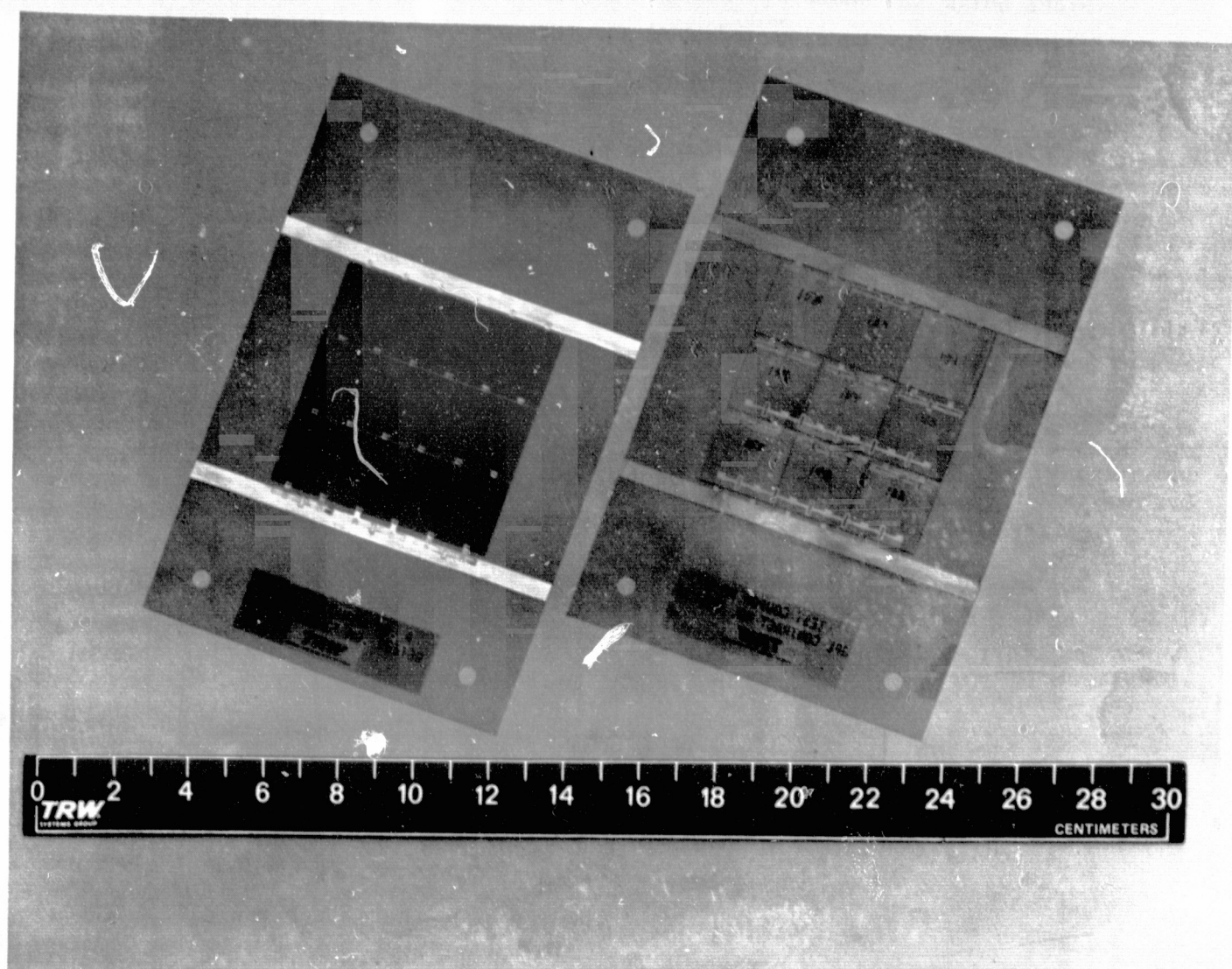


Figure 3.5-1. Typical Nine Cell Test Coupon on Kapton Substrate

Table 3.5-1. Cells Used in Coupon Assembly. Short Circuit Current (Isc)
at 135.3 mW/cm Intensity, 28°C Test Temperature

CELL NO.	INITIAL Isc	AFTER FRONT CONTACT WELDING	AFTER GLASSING
103	122	122	126
104	124	124	127
106	120	120	124
108	124	123	124
109	119	119	124
110	118	119	122
113	117	118	121
115	117	117	122
116	116	117	121
119	119	120	124
120	125	126	129
122	123	125	128
123	120	121	125
126	120	124	124
127	119	120	124
128	118	118	131
130	119	125	131
141	124	124	128
142	123	122	126
143	121	121	122
153	124	125	128
154	115	116	119
155	119	119	124
157	122	122	125
158	117	117	121
159	127	128	130

CELL NO.	INITIAL Isc	AFTER FRONT CONTACT WELDING	AFTER GLASSING
201	119	---	122
202	126	---	129
203	126	---	129
207	119	---	122
211	120	---	122
214	120	---	123
215	124	---	127
216	124	---	126
217	121	---	124
222	124	---	127
227	122	---	126
228	126	---	129
233	126	---	129
234	122	---	124
235	119	---	123
237	121	---	124
238	122	---	122
240	123	---	125
AVG.	121	121	123

0

1.6%

Table 3.5-2. Cells Used in Coupon Assembly. Open Circuit Voltage (Voc)
at 135.3 mW/cm² Intensity, 28°C Test Temperature

CELL NO.	INITIAL VOC	AFTER FRONT CONTACT WELDING	AFTER GLASSING
103	545	543	545
104	551	549	551
106	550	550	550
108	550	548	549
109	551	551	551
110	542	542	542
113	553	553	555
115	557	556	558
116	554	553	553
119	551	543	548
120	555	551	552
122	547	547	550
123	557	556	556
126	555	555	553
127	541	541	541
128	552	552	543
130	554	553	553
141	547	542	541
142	556	555	556
143	542	542	542
153	555	553	553
154	554	549	551
155	546	545	547
157	551	550	547
158	552	550	551
159	551	550	551

CELL NO.	INITIAL VOC	AFTER FRONT CONTACT WELDING	AFTER GLASSING
201	540	---	543
202	544	---	543
203	553	---	553
207	541	---	541
211	541	---	540
214	544	---	544
215	547	---	548
216	545	---	542
217	543	---	540
222	545	---	538
227	542	---	541
228	545	---	553
233	544	---	547
234	546	---	545
235	541	---	542
237	545	---	544
238	544	---	542
240	542	---	544
AVG.	548	549	547

Table 3.5-3. Cell Used in Coupon Assembly. Current (MA) at 0.46 Volt,
135.3 mW/cm² Intensity, 28°C Test Temperature

CELL NO.	INITIAL I(.46V)	AFTER FRONT CONTACT WELDING	AFTER GLASSING
103	111	110	112
104	114	109	114
106	112	110	113
108	112	111	109
109	111	110	114
110	108	107	111
113	110	107	112
115	111	111	116
116	108	109	113
119	112	109	113
120	116	113	116
122	114	114	116
123	113	114	118
126	111	116	108
127	110	110	113
128	108	106	119
130	119	116	120
141	115	109	108
142	114	114	117
143	111	110	111
153	118	114	117
154	107	104	105

CELL NO.	INITIAL I(.46V)	AFTER FRONT CONTACT WELDING	AFTER GLASSING
201	105	---	112
202	116	---	116
203	117	---	119
207	111	---	112
211	111	---	110
214	112	---	113
215	111	---	116
216	114	---	107
217	112	---	114
222	114	---	116
227	112	---	112
228	115	---	117
233	115	---	119
234	113	---	112
235	109	---	111
237	111	---	112
238	113	---	112
240	113	---	113
AVG.	112.2	110.3	113.4
		.983	1.011
		-1.7%	+1.1%

The electrical performance variations, due to assembly of the second coupon group have been summarized in Tables 3.5-4 through 3.5-6. The results show a glassing gain in I_{sc} and that of the current at 0.46 volt ($I_{.46V}$) of 2.5 percent and 2.1 percent respectively.

The weld schedule for the first and second group of test coupons is given in Table 3.3-3. Figures 3.5-2 through 3.5-4 show the solar cell distribution by electrical performance for each test coupon made. The individual coupon groups were matched electrically based on the availability of cells at that time. The cell performance improved as more cell groups were received. The final electrical performance measurement was conducted under the Large Area Pulsed Solar Simulator (LAPSS). The current-voltage characteristics of a typical test coupons is shown in Figures 3.5-5. The comparison of the test results with those computed from the single glassed cell performance is illustrated in Table 3.5-7.

3.5.3 Module Solar Blanket

The three, eighty cell module solar blankets were assembled with four cells connected in parallel and twenty cells connected in series. Only one of the solar module blankets was to undergo thermal vacuum cycle testing prior to shipment to JPL. The front and rear views of the completed module solar blankets are shown in Figures 3.5-6 through 3.5-8.

The individual cells were matched into parallel configurations of four cells to provide a minimum module current of 540 mA at 0.46 volt for the first module and 524 mA for the second and third module blankets. The resulting cell distribution for each of these modules is summarized in Figures 3.5-9 through 3.5-11. The modules current-voltage characteristic, as measured under the LAPSS is illustrated in Figures 3.5-12 through 3.5-14. The inspection records of the modules after fabrication is shown in Figures 3.5-15 through 3.5-17.

A preliminary performance test of the modules revealed that module blanket S/N 2 had a shorted cell in the fourth parallel group after assembly, requiring the exchange of 2 cells in that group. The shorted cell No. 873 was exchanged with cell No. 896, and cracked cell No. 856 was exchanged with cell No. 899. The cell replacement method was the same as that described in concept (A), the first of the three concepts discussed in Section 3.7 of this report.

Table 3.5-4. Electrical Performance Variation due to Assembly of Test Coupon. Light Intensity: 135.3 mW/cm²; Temperature: 28°C; Cell Parameter: ISC

CELL NO.	Isc (mA)	
	Initial Readg.	After Weldg. & Glassg.
301	122.7	125.6
302	127.2	128.8
303	126.4	127.3
304	128.6	129.2
305	130.6	131.5
307	126.8	126.8
309	126.0	127.0
311	127.5	127.9
312	126.1	129.2
313	124.3	128.0
314	126.6	131.0
316	127.1	129.1
317	135.8	137.5
318	124.2	126.0
319	129.2	133.8
321	128.8	132.2
322	128.5	132.1
323	121.9	126.2
324	129.7	132.5
325	125.5	128.8
326	133.3	135.3
327	134.6	135.8
328	122.6	127.7
329	124.6	130.2
330	124.0	129.9
331	123.8	129.2
332	129.9	134.8
334	122.8	128.9
335	125.3	130.5
339	122.9	128.6

CELL NO.	Isc (mA)	
	Initial Readg.	After Weldg. & Glassg.
340	126.9	131.9
341	131.2	134.4
344	123.9	128.0
345	125.7	129.2
346	121.7	125.9
347	124.4	127.3
348	127.0	131.2
350	131.7	135.8
351	128.4	129.8
352	108.2	113.2
356	129.7	133.3
357	123.0	126.7
359	115.5	118.4
360	127.9	132.5
361	111.6	116.1
363	114.2	120.5
364	120.0	125.1
365	125.3	128.2
369	116.1	118.6
370	116.9	120.2
371	123.7	126.1
372	115.9	120.1
373	110.5	115.1
375	108.6	112.6
376	117.8	119.9
380	124.9	128.4
381	122.2	125.2
382	120.4	123.5
386	124.0	125.9
380	121.7	122.8

CELL NO.	Isc (mA)	
	Initial Readg.	After Weldg. & Glassg.
392	116.3	120.0
394	131.5	134.1
395	129.3	129.2
403	126.0	127.3
404	129.4	131.8
406	129.2	131.4
407	129.4	132.2
408	121.7	125.2
409	122.0	124.1
414	130.6	133.0
415	119.6	122.8
416	123.6	125.9
417	130.0	132.8
420	130.7	133.8
422	125.2	129.5
423	120.8	125.9
424	124.9	128.5
425	125.4	129.6
427	120.8	125.8
430	121.7	125.2
431	122.4	125.1
436	120.4	124.1
439	121.8	125.5
440	119.8	122.7
441	125.2	127.9
442	121.7	125.2
446	121.1	122.1
448	123.3	126.9
449	118.1	120.1
450	125.8	127.8
AVG	124.2	127.4

Table 3.5-5. Electrical Performance Variation due to Assembly of
Test Coupon. Light Intensity: 135.3 mW/cm²;
Temperature: 28°C; Cell Parameter: Voc

CELL NO.	Voc (v)	
	Initial Readg.	After Weldg. & Glassg.
301	543.3	543.3
302	543.7	541.7
303	543.7	543.3
304	543.2	540.3
305	539.3	538.5
307	537.2	537.2
309	536.8	537.3
311	536.3	536.2
312	570.2	569.9
313	564.5	563.7
314	564.7	564.7
316	562.2	563.1
317	575.5	575.3
318	566.7	566.8
319	563.3	564.2
321	569.0	568.2
322	562.7	560.4
323	558.3	558.7
324	561.7	561.2
325	564.3	565.6
326	568.0	568.0
327	565.3	563.1
328	565.2	563.7
329	570.0	569.6
330	563.7	564.6
331	561.0	560.8
332	556.4	556.4
334	565.2	565.8
335	573.4	574.8
339	573.3	573.0

CELL NO.	Voc (v)	
	Initial Readg.	After Weldg. & Glassg.
340	563.7	563.0
341	563.7	564.9
344	560.7	562.0
345	568.0	561.5
346	568.9	568.9
347	563.3	563.5
348	564.3	565.1
350	538.7	539.0
351	543.1	544.9
352	546.5	547.9
356	561.3	561.1
357	570.5	570.9
359	535.4	542.3
360	554.3	546.6
361	552.0	552.1
363	554.1	551.2
364	545.1	543.4
365	548.5	550.0
369	544.2	542.2
370	545.2	544.4
371	544.4	544.1
372	548.4	546.7
373	546.0	544.2
375	545.5	543.5
376	543.3	540.2
380	561.2	558.6
381	546.4	545.4
382	550.8	549.8
386	550.0	549.1
390	546.9	548.1

CELL NO.	Voc (v)	
	Initial Readg.	After Weldg. & Glassg.
392	546.8	549.1
394	550.2	551.8
395	549.2	546.0
403	544.4	547.6
404	555.0	554.4
406	552.0	553.0
407	547.6	549.4
408	549.8	549.7
409	546.1	547.2
414	544.3	534.8
415	538.8	538.3
416	543.2	544.6
417	550.4	549.8
420	551.8	553.1
422	543.0	545.0
423	554.8	555.9
424	548.0	549.0
425	547.5	550.7
427	544.0	544.9
430	545.6	548.1
431	542.9	543.5
436	550.3	551.7
439	550.5	550.3
440	548.1	543.1
441	546.2	545.2
442	551.7	551.6
446	546.2	546.5
448	551.6	552.2
449	546.2	548.7
450	547.6	546.2
AVG	553.1	558.7

Table 3.5-6. Electrical Performance Variation due to Assembly of Test Coupon. Light Intensity: 135.3 mW/cm²; Temperature: 28°C; Cell Parameter: I_{46V}

CELL NO.	I _{46V} (mA)	
	Initial Readg.	After Weldg. & Glassg.
301	116.8	115.0
302	114.3	114.4
303	113.4	113.8
304	113.3	111.6
305	115.7	115.8
307	111.4	110.9
309	110.4	110.8
311	111.2	110.8
312	119.6	121.9
313	115.0	116.7
314	118.2	122.0
316	115.5	116.9
317	129.2	131.6
318	117.2	119.0
319	121.6	126.6
321	117.9	121.6
322	126.8	122.2
323	113.9	118.8
324	116.3	118.6
325	117.8	122.8
326	125.7	127.2
327	126.6	127.3
328	113.8	119.6
329	115.9	123.1
330	116.3	121.1
331	115.3	121.3
332	114.9	118.0
334	115.9	121.8
335	119.5	123.5
339	116.3	120.2

CELL NO.	I _{46V} (mA)	
	Initial Readg.	After Weldg. & Glassg.
340	117.0	120.9
341	123.9	127.5
344	115.3	120.7
345	118.2	121.4
346	114.2	119.5
347	115.2	119.4
348	120.3	123.5
350	117.5	120.9
351	117.1	119.3
352	100.2	104.4
356	121.3	124.4
357	117.6	120.8
359	84.1	100.9
360	118.1	100.3
361	104.4	108.9
363	107.2	111.7
364	109.0	111.8
365	116.8	119.5
369	106.2	108.7
370	106.2	108.7
371	100.7	102.5
372	105.6	109.1
373	101.7	103.5
375	99.0	101.6
376	108.2	108.2
380	115.2	118.4
381	111.7	113.9
382	112.7	115.1
386	114.1	115.1
390	112.9	113.5

CELL NO.	I _{46V} (mA)	
	Initial Readg.	After Weldg. & Glassg.
392	107.7	111.2
394	120.9	123.2
395	120.3	119.2
403	115.1	118.4
404	120.1	121.9
406	118.5	120.5
407	118.8	120.0
408	113.6	117.0
409	112.8	115.2
414	118.2	97.8
415	108.2	109.9
416	110.8	112.8
417	119.7	120.9
420	121.6	125.2
422	113.4	118.2
423	112.5	116.9
424	114.8	118.4
425	110.0	120.3
427	110.9	114.0
430	110.8	115.2
431	109.3	111.8
436	111.9	115.2
439	113.3	110.4
440	109.0	111.9
441	113.9	110.8
442	112.2	115.3
446	110.8	112.2
448	110.8	117.1
449	108.7	111.8
450	114.8	116.1
AVG.	113.9	116.3

#1

#103 112 mA	#104 114 mA	#106 113 mA
#115 116 mA	#110 111 mA	#116 112 mA
#119 113 mA	#123 118 mA	#126 108 mA

#2

#118 120 mA	#108 109 mA	#113 111 mA
#109 114 mA	#120 116 mA	#128 119 mA
#142 117 mA	#127 113 mA	#157 110 mA

#4

#201 111 mA	#203 119 mA	#211 110 mA
#202 116 mA	#207 111 mA	#214 113 mA
#215 116 mA	#216 107 mA	#233 119 mA

#3

#122 116 mA	#143 111 mA	#155 112 mA
#153 116 mA	#154 105 mA	#159 119 mA
#141 108 mA	#130 120 mA	#158 111 mA

#5

#227 112 mA	#217 114 mA	#240 113 mA
#222 116 mA	#234 112 mA	#237 112 mA
#228 117 mA	#238 111 mA	#235 111 mA

Figure 3.5-2. Solar Cell Distribution by Electrical Performance
(Matched to provide coupon current of 339 mA at
1.38 volts)

#6

#301	#302	#313
115.0	114.4	116.7
#303	#307	#312
113.8	110.9	121.9
#304	#311	#325
111.6	110.8	122.8

#7

#305	#309	#323
115.8	110.8	118.8
#314	#364	#364
122.0	111.7	111.8
#318	#365	#369
119.0	119.5	108.7

#9

#392	#394	#350
111.2	123.2	120.9
#386	#390	#395
115.1	113.5	119.2
#361	#382	#329
108.9	115.1	123.1

#8

#332	#352	#356
118.0	104.4	124.4
#324	#326	#359
118.6	127.2	100.9
#327	#351	#360
127.3	119.3	100.3

#10

#375	#381	#317
101.6	113.9	131.6
#371	#316	#341
102.5	116.9	127.5
#370	#380	#321
108.7	118.4	121.6

Figure 3.5-3. Solar Cell Distribution by Electrical Performance
(Matched to provide minimum coupon current of 345 mA
at 1.38 volts)

#11	#373	#335	#346
	103.5	123.5	119.5
	#376	#339	#347
	108.2	120.2	119.4
	#372	#357	#344
	109.1	120.8	120.7

#12	#331	#319	#328
	121.3	126.6	119.6
	#322	#340	#345
	122.2	120.9	121.4
	#348	#330	#334
	123.5	121.1	121.8

#14	#422	#430	#446
	118.2	115.2	112.2
	#416	#408	#450
	112.8	117.0	116.1
	#417	#415	#442
	120.9	109.9	115.3

DOUBLE LOOP

#13	#409	#425	#439
	115.2	120.3	110.4
	#407	#431	#436
	120.0	111.8	115.2
	#404	#414	#420
	121.9	97.8	125.3

#15	#423	#448	#449
	116.9	117.1	111.8
	#406	#427	#441
	120.5	114.0	110.8
	#403	#424	#440
	118.4	118.4	111.9

Figure 3.5-4. Solar Cell Distribution by Electrical Performance
(Matched to provide minimum coupon current of 345 mA
at 1.38 volts)

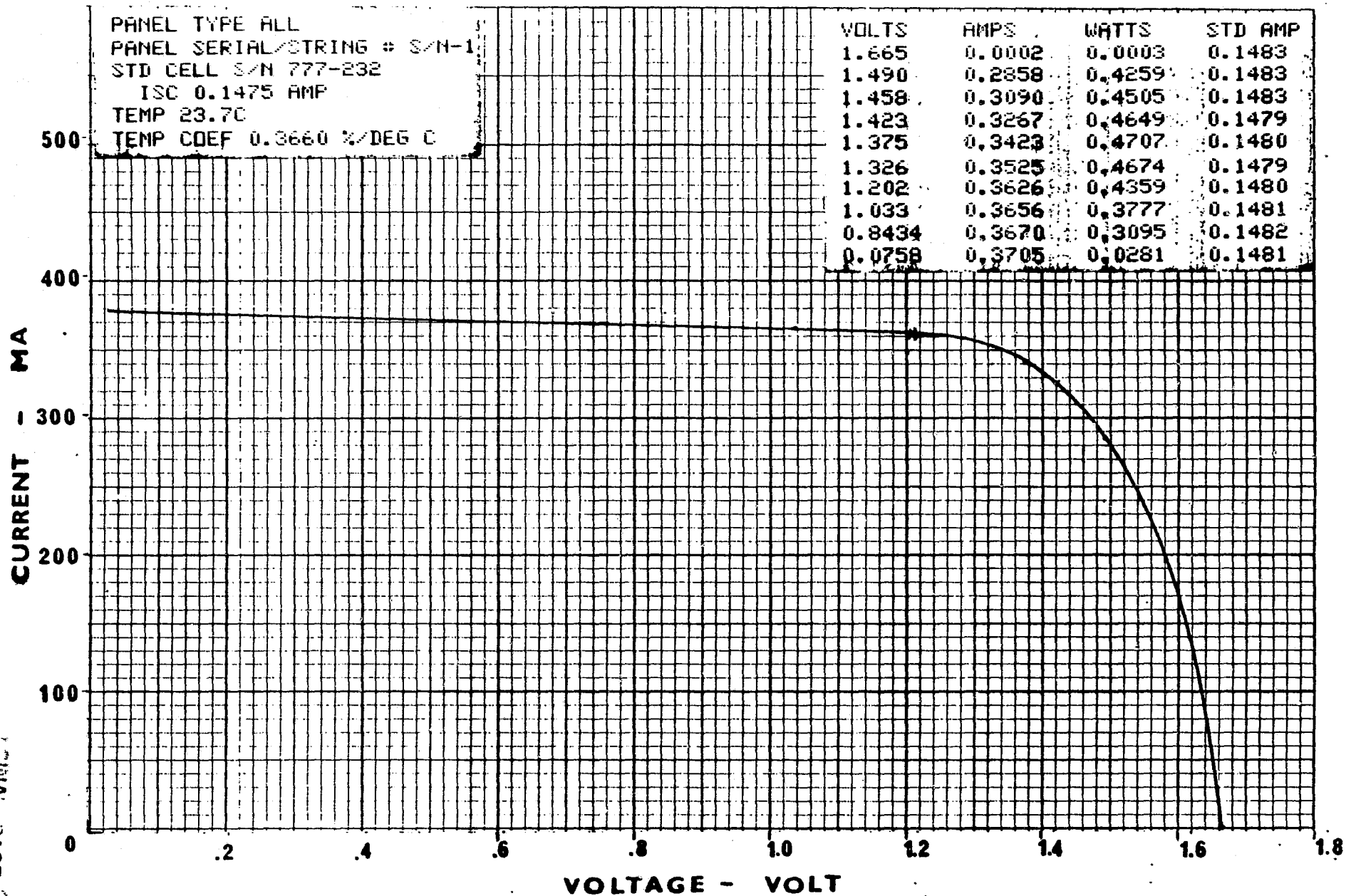
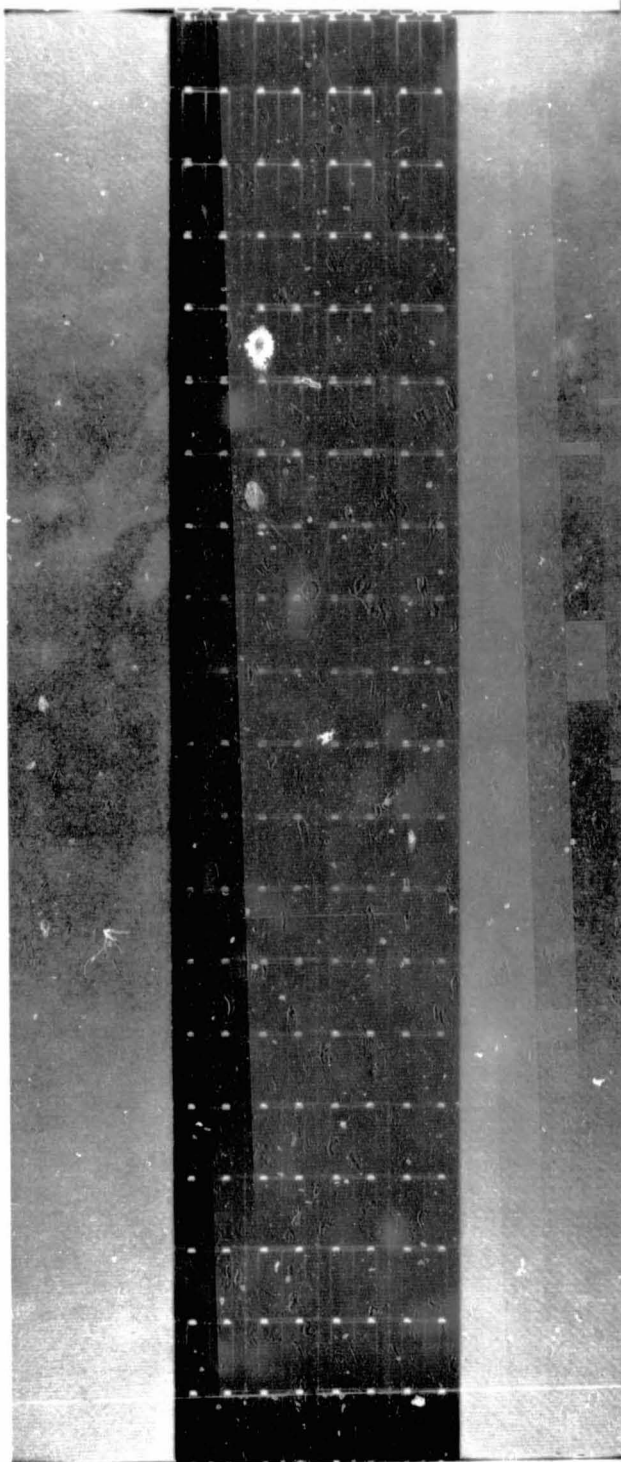


Figure 3.5-5. Test Coupon Current-Voltage Characteristic

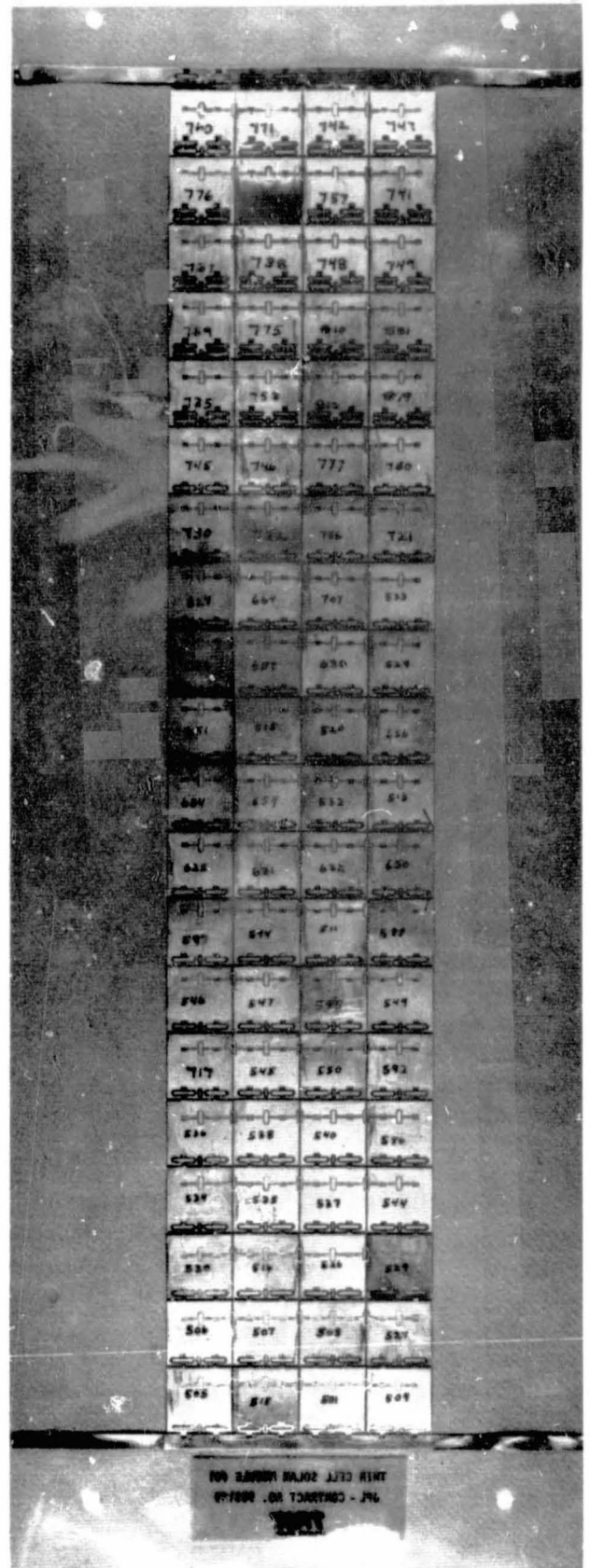
Table 3.5-7. Final Electrical Performance of Test Coupons

COUPON NO.	Computed (C) Coupon Performance I(1.38v)	Measured (M) Coupon Performance I(1.38v)	$\frac{M}{C}$
1	339	346	1.021
2	339	341	1.006
3	339	341	1.006
4	339	335	0.988
5	339	331	0.976
6	345	354	1.026
7	345	351	1.017
8	347	352	1.014
9	347	352	1.014
10	347	354	1.020
11	347	356	1.026
12	365	380	1.041
13	345	340	0.986
14	346	348	1.006
15	345	350	1.014



TWIN CELL SOLAR MODULE #01
JPL - CONTRACT NO. 955139

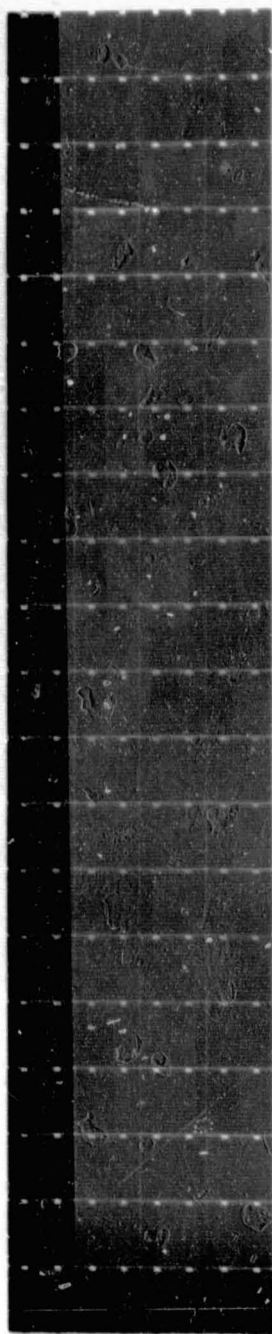
TRW
AEROSPACE GROUP



THIS CELL SOLAR MODULE #01
JPL - CONTRACT NO. 955139

TRW

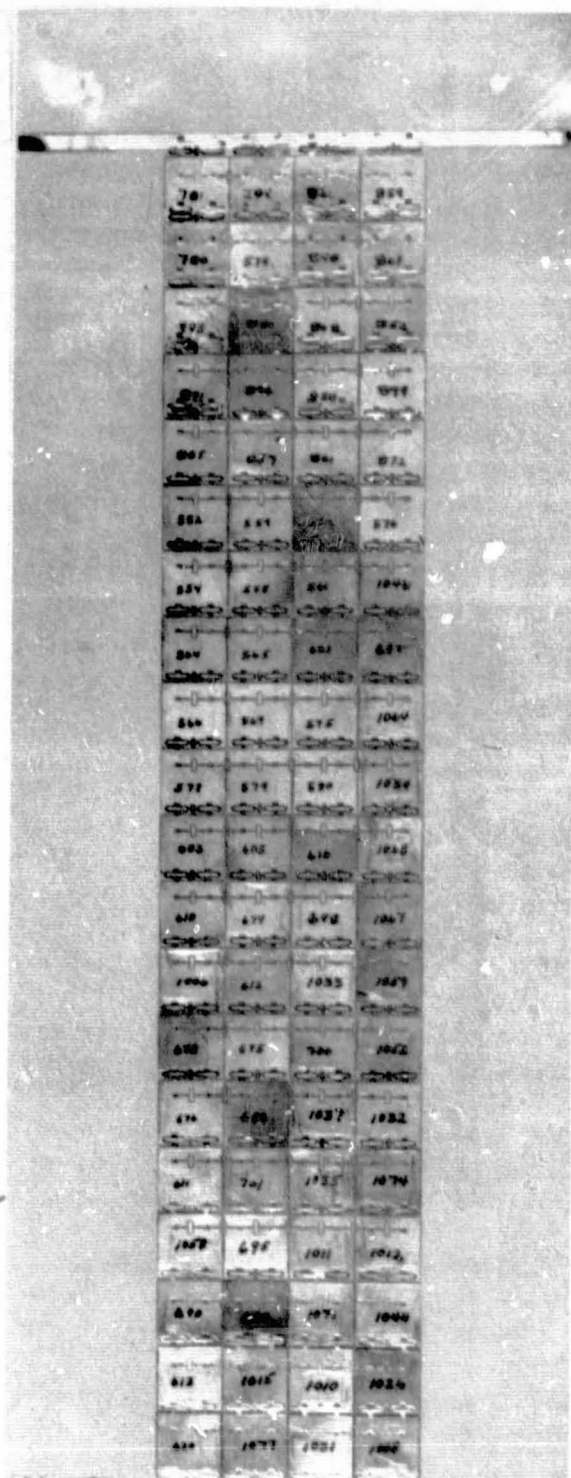
Figure 3.5-6. Module Solar Blanket, S/N 01 Front and Rear View



THIN CELL SOLAR MODULE S/N 02
JPL - CONTRACT NO. 955139

TRW

DEFENSE AND SPACE ELECTRONICS GROUP



THIN CELL SOLAR MODULE S/N 02
JPL - CONTRACT NO. 955139

TRW

DEFENSE AND SPACE ELECTRONICS GROUP

Figure 3.5-7. Module Solar Blanket, S/N 02 Front and Rear View
3.5-16

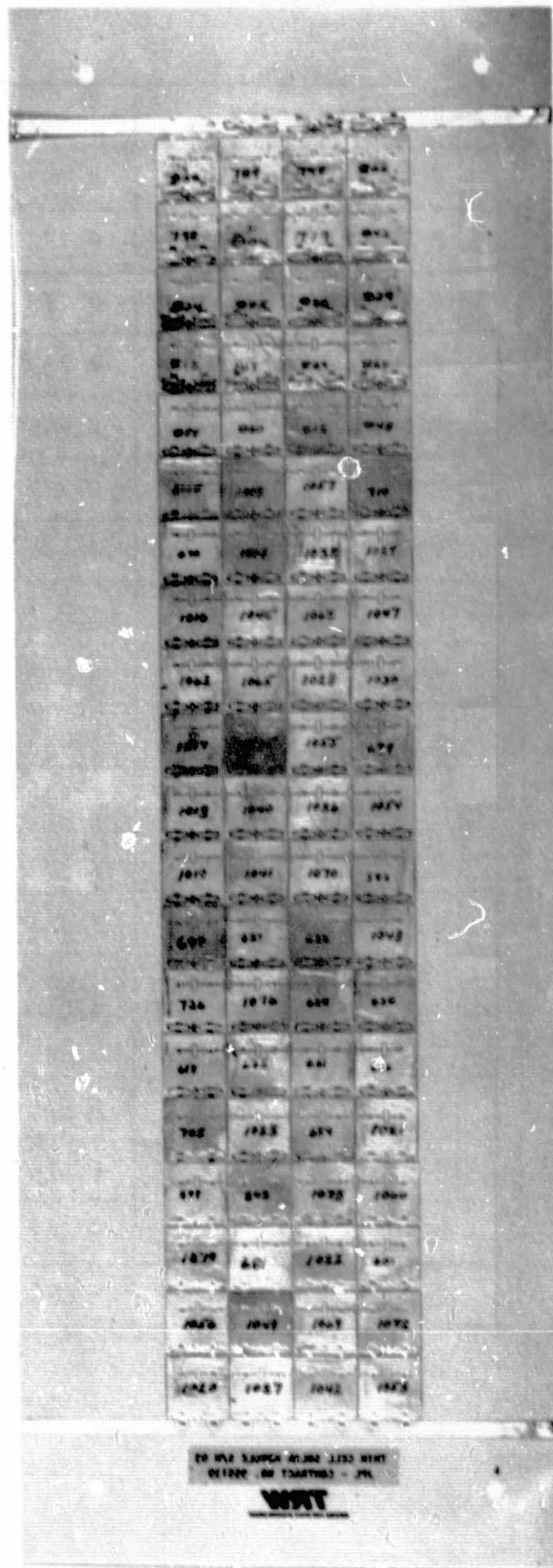
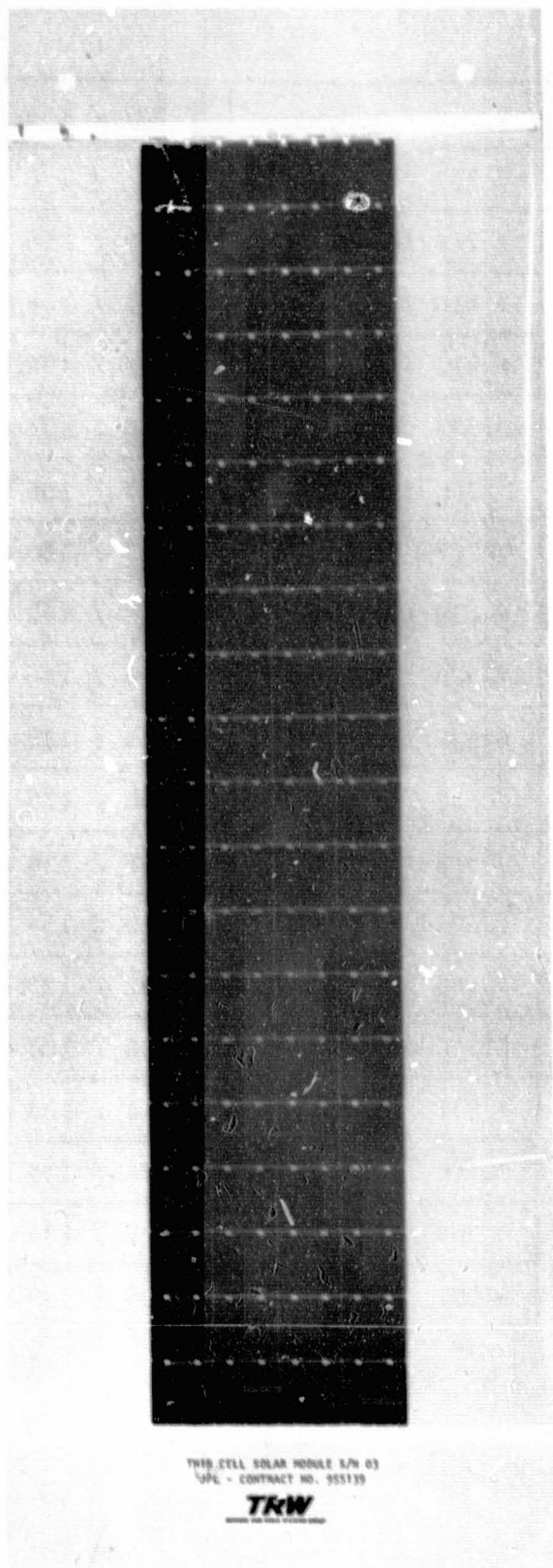


Figure 3.5-8. Module Solar Blanket, S/N 03 Front and Rear View

DOUBLE LOOPS	# 517 / 139 mA	# 771 / 129 mA	# 742 / 135 mA	# 747 / 139 mA
	# 776 / 131 mA	# 782 / 134 mA	# 757 / 138 mA	# 741 / 138 mA
	# 737 / 128 mA	# 738 / 138 mA	# 748 / 137 mA	# 749 / 136 mA
	# 759 / 133 mA	# 775 / 132 mA	# 810 / 139 mA	# 831 / 136 mA
	# 735 / 133 mA	# 753 / 137 mA	# 812 / 135 mA	# 849 / 134 mA
	# 745 / 130 mA	# 746 / 129 mA	# 777 / 143 mA	# 750 / 137 mA
	# 730 / 129 mA	# 722 / 136 mA	# 706 / 138 mA	# 721 / 136 mA
	# 627 / 139 mA	# 664 / 133 mA	# 707 / 133 mA	# 533 / 138 mA
	# 655 / 127 mA	# 657 / 130 mA	# 630 / 140 mA	# 528 / 142 mA
	# 651 / 123 mA	# 515 / 142 mA	# 520 / 139 mA	# 656 / 136 mA
SINGLE LOOPS	# 634 / 129 mA	# 654 / 129 mA	# 532 / 144 mA	# 513 / 138 mA
	# 625 / 135 mA	# 631 / 135 mA	# 632 / 135 mA	# 650 / 135 mA
	# 587 / 127 mA	# 594 / 141 mA	# 511 / 140 mA	# 588 / 130 mA
	# 546 / 133 mA	# 547 / 133 mA	# 595 / 137 mA	# 549 / 136 mA
	# 717 / 138 mA	# 545 / 133 mA	# 550 / 141 mA	# 592 / 135 mA
	# 536 / 124 mA	# 538 / 141 mA	# 540 / 144 mA	# 586 / 130 mA
	# 534 / 127 mA	# 535 / 137 mA	# 537 / 137 mA	# 544 / 138 mA
	# 530 / 134 mA	# 516 / 136 mA	# 526 / 135 mA	# 529 / 135 mA
	# 506 / 136 mA	# 507 / 130 mA	# 508 / 140 mA	# 527 / 134 mA
	# 505 / 136 mA	# 518 / 124 mA	# 501 / 140 mA	# 509 / 139 mA

Figure 3.5-9. Solar Cell Distribution by Electrical Performance (I_{46V})
Matched to Provide Minimum Module Current of 540 mA at
9.2 Volts, Module S/N 1

DOUBLE LOOPS	# 781 / 139 mA	# 784 / 138 mA	# 821 / 111 mA	# 859 / 136 mA
	# 780 / 134 mA	# 574 / 139 mA	# 848 / 129 mA	# 867 / 125 mA
	# 793 / 134 mA	# 850 / 128 mA	# 868 / 136 mA	# 852 / 127 mA
	# 871 / 144 mA	# 896 / 137 mA	# 858 / 130 mA	# 899 / 116 mA
	# 855 / 130 mA	# 857 / 131 mA	# 861 / 131 mA	# 872 / 138 mA
	# 552 / 139 mA	# 559 / 129 mA	# 602 / 128 mA	# 576 / 128 mA
	# 554 / 132 mA	# 558 / 139 mA	# 561 / 129 mA	#1046 / 124 mA
	# 564 / 141 mA	# 565 / 132 mA	# 621 / 133 mA	# 687 / 118 mA
	# 566 / 135 mA	# 569 / 130 mA	# 575 / 131 mA	#1064 / 128 mA
	# 577 / 130 mA	# 579 / 132 mA	# 580 / 130 mA	#1034 / 132 mA
SINGLE LOOPS	# 603 / 135 mA	# 605 / 134 mA	# 616 / 131 mA	#1068 / 125 mA
	# 610 / 140 mA	# 674 / 130 mA	# 698 / 131 mA	#1067 / 123 mA
	#1006 / 136 mA	# 612 / 137 mA	#1033 / 126 mA	#1059 / 125 mA
	# 673 / 135 mA	# 675 / 134 mA	# 700 / 130 mA	#1052 / 126 mA
	# 676 / 134 mA	# 686 / 134 mA	#1037 / 127 mA	#1032 / 129 mA
	# 611 / 141 mA	# 701 / 131 mA	#1035 / 127 mA	#1074 / 125 mA
	#1058 / 135 mA	# 695 / 134 mA	#1011 / 130 mA	#1012 / 130 mA
	# 690 / 135 mA	# 694 / 135 mA	#1071 / 129 mA	#1044 / 130 mA
	# 613 / 136 mA	#1015 / 130 mA	#1010 / 130 mA	#1026 / 131 mA
	# 620 / 138 mA	#1077 / 128 mA	#1031 / 146 mA	#1008 / 131 mA

Figure 3.5-10. Solar Cell Distribution by Electrical Performance ($I_{sc} = 46V$)
Matched to Provide Minimum Module Current of 524 mA at
9.2 Volts, Module S/N 2

DOUBLE LOOP	# 808 / 135 mA	# 789 / 131 mA	# 795 / 126 mA	# 800 / 132 mA
	# 798 / 133 mA	# 804 / 132 mA	# 779 / 136 mA	# 842 / 123 mA
	# 824 / 140 mA	# 835 / 125 mA	# 838 / 126 mA	# 829 / 133 mA
	# 813 / 130 mA	# 817 / 131 mA	# 834 / 131 mA	# 864 / 132 mA
	# 854 / 130 mA	# 860 / 135 mA	# 875 / 128 mA	# 843 / 131 mA
SINGLE LOOP	#1004 / 138 mA	#1009 / 135 mA	#1057 / 132 mA	# 714 / 123 mA
	# 670 / 132 mA	#1014 / 134 mA	#1038 / 132 mA	#1029 / 145 mA
	#1016 / 137 mA	#1045 / 131 mA	#1063 / 132 mA	#1047 / 130 mA
	#1062 / 133 mA	#1065 / 133 mA	#1028 / 142 mA	#1030 / 141 mA
	#1017 / 135 mA	#1075 / 134 mA	#1055 / 135 mA	# 679 / 134 mA
	#1013 / 134 mA	#1040 / 134 mA	#1036 / 134 mA	#1054 / 135 mA
	#1019 / 139 mA	#1041 / 137 mA	#1070 / 136 mA	# 582 / 124 mA
	# 697 / 129 mA	# 637 / 126 mA	# 623 / 128 mA	#1048 / 142 mA
	# 726 / 129 mA	#1076 / 128 mA	# 624 / 137 mA	# 638 / 131 mA
	# 617 / 132 mA	# 635 / 133 mA	# 661 / 132 mA	# 646 / 132 mA
	# 705 / 133 mA	#1023 / 141 mA	# 659 / 134 mA	#1021 / 143 mA
	# 599 / 138 mA	# 593 / 137 mA	#1073 / 134 mA	#1066 / 137 mA
	#1078 / 136 mA	# 681 / 137 mA	#1022 / 141 mA	# 601 / 139 mA
	#1056 / 138 mA	#1049 / 139 mA	#1069 / 136 mA	#1072 / 139 mA
	#1020 / 137 mA	#1027 / 135 mA	#1042 / 137 mA	#1053 / 136 mA

Figure 3.5-11. Solar Cell Distribution by Electrical Performance (I_{sc} 46V)
Matched to Provide Minimum Module Current of 524 mA at
9.2 Volts, Module S/N 3

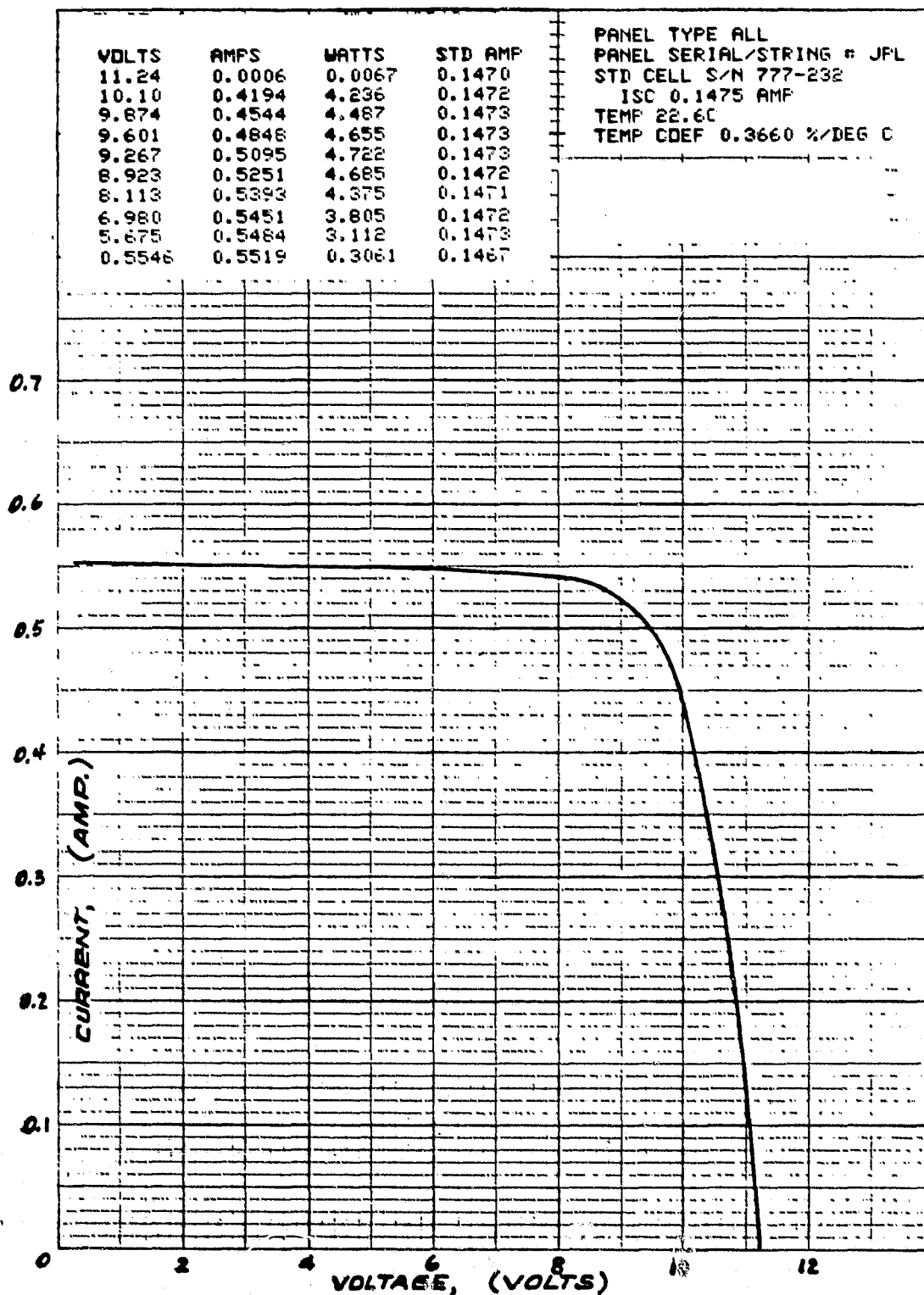


Figure 3.5-12. Module Solar Blanket Current-Voltage Characteristic, S/N 01

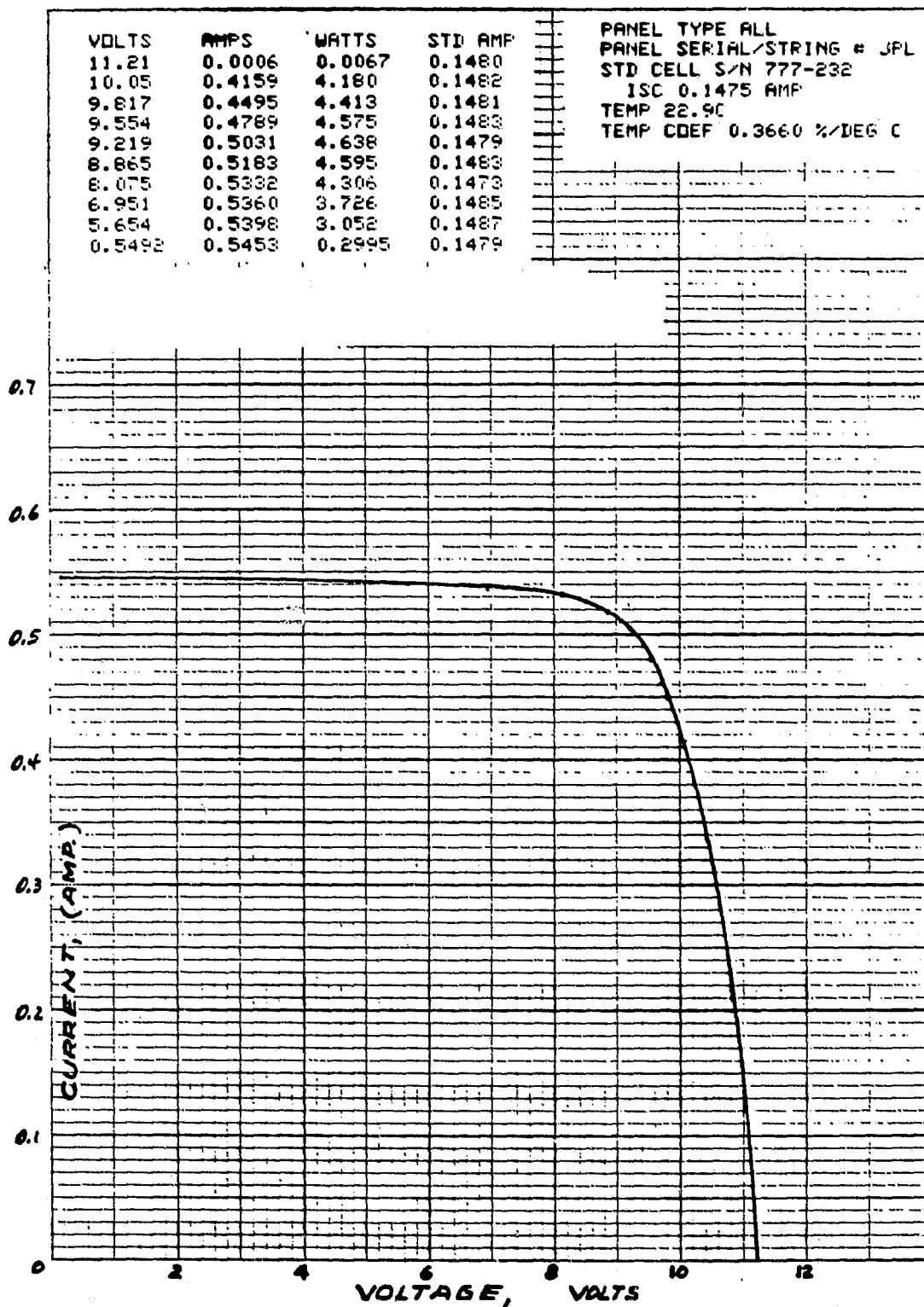


Figure 3.5-13. Module Solar Blanket Current-Voltage Characteristic, S/N 02

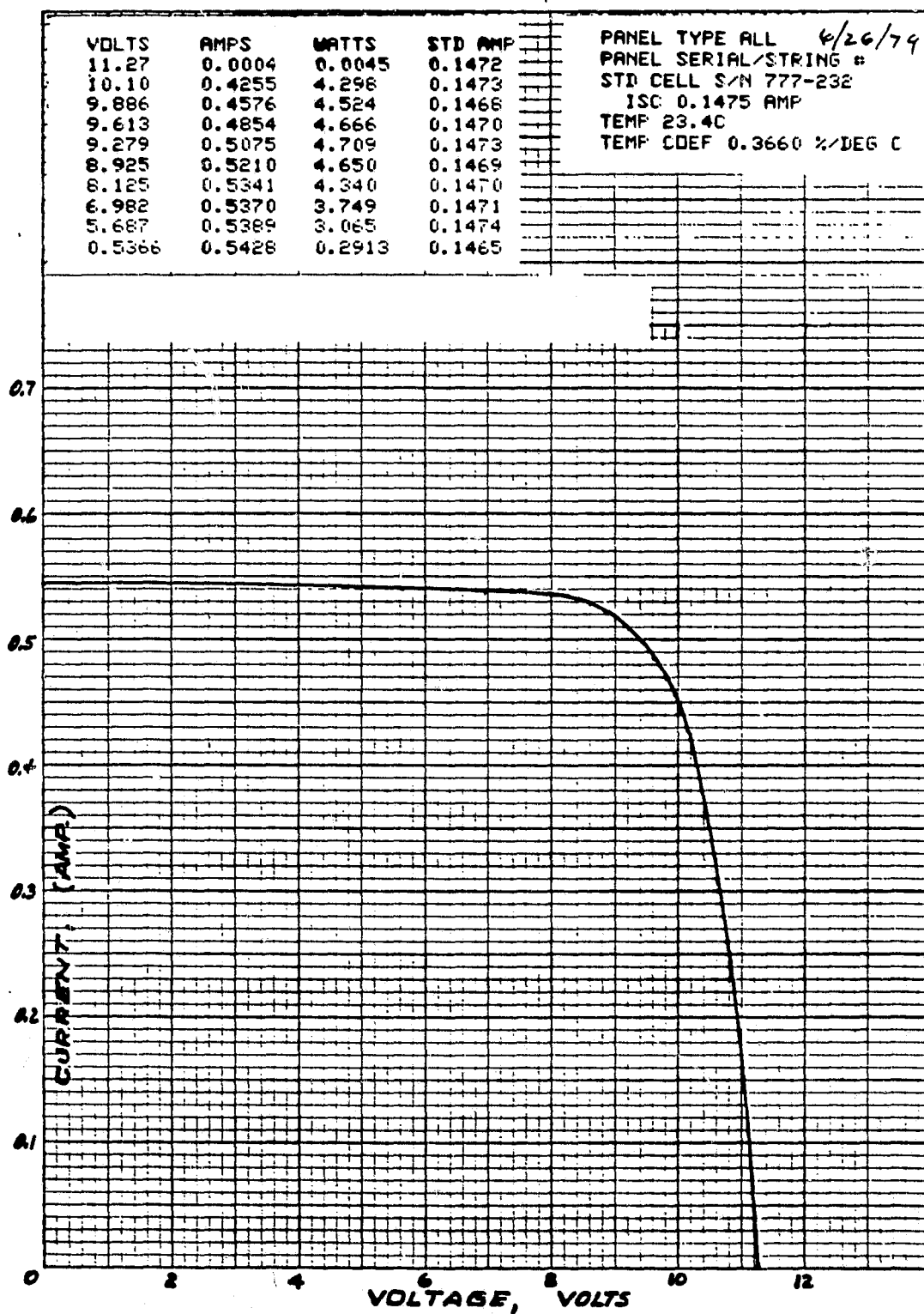
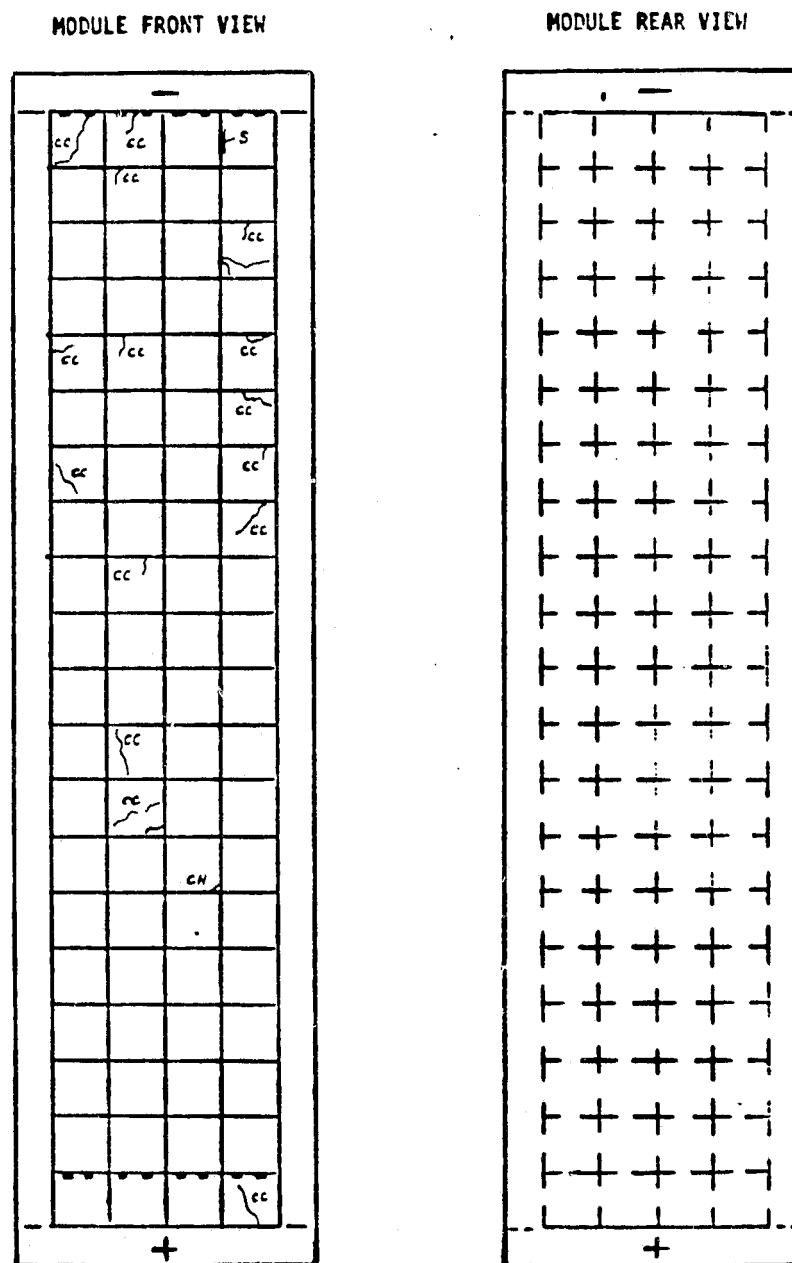
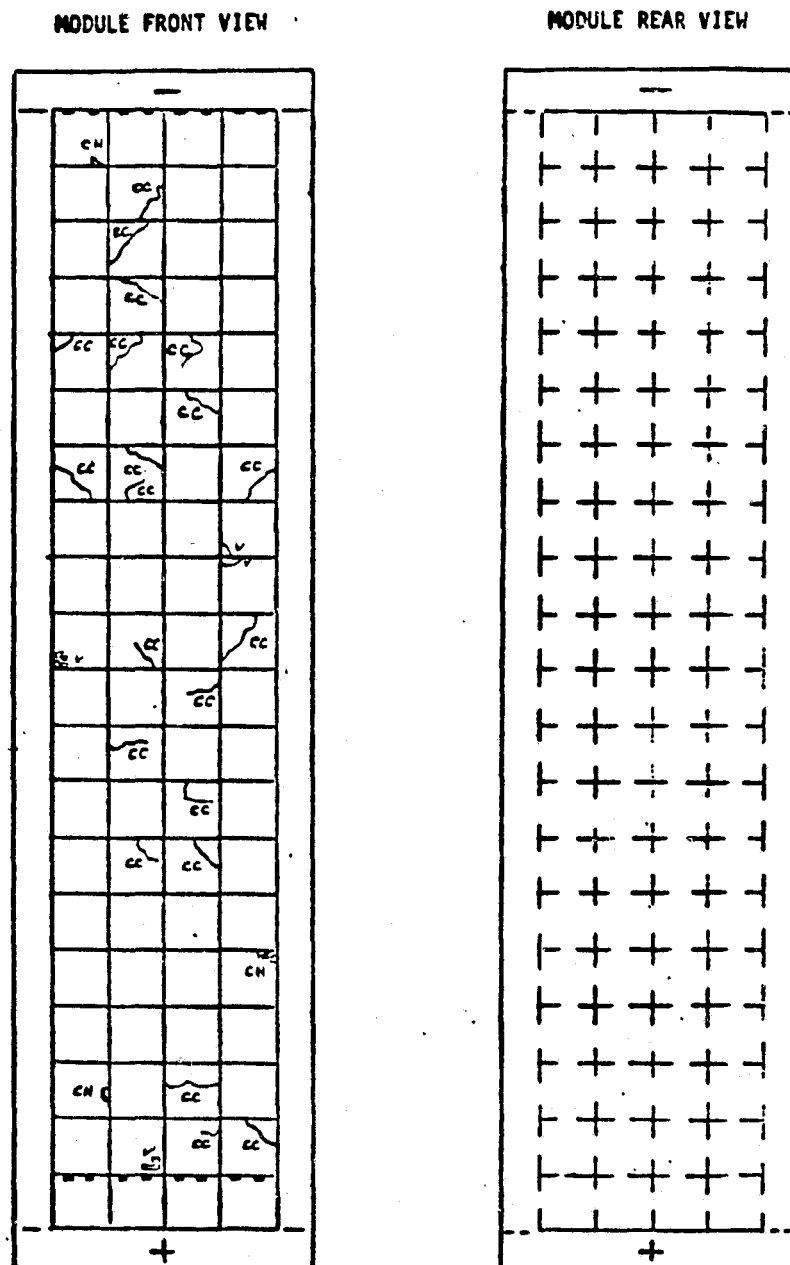


Figure 3.5-14. Module Solar Blanket Current-Voltage Characteristic, S/N 03



DISCREPANCIES: CC = Cracked Coverglass
 CH = Chipped Coverglass
 V = Void under Coverglass
 S = Spacing between Coverglass out of Spec.

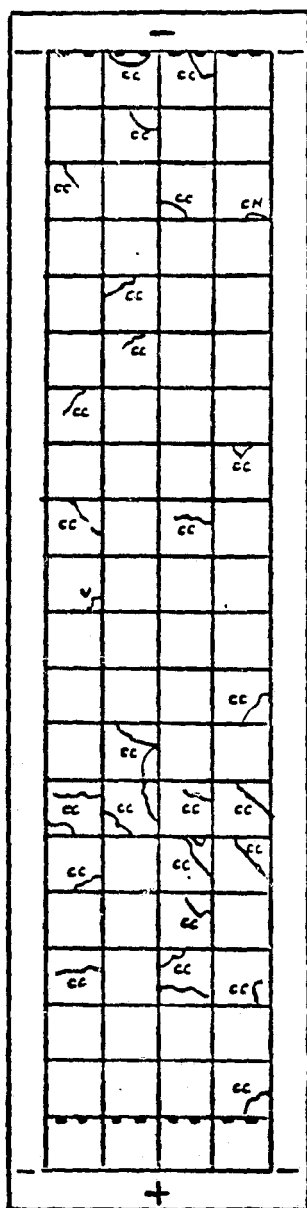
Figure 3.5-15. Inspection Record of First Module Solar Blanket (S/N 01) After Assembly



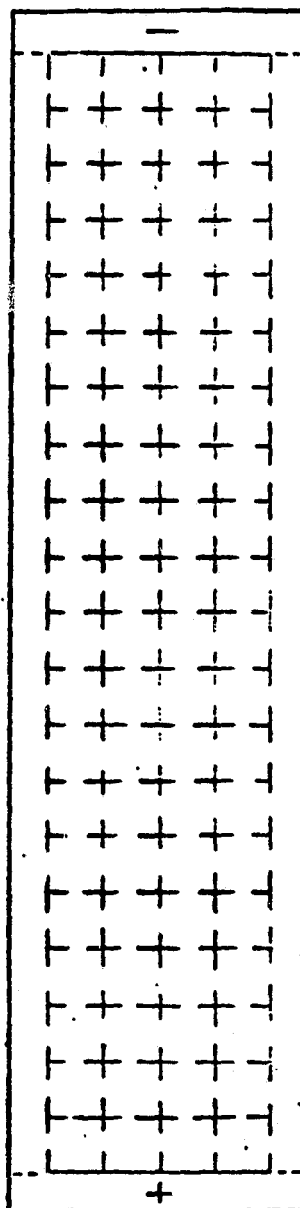
DISCREPANCIES: CC = Cracked Coverglass
 CH = Chipped Coverglass
 V = Void under Coverglass
 S = Spacing between Coverglass out of Spec.

Figure 3.5-16. Inspection Record of Module Solar Blanket (S/N 02)

MODULE FRONT VIEW



MODULE REAR VIEW



DISCREPANCIES: CC = Cracked Coverglass
 CH = Chipped Coverglass
 V = Void under Coverglass
 S = Spacing between Coverglass out of Spec.

Figure 3.5-17. Inspection Record of Module Solar Blanket (S/N 03)

The weight of each completed module solar blanket was determined: (a) for their overall weights, and (b) for the module blanket area covered by solar cells only. For this 4.02 grams were subtracted from the module weight for the excess Kapton substrate surrounding the cell-occupied area. The weight data is summarized in Table 3.5-8. From this data and the electrical performance of the first module assembled, a power-to-mass ratio of 250 W/kg has been determined (for 1 Sun, AM = 0, 28°C conditions). The average bare single cell performance of the cells used in the first module was 62.47 mW. The optimum module performance at 9.4 volts is 4.75 watt (Figure 3.5-12).

Table 3.5-8. Module Solar Blanket Weight Summary

Module No.	Overall Weight (g)	Weight of Cell Occupied Area (g)	P _{max} (W)	W/Kg
1	23.04	19.02	4.75	250
2	23.27	19.25	4.66	242
3	23.46	19.44	4.70	242
Average	23.257	19.237	4.703	245

3.6 DEVELOPMENT TESTING

Development tests were performed to verify the compliance of the solar cell test coupons with the requirements established in the contract and to gain the understanding of the test coupon's electrical and mechanical behavior under typical environmental stresses, such as thermal soaks, and thermal vacuum cycling-testing.

Ten test coupons were subjected to four thermal soak tests, with a duration of 24 hours for each test. The test temperatures were 120°C, 170°C and -120°C, -180°C for the temperature soaks. This test was followed by 100 thermal vacuum cycles between 120°C to -180°C with 30-minute soaks at the temperature extremes employing the facilities shown in Figure 3.6-1. The ten test coupons, each 4- by 6-inch in size, were suspended in a fiberglass frame using wires (Figure 3.6-2). The fiberglass frame was mounted in the vertical position onto the rotatable inner chamber assembly which in turn is able to rotate about its central axis by 90 degrees and back. In one location the test coupons were facing tungsten filament heaters and in the other location a liquid nitrogen cooled wall. Cold wall and heater were maintained at constant temperature. Temperature cycling of the coupons is achieved by rotating the inner chamber assembly into alternate positions. Two thermocouples were attached to two additional control modules. The temperature profile is shown in Figure 3.6-3. The chamber vacuum was held at 2×10^{-6} torr.

The ten test coupons were inspected and their electrical performance tested prior to and following each environmental exposure. Nine of the ten test coupons showed no electrical degradation, one coupon showed a 3.4 percent reduction in power after the first temperature soak at 120°C and an additional 3 percent reduction in power after the 100 thermal vacuum cycles. The failure is believed to be caused by a broken cell in the module (S/N 8), which could not be confirmed during the original inspection. The module performance data is summarized in Table 3.6-1.

No weld-joint facilities were formed after testing. The major discrepancies recorded, prior to and after the various thermal soak and temperature cycling tests were in the area of cover glass cracking. The distribution of the cover glass cracks is summarized in Table 3.6-2, showing 37 cracks occurring after coupon fabrication, and additional cracks

after the various thermal-soak and - cycling tests bringing the total number of cracks to 71, and thus affecting a total of 49 covers.

Additional thermal cycling was performed on the second (S/N 02) of 3 module solar blankets. The module was subjected to 24 thermal vacuum cycles between +70° and -110°C with 30 minute soaks at the temperature extremes. The electrical module performance following this test showed that the module solar blanket has not degraded electrically; however, about 50% more coverglass cracks were formed after the test.

ORIGINAL PAGE IS
OF POOR QUALITY

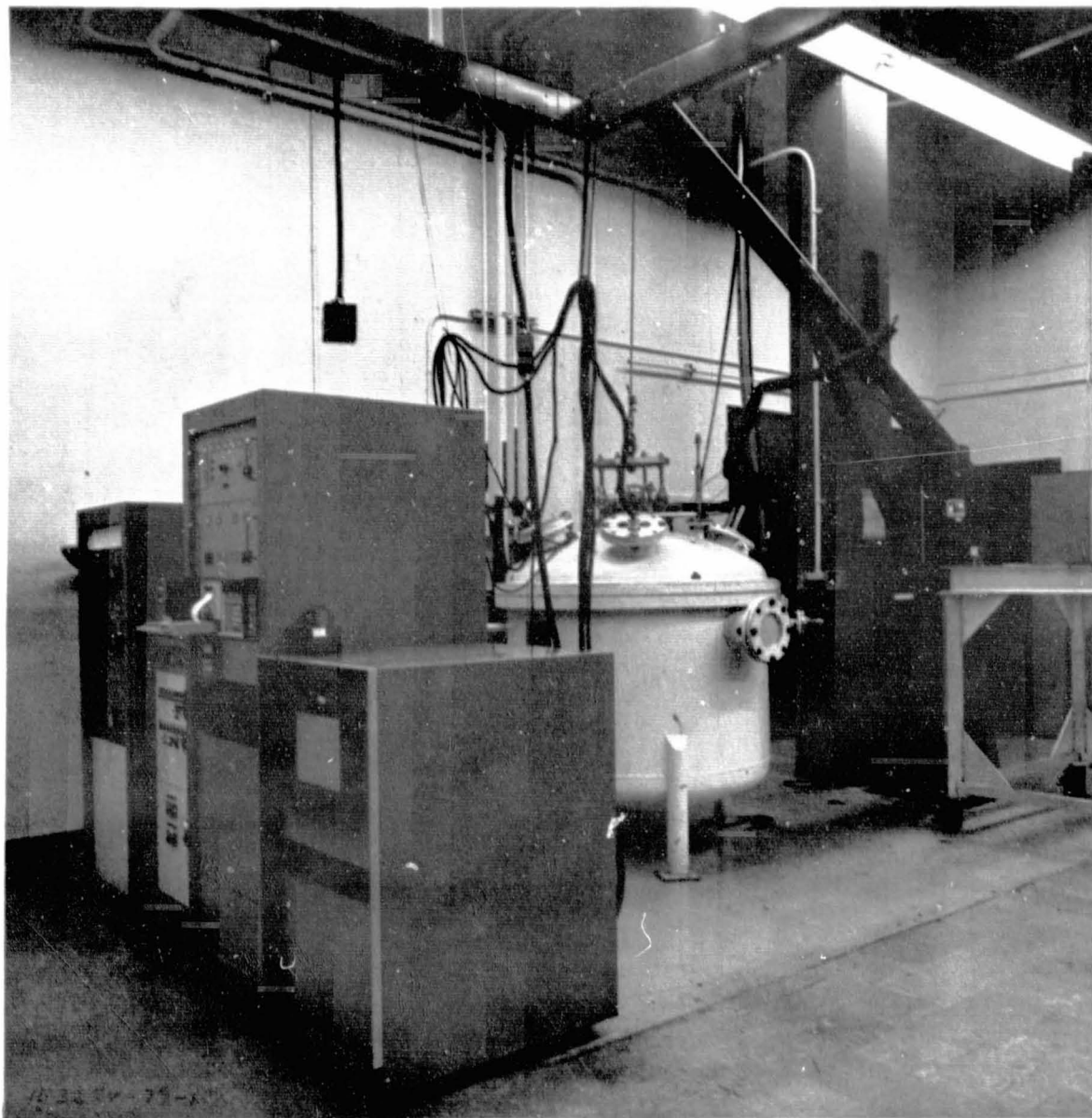
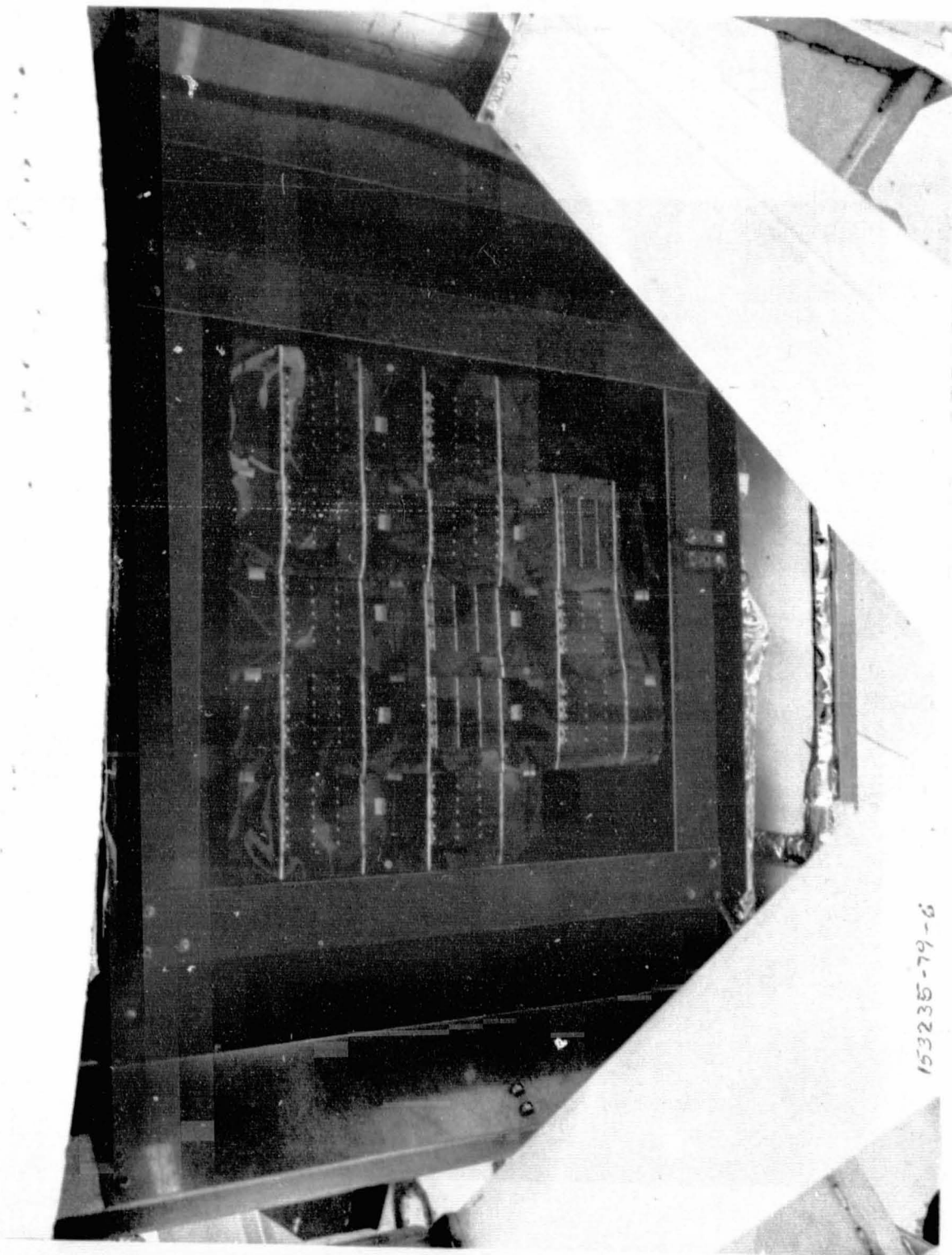


Figure 3.6-1. Overall View of Thermal Vacuum Test Facility Employed for Test Coupon Thermal Cycling Test

Figure 3.6-2. View into Thermal Vacuum Test Fixture Showing Ten (JPL) Test Coupons Suspended in Fiberglass Frame



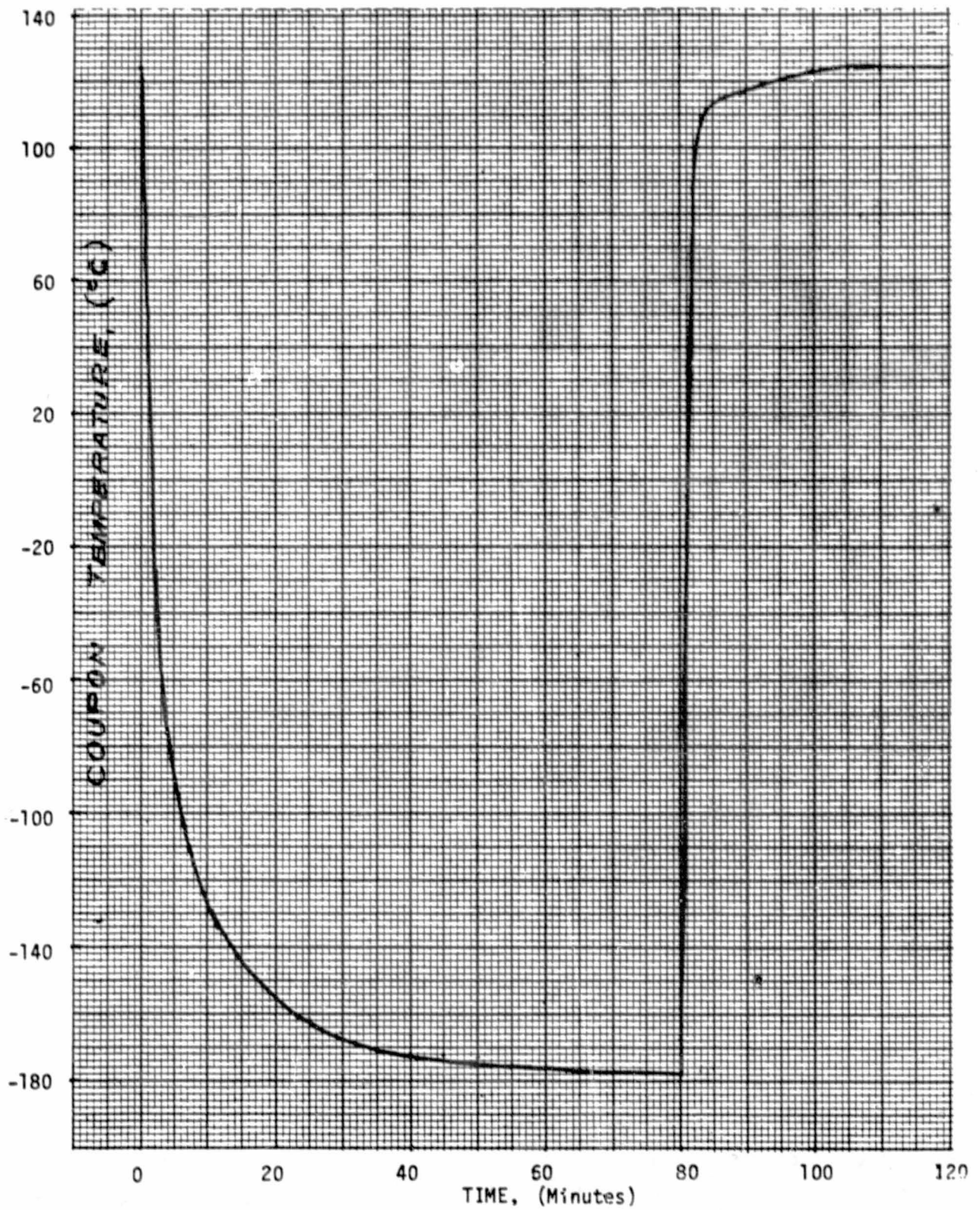


Figure 3.6-3. Typical Temperature Profile of Test Coupon (Chamber Vacuum was held at 2×10^{-6} Torr.)

Table 3.6-1. Electrical Performance of Test Coupons

Coupon No.	COUPON CURRENT AT 1.38 VOLTS (mA)					
	Initial Measurement	Post 24 Hr. Soak at 120°C	Post 24 hr. Soak at 170°C	Post 24 hr. Soak at -120°C	Post 24 hr. Soak at -180°C	Post Therm. Vacuum Cycl.
6	354	352	351	352	352	357
7	351	350	351	351	350	351
8	352	340	342	342	342	330
9	352	351	352	352	360	358
10	354	355	357	357	359	360
11	356	360	359	360	360	362
12	380	380	381	381	381	384
13	340	340	338	336	340	344
14	348	343	349	347	345	350
15	350	346	347	350	348	350

Table 3.6-2. Count of Cracked Cover Slides

COUPON NO.	INITIAL INSPECTION	AFTER 24 HR - THERMAL SOAK TEST AT				AFTER 100 Vacuum Thermal Cycles FROM 120°C TO -180°C
		120°C	170°C	-120°C	-180°C	
6	5	1	1	1	0	0
7	3	1	2	0	1	1
8	3	1	1	1	1	0
9	2	1	0	0	0	0
10	2	1	0	0	1	1
11	2	0	0	0	0	0
12	2	1	0	0	0	0
13	5	1	1	2	0	0
14	4	0	3	1	2	0
15	9	3	2	0	0	2
TOTAL	37	10	10	5	5	4

3.7 REPAIR STUDY

Several thin cells were removed from a typical 9-cell module assembly. A 75 m (0.003-inch) thick sharpened spatula was developed for the separation of the cell from the substrate. The weld joints was separated using a fork-type tool. None of the surrounding cells was damaged during the cell removal.

For the cell replacement, three options were evaluated which are best illustrated in Figure 3.7-1. Concepts A and B show the welded approach, employing conventional welding; i.e., the weld electrodes are in the vertical position requiring a firm flat horizontal substrate. In concept A both interconnector contacts are bent over the cells to which they remain attached after the faulty cell is removed. The new bare thin cell is pushed below the left interconnector, face down, where it is positioned properly on top of the neighboring cell. The interconnector is welded to the rear side of the new cell. Thereafter the new cell is rotated 180 degrees using a flat support. The interconnectors on the right side are bent over the new cell contacts and welded to the new cell in the same manner. This process is followed by the bondings of cover-to-cell and cell-to-substrate. This method works quite well and is the recommended technique.

An alternate approach of cell replacement is shown in Figure 3.7-1b. An interconnector ribbon is welded separately, first to the rear cell side, using a conventional welding fixture. From there the cell with the tab is transferred to the module where the tab is welded to the existing interconnector, thus completing the rear cell contact connection. Front side welding is performed in the same manner as described for Figure 3.7-1a.

The third cell replacement method is applied only in those areas where weld equipment cannot be handled, such as super large array blankets or areas where a firm flat substrate below the cell to be replaced may not be available. In this case cell replacement is achieved by means of reflow soldering, utilizing a 250-watt floodlight (about 2 to 3 inches above the replacement cell). High temperature solder-preforms, held in place with flux, will provide the means to join the cell contact with the interconnector. During this operation the surrounding cells are protected by a heat shield, consisting of five layers of aluminum foil separated by four layers

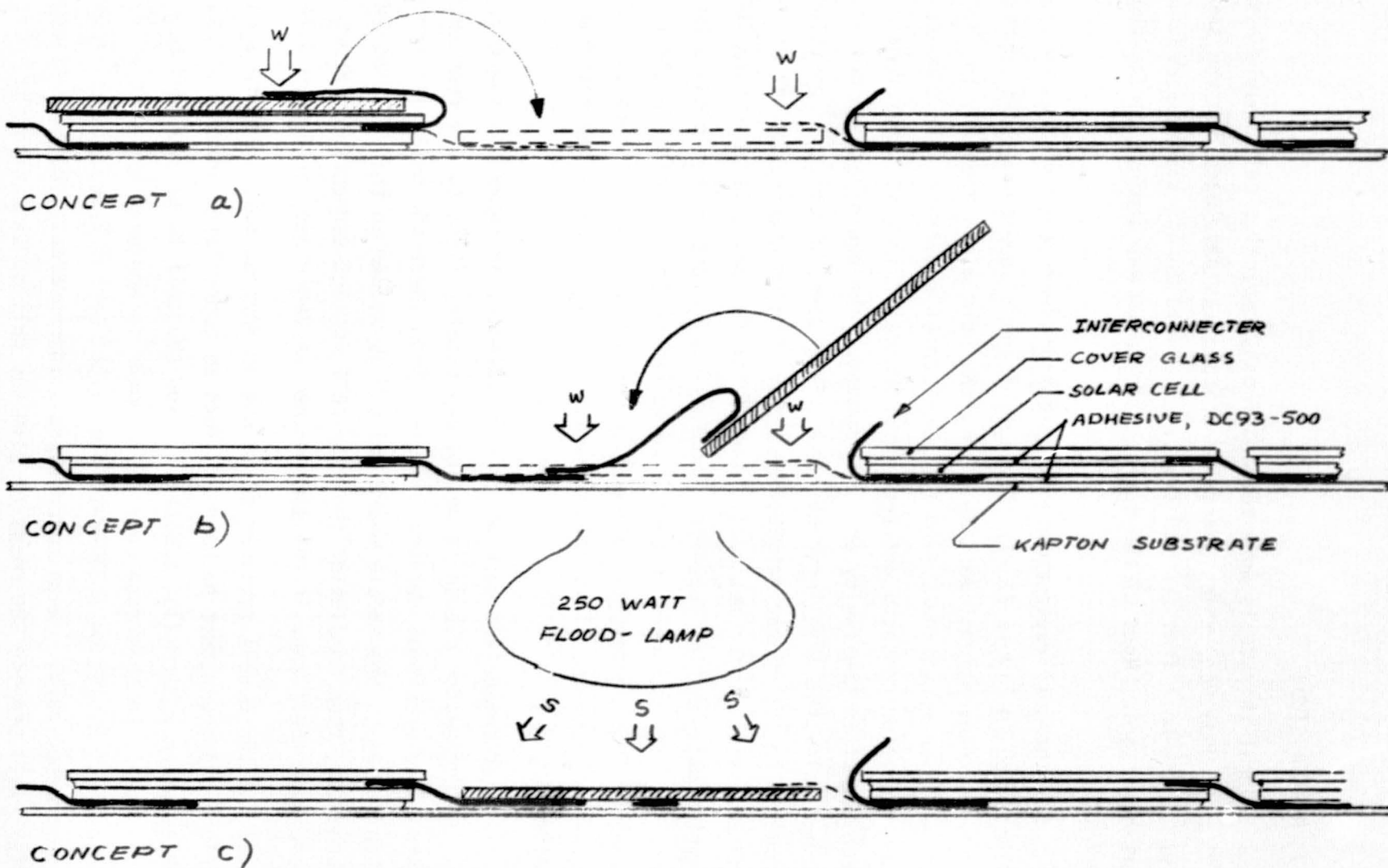


Figure 3.7-1. Three Options of Cell Replacement, Employing Welding and Reflow Soldering

of paper. The replacement cell is exposed through the center opening of the heat shield, 2.3 by 2.3 cm in size.

For all cell replacement approaches, with the exception of the reflow soldered method, the interconnector bar connecting the replacement cell in parallel with the other cells has been omitted thus far. This shortcoming will not alter the module performance.

3.7.1 Detailed Solar Cell Replacement

The following section describes the detailed procedure employed for the replacement of solar cells in solar module blankets.

3.7.1.1 Cell Removal

The filter glass, covering the interconnector on the front side of the faulty cell, is chipped away until both interconnector tabs are exposed. The interconnectors tabs are separated from the cell and bent over the cell to which they remain attached. A thin sharpened spatula is carefully inserted from three different sides below the faulty cell in order for the cell to be separated from the substrate and from the interconnector welded to the rear side of the cell. Periodic wetting of the spatula with alcohol helps in the separation of the faulty cell.

3.7.1.2 Preparation of Interconnectors and Substrate

Once the faulty cell is freed, the adhesive is removed from the interconnectors (formerly below the cell) and the interconnector is bent over the cell to which it is attached. The back side of the interconnector is cleaned in this position, as it is resting on the cover glass. Afterwards the adhesive is removed from the substrate. Next, the silicon particles from the faulty cell left on the interconnector tabs need to be removed. An X-acto knife will serve best for this operation, as a thin metallic shim is placed below the interconnector for the protection of the filter glass below. In some cases it will be difficult to completely remove all silicon particles from the interconnector tabs; for this reason the weldable interconnector area will be insufficient for a good weld joint. In these instances the interconnector tabs facing the front cell contacts are tinned.

3.7.1.3 Installation of New Cells

The new bare solar cell is placed face down, below the interconnector loop on top of the neighboring cell, as shown in Figure 3.7-1a. The replacement cell is aligned with the edge of the interconnector; the cell sides are aligned with the cell on which the replacement cell rests. After the interconnector is welded to the rear side of the replacement cell, the same cell is then rotated 180 degrees using the flat shim to support the thin cell during this operation. Once good cell positioning is assured the new cell is gently lifted, a drop of adhesive is placed below the cell and then brought back to its normal position. A weight on top of the cell assures proper cell-to-substrate bonding. Approximately 30 minutes later the interconnector tabs, connecting the front cell contacts, are rotated onto the replacement cell and soldered using the weld electrodes to generate the required heat. The active cell area cleaning operation is followed by the application of glassing adhesive and the cover slide. Again, a weight is placed on top of the assembly, which will remain in position for a 12-hour adhesive cure at room temperature.

3.7.1.4 Discussion

The cell removal operation is tedious and must be performed very carefully, preferably under the magnification of a 10-power microscope, so that the cells next to the faulty cell are not cracked or chipped in the process.

The removal of the adhesive from interconnector tabs and substrate is the most time-consuming operation because of the primer used in the original bonding operation. Again, care must be exercised not to deform interconnectors. A thin metallic shim between interconnector and cell has been shown to be very helpful during the cleaning operation.

If silicon particles should remain on the interconnector tab prior to welding it to the replacement cell, cell cracking can almost be assured. It is important, therefore, to remove all particles carefully without disturbing the silver plating surrounding the silicon nugget. Should the silver-plated area be too small for welding, then solder coating is recommended. Solder reflow occurs on the replacement cell when the weld

pulse heats the interconnector tab on top of the replacement cell. Considerably more area is available on the rear contact interconnectors, so that welding should always be possible here.

Good results have been obtained when welding the replacement cell right on top of the neighboring cell without cracking either cell. However, care must be exercised when rotating the thin bare replacement cell and interconnector 180 degrees.

3.8 USABLE DEVICE YIELD

The cell damage experienced during test coupon and module solar blanket fabrication was carefully monitored throughout the various assembly steps. Cell breakage occurred in almost all assembly phases, mainly in the cell glassing operation. A reduction in cell and cover glass breakage was seen after the modification of the glassing fixtures and the use of the proper mold release. The most damage incurred next to the glassing process, was in the area of the interconnect to bare cell welding operation. It was the second highest factor determining yield. A considerable amount of time was spent in modifying the weld electrode pressure system, in the hope of reducing the cell breakage which was incurred as operators were interchanged. Throughout the development program a total of three operators were employed (operators A, B and C as shown in Table 3.8-1). The years of experience these operators had was: A = 3 years, B = 4 years, and C = 15 years. All operators have been known to be competent workers for the assembly of conventional solar array assemblies, where cell thicknesses of 200 μ m (0.008 inch) and thicker have been involved. Each operator received the same instructions, generally in writing.

It is felt that handling of the thin cells induced the largest damage rate. Consistently good coordination of each move is required as a cell is transferred, from one location to another (using tweezers). Future automated assembly techniques will reduce cell and cover breakage as well as assembly time.

Table 3.8-1. Cell Damage Experienced During Coupon Fabrication

OPERATION	DAMAGED CELLS (%)			
	FIRST GROUP (5) TEST COUPONS	SECOND GROUP (10) TEST COUPONS	MODULE SOLAR BLANKET S/N 01	MODULE SOLAR BLANKET S/N 02 & 03-
Operators	A	B	C	B
1. Interconnector Welding	5	8	31	11
2. Cell Glassing				
• Adhesive Voids Cover slippage	4	1	13	2
• Cell Removal from Fixture	9	7	9	2
• Adhesive Clean-up	3	3	6	1
3. Module Welding	0	0	0	1
TOTAL	21%	19%	59%	22%

3.9 QUALITY ASSURANCE PROCEDURES

- a) The following is a Quality Assurance outline for the verification of integrity of the components employed for the high temperature-low mass solar blanket.
- b) The Quality Assurance Procedure outline for the verification of integrity of solar cell welded joints, bonded coverglass, assembled and bonded to Kapton substrate.

3.9.1 Solar Cell

Quality verification of the integrity of solar cells will be performed at supplier by TRW Source Inspection. Conformance to specifications and process requirements will be verified at source by TRW quality assurance representatives. The electrical cell integrity will be verified and witnessed by TRW Quality Representatives at supplier facility.

The solar cell specification covers the following requirements for space flight applications:

- 1. Design and Construction
 - 1.1 Uniformity of product
 - 1.2 Cell material
 - 1.3 Anti-reflective coating
 - 1.4 Cell contacts and gridlines
 - 1.5 Solar cell junction area
- 2. Performance
 - 2.1 Electrical output
 - 2.2 Electrical output (after cover installed)
 - 2.3 Electrical output (after charged particle radiation)
 - 2.5 Cell contact integrity, (contact pull testing before and after humidity and temperature exposure)
- 3. Dimensions and Weight

- 4. Color and Finish
 - 4.1 Color and appearance
 - 4.2 Mechanical imperfections
- 5. Identification and Packaging

3.9.2. Coverglass

Quality verification of the integrity of coverglass will be performed at supplier by Source Inspection. Conformance to specifications and process requirements will be verified at source by TRW quality assurance representatives. All items will be fabricated, cleaned, and packaged in accord with contract requirements and approved procedures.

The coverglass specification outlines the following requirements for space flight applications:

- 1. Design and Construction
 - 1.1 Substrate material
 - 1.2 Anti-reflective coating (if appropriate)
 - 1.3 Blue-reflective coating (if appropriate)
 - 1.4 Uniformity of product
- 2. Performance
 - 2.1 Cut-off wavelength
 - 2.2 Transmission
 - 2.3 Ultraviolet rejection
 - 2.4 Radiation resistance
 - 2.5 Storage
 - 2.6 Temperature cycling
 - 2.7 Radiometric properties
- 3. Chemical and Physical Properties
 - 3.1 Chemical and physical compatibility
 - 3.2 Coating orientation marking

- 3.3 Surface quality
- 3.4 Edge and corner chips
- 3.5 Abrasion resistance
- 4. Dimensions and Weight
- 5. Color and Finish
 - 5.1 Appearance
 - 5.2 Coating imperfections

3.9.3 Component and Assembly

The following section discusses the verification of integrity of solar cell weld joints, cover glass bonding and cell-to-substrate bonding.

3.9.3.1 Weld Joint Integrity (Front Cell Contact Welding of Interconnect to Cell)

- a) Verification of weld machine settings
- b) Sample pull testing (1 cell per pull test, two weld joints minimum). This operation to be performed at the start of operations in the morning and again in the afternoon. Two entries in data log sheets per day.
- c) Visually inspect for weld imprint.

3.9.3.2 Coverglass to Cell Bond Integrity

- a) Prior to cell glassing operation:
 - 1) Verification of adhesive type and mix ratio
 - 2) Adhesive cure sample inspection
 - 3) Recording of data into log sheets.
- b) After cell glassing:
 - 1) Cells:
 - Inspect for broken or cracked cells (none allowed)
 - Edge chips: not larger than 0.040 by 0.200 inch
 - Corner chips: 0.080-inch hypotenuse maximum

2) Interconnect

- No damaged or deformed interconnect

3) Coverglass:

- Corner chips, edge nicks and broken covers are acceptable as long as the active cell area is not exposed.
- Adhesive is not permitted on top side of covers and below cell (cell P-contact).
- Adhesive voids shall not be larger than 0.050 inch in diameter.

3.9.3.3 Interconnect Integrity (BACK Side Cell Contact--
for Module or String Assembly)

- a) Verification of weld machine settings.
- b) Sample pull tests (1 cell per pull test, two weld joints minimum). This operation to be performed at the start of operations in the morning and again in the afternoon. Two entries in data log sheets per day.
- c) Visually inspect for weld imprint (cell P-contacts).

3.9.3.4 Substrate to Cell Integrity

- a) Prior to bonding:
 - 1) Verify adhesive type and application
- b) After module bonding:
 - 1) Verify cure time.
 - 2) Inspect for adhesive bond area coverage, 70 percent minimum.
 - 3) Inspect for coverglass spacing.
 - Series spacing: 0.016 inch minimum.
 - Parallel spacing: 0.006 inch minimum
 - Inspect for broken covers (record on discrepancy road map).

- c) Prior to module electrical test:
 - 1) Verify equipment calibration and proper standard cell selection.
- d) After module electrical test:
 - 1) Plot I-V Characteristic (at AMO, 28°C conditions).

4. CONCLUSIONS

The results of the work accomplished to date have been encouraging. Modified standard assembly processes can be used to assemble very thin silicon solar cells into module solar blankets that can survive exposure to the typical environments encountered in space without significant degradation. The major conclusions of the study are summarized below.

- o Improved interconnectors geometrics have been developed for optimizing low electrical resistance and stress relief trade-off. The interconnector design lends itself to automation and may be used for either soldering or welding.
- o Weld schedules for front and rear cell welding have been optimized; weld joint pull strength between 0.3 and 0.7 kg have been obtained for front cell contact welding and joint pull strength between 0.6 and 1.0 kg for rear cell contact welding. Smoother cell surfaces are desired.
- o Cell fracturing during rear cell contact welding has been overcome by employing larger weld electrodes.
- o Glassing fixtures have been developed and a mold release agent was found that will permit glassing of bowed thin cells without solar cell and cover glass breakage.
- o It was found that limited thermal soak and thermal cycling testing do not degrade bonded cell assemblies, interconnected by means of welded Invar interconnectors.
- o Module solar blanket repair and rework techniques have been established and proven.
- o A module solar blanket power-to-mass ratio of 250 W/kg can be demonstrated without difficulty.
- o Increased assembly time is generally required when dealing with solar cell and cover glass assemblies.
- o Presently employed automated equipment requires modification to handle thin cell assemblies.

Future automated assembly techniques will reduce solar cell and cover glass breakage and assembly time as well.

5. RECOMMENDATIONS

It is recommended that laser welding be evaluated in order to reduce the pressure exerted mainly onto the rear cell contact during interconnector attachment.

Several solar cell improvements will improve array reliability and production yield: cell edge cracking should be eliminated and the cell bowing minimized. Smoother solar cell contact surfaces are recommended (<500 nm rms), which in turn will improve the weld joint pull strength.

Additional work is required to positively identify the cause of cover glass breakage after cover glass installation, as well as finding a cure for the problem. Controlled glassing experiments are suggested using thin cells with different cell-bow-radii, followed by a series of inspections in order to determine the cover glass breakage as a function of time.

Automated module assembly methods should be studied for all subassembly stages in order to reduce component breakage and improve yield and productivity.

6. NEW TECHNOLOGY

This report does not contain items of new technology developed by TRW Defense and Space Systems Group under this contract.

7. REFERENCES

1. J. Lindmayer and C.Y. Wrigley, "Ultrathin Silicon Solar Cells," Thirteenth Photovoltaic Specialists Conference, Washington, D.C., June 1978.
2. TRW 78-8725.6-122, "In Plane Stress Relief Loop Interconnects-Conductivity versus Stress Relief," M.D. Cannady, 10 October 1978.
3. "Solar Cell Array Handbook," Vol. 1, Jet Propulsion Lab, October 1976.
4. A. Kaplan, "Fatigue Life Study of Solar Cell Welds," Report No. MEL-73-C-60, September 1973.
5. A. Kaplan, "Fatigue Analysis of Solar Cell Welds," IEEE 1973 Photovoltaic Specialists Conference, Palo Alto, California, November 1973.
6. H.G. Mesch, "Parallel Gap Welding of Silver-Plated Solar Cells," IEEE Photovoltaic Specialists Conference, Palo Alto, California, November 1973.

ACKNOWLEDGEMENT

The author would like to thank the TRW personnel who have contributed to this project. In particular, the contributions of A. Kaplan for the "Interconnector Stress and Fatigue Analysis." Rita Seruse, Doris Sims, and Belinda Zamora for the coupon and module assembly, Jim Sung and J. Globitz for the Photomicrography work and Larry Miller for the numerous Electro-Optical Measurements.